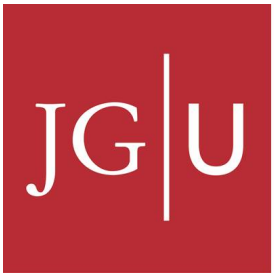

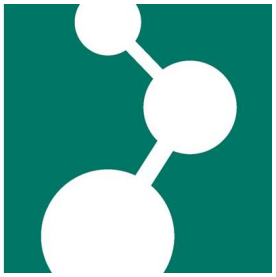

Saccharide based nanocapsules - From monomer building blocks to improved capsules properties

Dissertation
zur Erlangung des Grades
Doktor der Naturwissenschaften
im Promotionsfach Chemie

am Fachbereich Chemie, Pharmazie und Geowissenschaften
der Johannes Gutenberg-Universität Mainz

Kerstin Malzahn

geboren in München
Mainz, 2014

Die vorliegende Arbeit wurde am Max-Planck-Institut für Polymerforschung in Mainz unter der Betreuung von ... von Juli 2011 bis Juni 2014 angefertigt. Ich versichere, die vorliegende Arbeit selbstständig angefertigt zu haben. Alle verwendeten Hilfsmittel und Quellen habe ich eindeutig als solche kenntlich gemacht.

Dekan:
1. Gutachterin:
2. Gutachter:
Tag der mündlichen Prüfung: 21.07.2014

Contents

Chapter 1

Introduction

"There is nothing permanent except change." - Heraclitus of Ephesus (535-475 BCE)

Even though this quote is very old, it is still true - especially in science. Scientific evolution is a road that has led us into the age of complexity.[1] To stick with the road as metaphorical image of scientific evolution one should mention that it is neither a cul-de-sac nor a one-way street. Research creates knowledge and allows us to invent new applications thereof. Having reached a metaphorical pass, we can already see the next one on the horizon. However, the road remains hidden. Similarly, not only research promotes knowledge but new applications also pose new challenges. These challenges need to be answered by research to pave the way towards further knowledge and applications. The iterative principle of scientific evolution is visualized schematically in Figure 1.1.

The development of polymer capsules with a hydrophilic core is a good example for the scientific evolution over the last decades. Prior to nanocapsules, microcapsules were known. Chang already reported the formation of microcapsules with a hydrophilic core by polycondenstion in 1964.[2] He used the encapsulation of enzymes to mimic the function of red blood cells. In 1973 a process was introduced, which allows the preparation of structures in the submicrometer range.[3] This concept evolved in the miniemulsion process, where high shear forces are induced by ultrasonication.[4] The formation of capsules with an aqueous core by interfacial polymerization was transferred to the nanometer regime.[5] Within 40 years of scientific evolution, the diameter of the capsules was reduced by orders of magnitude. Nowadays, challenges in the preparation of nanocapsules for biomedical applications are the design of (multi)functional

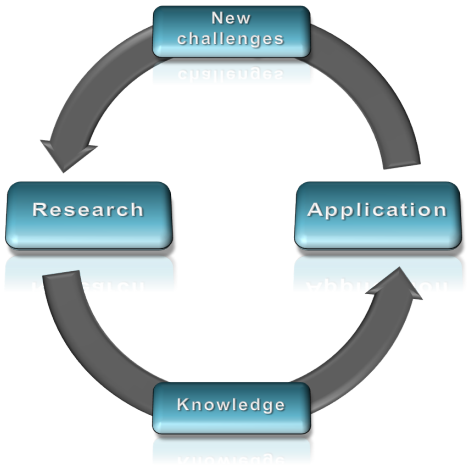

Figure 1.1: Schematic representation of the infinite cycle of scientific evolution.

nanocapsules, which should respond to specific triggers, be biodegradable, and biocompatible.

In this work, three nanocapsular systems were studied. They all share the use of saccharides, a biocompatible and sustainable class of materials. Nanocapsules with an aqueous core are thought to be a suitable vehicle for the targeted transport of hydrophilic drugs in the body. Upon drug delivery, no organic solvents are being released together with the cargo molecule. The cargo of DNA or proteins is of importance for drug-delivery, e.g. in neurosciences.[6] The functional groups of biomolecules (hydroxyl, amine, or thiol groups) should not participate in the capsule forming reaction to maintain their activity. These type of reactions are referred as bio-orthogonal. In the first part of the thesis, a new and facile route for the formation of biocompatible nanocapsules was invented. Olefin cross-metathesis was evaluated for its potential to replace the current interfacial polymerization reactions like polyaddition reactions based on diisocyanates without the use of toxic monomers. The employed metal catalyst is considered removable. A polysaccharide was modified and used as a hydrophilic capsule forming monomer, which should react with the hydrophobic poly(phosphoesters) at the interface.

Beside the invention of new transporters it is also of interest to modify the mode of action of existing drug-delivery systems. "Smart"/responsive drug-delivery systems are being designed e.g. for use in antimicrobial coatings. The

drug-delivery systems should become active only when a threat to the human body is present.

The second project, described in this thesis, marries the advantages of nanogels and nanocapsules to form a core-shell system. Similar to the first project, the presented approach also employs a modified model polysaccharide as a molecular building block. Initial studies regarding the antibacterial activity and cytotoxicity of the core-shell system were carried out to prove its potential for application for wound dressings. The facile exchange of the polysaccharide from dextran to sodium hyaluronate would enable the core-shell system to act as a smart drug-delivery system.

A German proverb says "he who heals is right", which could be translated literally as "whatever treatment works is good". Based on this principle many carriers for medical application are studied rather empirically. However, a profound understanding of the nanocarriers influence on the drugs properties is a major advantage in the successful drug delivery. This is of importance to increase the sensitivity of contrast agents for magnetic resonance imaging (MRI) by encapsulation or conjugation to macromolecules. MRI poses the special prerequisite of a sufficient water exchange between encapsulated contrast agent and the surrounding bulk fluid. The third project is aimed to understand how the nanocapsules properties are influenced by their preparation conditions. The exchange between nanocapsules interior and exterior was studied by means of change in contrast agent relaxivity. Secondly, the nanocapsule core was modified. The encapsulation of high viscosity liquids was thought to enhance the nanocapsules relaxivity. With this regard, (poly)saccharides were not used as building blocks but rather as an interior filling.

The thesis is subdivided into different chapters, which can be summarized as follows. This first introductory chapter is followed by theoretical considerations that are relevant for the understanding of this thesis (Chapter 2). It deals with the fundamentals about saccharides and strategies used for nanocapsule formation. Further the origin of antibacterial activity and the requirements for an improved sensitivity of contrast agents are laid-out. Chapter 3 gives an overview of the characterization techniques used throughout the thesis. Chapter 4 contains the results obtained in the course of the thesis and is divided into three sections as described above. The results of each section are highlighted in an abstract, which is followed by a short introduction. The observations made

and the results obtained are discussed in the course of each section, which is concluded with a summary and outlook. In chapter 5 the experimental details are given and structured with respect to chapter 4.

Chapter 2

Theory

2.1 Saccharides

Carbohydrates ("sugars") are the most abundant biomolecules on earth.[7] Most carbohydrates share the empirical formula $(CH_2O)_n$. One can differentiate between monosaccharides, oligosaccharides, and polysaccharides, when classifying by size. The latter consist of monosaccharides as repeating units. In the following sections polysaccharides and mono- or disaccharides are discussed in more detail.

2.1.1 Mono- and Disaccharides

From a structural point of view, monosaccharides are either poly(hydroxy aldehydes) or polyhydroxy ketones. In monosaccharides the hydroxyl groups can be partially substituted by other functional groups. Glucosamine and glucuronate for example are derivatives of glucose, in which one hydroxyl group is substituted by an amine or a carboxylic acid, respectively. For both types of monosaccharides, poly(hydroxy aldehydes) and the ketones, the cyclic acetal structure is preferred, if n $\geq$ 4. The resulting molecules are referred to as pyranose (six membered ring) and furanose (five membered ring), respectively. Monosaccharides are chiral molecules, often with several stereo centers. Due to its 4 stereo centers, 16 different types of pyranose exist, which carry hydroxyl groups only. Depending on orientation of the hydroxyl groups one differentiates 8 monosaccharides, one of them is glucose. All eight monosaccharides can either exist in L- or D-form. The cyclic acetal structure contains an additional sterocenter, which leads to a, so-called, α or β confor-

mation of the monosaccharide. The metabolism of many organisms relies on D-glucose, the most abundant monosaccharide. However, plants and animals often rely on disaccharides as transport sugars. Commonly known disaccharides are maltose (α-D-glucopyranosyl-(1-4)-α-D-glucopyranose), lactose (D-galactopyranosyl-β-(1-4)-D-glucopyranose) and sucrose α-D-glucopyranosyl-(1-2)-β-D-fructofuranosid. The sucrose is of major commercial importance among the oligosaccharides. It is synthesized by plants and extracted industrially from sugar cane or sugar beet. Because sucrose does not contain an anomeric hydroxyl group it is referred to as non-reducing sugar. Sucrose is cleaved into its monosaccharides during digestion by the enzyme invertase. This is a necessary step prior to resorption in the small intestine. The degradation of carbohydrates is discussed in section 2.1.3.

2.1.2 Polysaccharides

Polysaccharides are ubiquitous and can be found in organisms of all realms. Plants synthesize polysaccharides like guar gum, pectin, cellulose or starch. Chitin is of animal origin and the precursor for chitosan.[8] Microbes produce a variety of polysaccharides like dextran. Some of them are exopolysaccharides, which can take part in biofilm formation.[9] Polysaccharides can be subdivided in homopolysaccharides and heteropolysaccharides based on the number of different monosaccharide repeating units they contain. Polyglucans are polysaccharides, which are only composed of glucose units. The repeating unit of a polyglucan is called anhydroglucose. The naturally most abundant polysaccharides like cellulose or starch belong to the polyglucans. Polysaccharides can have either a linear or a branched structure. Starch, for instance, consist of the linear amylose and branched amylopectin. Both blocks consist of a main chain, wherein the monosaccharides are connected by α-1,4 glycosidic linkages. The branches itself consist of α-1,4 linked glucose molecules. The branches are connected to the main chain via α-1,6 glycosidic linkage. Cellulose is a linear polysaccharide, which is connected by β-1,4 glycosidic linkages. It is a major constituent of plant cell walls. Cellulose readily forms intermolecular hydrogen bonds, due to its linear structure and the orientation of the monosaccharide units. This makes it a very strong and insoluble material. Dextran is a branched polyglucan. It was used throughout the projects in this work. The properties of dextran and the applications resulting from its modification will be discussed in the following sections.

2.1.2.1 Dextran

Dextran and its microbial origin was discovered by Pasteur 1861.[10] Dextran consists of anhydroglucose units, which are connected via α-1,6 glycosidic linkages (Figure 2.1). Branches, consisting of few monosaccharide units, are attached to the main chain in α-1,3 configuration. Dextran has a varying degree of branching, depending on its origin. Dextran is being synthesized on an industrial scale by Leuconostoc mesenteroides NRRL B512F with a degree of branching around 5%.[11] Leuconostoc mesenteroides belongs to the lactobacillae and uses a dextran sucrase to synthesize dextran from sucrose. The native molecular weight of dextran is reported to be in the range of $M_w = 10^6$-10^8 g·mol^{-1}.[12] The obtained molecular weights and the degree of branching strongly depend on the conditions of microbial synthesis.[13] Commercially available dextrans of desired molecular weights are prepared by partial hydrolysis and subsequent fractionation.[14–16] Clinical grade dextran in the molecular weight range from 40000 to 70000 g·mol^{-1} is used as plasma expander in emergency treatment.[17, 18] Upon blood loss dextran can sustain the colloid osmotic pressure, which is usually maintained by blood proteins. Dextrans can decrease the blood viscosity and act antithrombogenic by inhibition of erythrocyte aggregation. Dextrans are soluble in a variety of solvents, including water, DMSO, and DMF/LiCl, due to the rotational chain mobility provided by the α-1,6 glycosidic linkage. This enables the modification with a variety of water-soluble and insoluble molecules. The modification will be discussed in the following section.

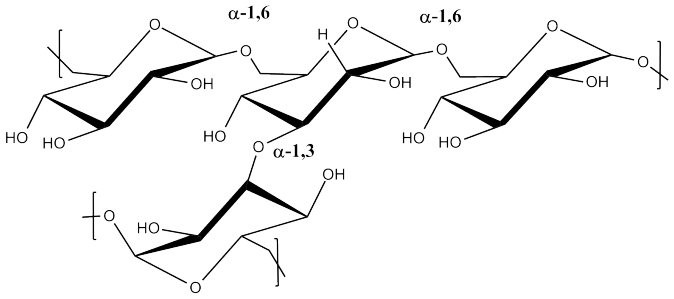

Figure 2.1: Schematic illustration of dextrans chemical structure. For reason of simplicity only three anhydroglucose units with α-1,6 glycosidic bond and one branching point (α-1,3) are depicted.

2.1.2.2 Modification of dextran and its application

The numerous hydroxyl groups of dextran enable its facile modification. Several routes for modification exist. Two common routes for the modification of dextran are depicted in Figure 2.2. Exemplarily for esterifications the reaction with an acid chloride is depicted. Another route is the etherification, which is represented here by the reaction of dextran with an alkoholate. Ester- and etherifications will be discussed in more detail.

Dextran sulfate is a commercially available inorganic dextran ester. A convenient way towards dextran sulfate is the reaction of dextran with sulfate complexes of DMF or pyridine.[19] Dextran sulfates have an anticoagulant activity and can be used has heparin analogue.[20] The charged dextran sulfate was also used to form layer-by-layer assemblies with cationic polyelectrolytes like chitosan. The enzymatic degradation time for such layer structures was significantly prolonged by the alternating polysaccharide assembly. Dextran derivatives have been linked to bioactive molecules directly or via spacers.[21] Among them were proteins, hormones or drugs.[22, 23] The conjugation was used to overcome various problems associated with the administration of drugs. The conjugation improved the solubility of drugs and extended their half-life time in plasma. Further, the conjugation suppressed undesired interactions and reduced the drugs toxicity.[24] The rather hydrophobic drug naproxen was conjugated to dextran to improve its transport in the human body.[23] Dextran molecules were not only conjugated to hydrophobic drugs, but have been modified hydrophobically, especially by esterification with carboxylic acids anhydrides or their derivatives to change their properties. The increased hydrophobicity made the modified dextrans more suitable for pharmaceutical coatings.[12, 25, 26] The etherification is of great importance for the hydrophobization of dextran as well. This will be discussed below.

Modified dextran can not only prolong the stability of biomolecules by direct conjugation but also by incorporation of drugs in dextran hydrogels. Therefore, dextran was modified with polymerizable groups like methacrylates.[27] Subsequently, the modified dextran was cross-linked by UV radiation or used as copolymer in radical polymerization. An example for the latter is the polymerization with isopropylacrylamide, which led to the formation of stimuli responsive hydrogels.[28] The cross-linking of allyl dextran with bisacrylamide has an importance in the formation of matrices for the separation of macromolecules (e.g. sephacryl).

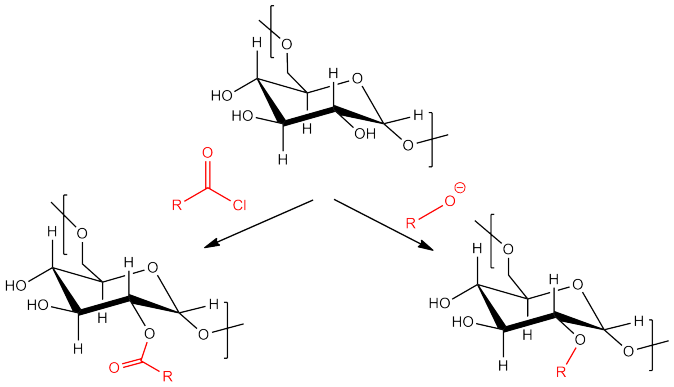

Figure 2.2: Possible routes for the functionalization of polysaccharides. Left: Esterification by acid chlorides, Right: Etherification by alcoholates. The depicted reactions stand exemplary for the respective type of reaction.

As indicated above, the etherification of dextran is of special importance for its hydrophobization. Landoll was the first to use modified polysaccharides (cellulose) as emulsifier.[29] The concept was transferred to the preparation of amphiphillic dextran. The resulting dextrans, like 2-hydroxy-3-phenoxy propyl dextran ethers, were utilized as surfactant in oil-in-water emulsions or for the stabilization of polylactide nanospheres.[30] A reduction of protein adsorption on the nanoparticles was observed additionally to the emulsifying properties for the modified dextran. This was attributed to the adsorption of a stiff layer of modified dextran on the nanoparticle surface, which acts as a corona, comparable to poly(ethylene glycol) (PEG). Not only were the emulsifying properties of polysaccharides altered by etherification but also their resistance to degradation. Dextran and starch were modified with hydroxyethyl groups by etherification with ethylene oxide.[31] However, this process has gained greater importance for the modification of starch to produce hydroxyethyl starch (HES). The purpose of the modification was to make amylose more inert against degradation by amylase. The degradation of carbohydrates will be discussed in more detail in the following section.

2.1.3 Degradation of carbohydrates

The degradation of carbohydrates can be specific or nonspecific. The latter is induced by a change in environmental conditions such as temperature or pH. The temperature induced degradation of sugars can start above 100 °C and is frequently used in food industry. However, the processes are still not fully

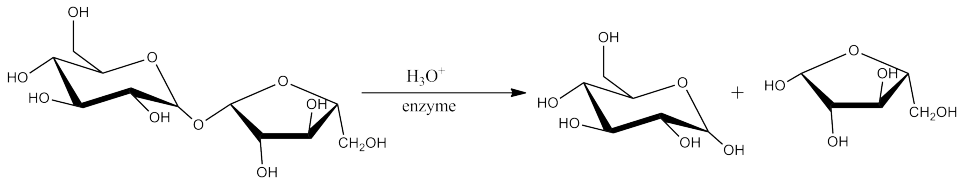

Figure 2.3: Degradation of carbohydrates, shown exemplarily for sucrose. Carbohydrates can be degraded enzymatically or by acid hydrolysis.

understood. Hydrolysis of carbohydrates can occur when the environmental pH is lowered. The acid hydrolysis leads to random degradation of the glycosidic bonds and a fragmentation of polysaccharides.

The enzymatic cleavage of carbohydrates is much more specific.[32] Specialized enzymes only cleave a specific type of polysaccharide. Similar to the nonspecific degradation the glycosidic bond is cleaved. This is depicted schematically in Figure 2.3. Enzymes do not necessarily have the ability to degrade the entire polysaccharide. In saliva e.g. α-amylases are present, which degrade starch into oligosaccharides. The enzyme glucosidase subsequently converts these oligosaccharides into D-glucose units. Dextran is degraded in the liver or the gastrointestinal tract by dextranases (EC 3.2.1.11).[12, 33] Polysaccharides can also be degraded by bacterial enzymes. These so-called exo-enzymes digest polysaccharides in the surrounding of the bacteria.[34] The resulting oligosaccharides can then be taken up by the bacteria. Another enzyme in the degradation of starch is the glucoamylase, which is excreted by fungi and splits off terminal glucose units from starch. The enzymatic degradation can be used for a (targeted) drug delivery. An example is the delivery of drugs to the colon. The multitude of polysaccharide degrading enzymes in the colon can be used to specifically release the drugs there, when encapsulated in polysaccharide based formulations. Another approach is the smart delivery of antibiotics to infection site. The drug-carriers are designed such that bacteria present in the infection site will specifically digest the carrier and be exposed to the antibiotic.[35]

2.2 Nanocapsules

Nanocapsules are considered accessible via two distinct pathways. One discriminates between techniques with and without a sacrificial core. A sacrificial core can be imagined as either a solid or liquid template, which is removed after

successful capsule wall formation. A recent example was given by Huang et al., who prepared nanocapsules by RAFT polymerization on a sacrificial silica core.[36] The layer-by-layer deposition is also a technique, which often relies on the use of a sacrificial core. The obtained nanocapsule structures are either cross-linked in a subsequent step or held together by physical interaction (e.g. ionic interactions).[37] The removal of the core material adds an additional step to the preparative process and makes the encapsulation of cargo molecules tedious. Therefore, current nanocapsule systems are often prepared without a sacrificial core. Preparative techniques without a sacrificial core include self-assembly and heterophase processes such as solvent evaporation and interfacial polymerizations.[38]

2.2.1 Nanocapsules obtained by self-assembly

Bader et al. described micelles and liposomes as synthetic drug-carriers on a vesicular basis, which form by self-assembly processes.[39] Micelles are formed from block copolymers when introduced in a suitable solvent, which is immiscible with one of the polymer blocks.[40] They commonly range in size from 10-100 nm.[41] The insoluble block is contained in the interior of the micelle. The formation of micelles occurs spontaneously once the critical micellar concentration (CMC) is exceeded. The CMC of block copolymers can be determined e.g. by surface tension measurements. Often micelles have a radius in the size range of the block-copolymer length. In biomedical application they are commonly used for the conjugation of drugs.[39, 42] Also swollen micelles are known and sometimes referred to as microemulsions.[43] They solubilize a compound, which is immiscible in the surrounding liquid. Microemulsions are thermodynamically stable, which leads to a long shelf-life time of the formulation. However, they provide only a limited loading capacity due to their small volume.
In contrast to swollen micelles, liposomes and polymersomes separate two miscible liquids. This is either realized by a double layer of amphiphilic molecules or tri-block polymers.[44, 45] Polymersomes are sometimes considered as synthetic analogs to liposomes, which are derived from natural lipids. Polymersomes often present an enhanced toughness and reduced permeability compared to liposomes.[46] This can be attributed to the versatility of block-copolymers, which enable a tuning of the membranes' properties. The membrane thickness can be adjusted by the block-copolymer length and its hydrophilicity/ hydrophobicity can be altered by the variation of the polymer blocks.[47] The miscibility

of the cargo in the polymer layer influences its retention. The incorporation of degradable polymer blocks enables a release of encapsulated cargo.[48] Various triggers for degradation of polymersomes were previously reported and have been reviewed by Onaca et al.[49] Examples include the temperature driven degradation of polymersomes, which contain polymerblocks with lower critical solution temperature.[50] Other stimuli are pH changes or oxidizing agents. The self-assembly approach has the advantage that no chemical reaction is required, which could affect the cargo molecules.

2.2.2 Nanocapsules obtained from heterophase systems

2.2.2.1 Nanocapsules prepared by a miniemulsion process

A well-established procedure for the formation of nanocapsules is the miniemulsion process.[51] Droplets of one phase are dispersed in a second, continuous phase. Droplets in the size range from 30 to 500 nm are formed by ultrasonication or high pressure homogenization. Miniemulsions are stabilized by surfactants, which hinder the collision of droplets and the resulting coalescence (Figure 2.4a). Between 0.1 - 20 wt% surfactant are used with respect to the dispersed phase.[38, 52, 53] Accordingly, the droplet surface is not covered completely by surfactant.This is considered a rather low surfactant concentration compared to microemulsions, which can contain more than 50% surfactant with respect to the dispersed phase.[54] Surfactants are either ionic or non-ionic in nature, which leads to an electrostatic or steric repulsion, respectively. More surface area can be populated with increasing amount of surfactant. Accordingly, the droplet diameter decreases with increasing amount of surfactant. The probability of droplet collision depends on their motion. They either move due to Brownian motion or induced by stirring. Therefore, increasing the viscosity of the continuous phase can further reduce the coalescence.

The second process, which destabilizes miniemulsions is called Ostwald ripening (Figure 2.4b).[55] It describes the consumption of smaller droplets by larger droplets. The Laplace pressure acting on smaller droplets is higher than for larger droplets. This results in a diffusion of material from smaller to larger droplets. This process can be counteracted by the addition of so called osmotic pressure agents (Figure 2.4c). These molecules are highly insoluble in the continuous phase and cannot diffuse with the other material in the process of Ostwald ripening. The Laplace pressure and osmotic pressure act oppositely.

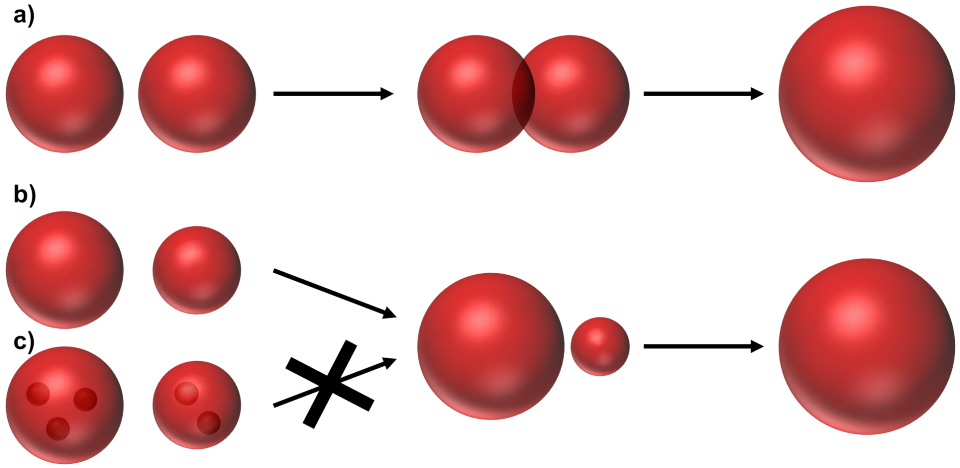

Figure 2.4: Processes of coalescence (a), Ostwald ripening (b) and its suppression by addition of an osmotic pressure agent (c).

Nanocapsules can be prepared with either a hydrophobic or a hydrophilic core. The emulsion of oil droplets in a water phase (o/w) is called direct miniemulsion. The emulsion of water droplets in an oil phase (w/o) is referred to as inverse emulsion. In direct miniemulsions molecules such as hexadecane are used as osmotic pressure agents, while salts are used in inverse miniemulsions.

For this work, the inverse miniemulsion process is of importance. The interfacial polymerization in an inverse miniemulsion is depicted schematically in Figure 2.5. Now, only the main steps will be pointed out, these are the dispersion by ultrasound (I to III) and the capsule formation by monomer addition (III to IV). The process will be described in more detail in section 2.2.2.3.

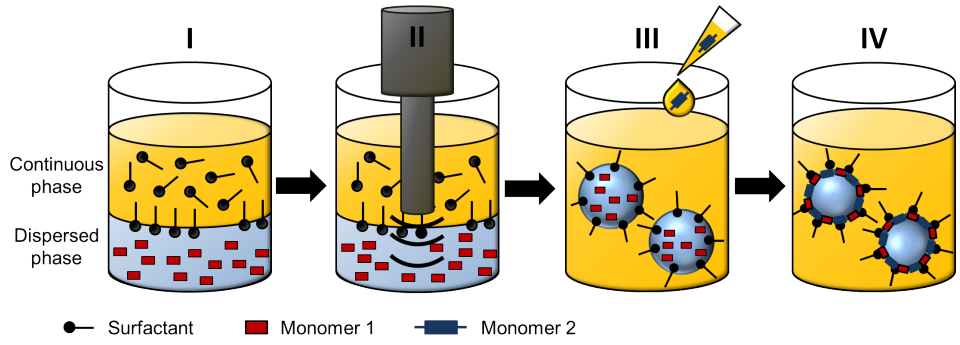

Figure 2.5: Schematic illustration of nanocapsule formation via interfacial polymerization in an inverse miniemulsion process.

2.2.2.2 Emulsion solvent evaporation

The emulsion solvent evaporation process was originally established for the formation of latexes.[56] However, it can be adapted for the nanocapsule formation with hydrophilic or hydrophobic core. The procedure will be explained exemplary for nanocapsules with a hydrophobic core. A preformed polymer is dissolved in a low-boiling solvent and dispersed together with a hydrophobic oil in an immiscible aqueous phase. The low-boiling solvent can be removed by elevated temperatures or vacuum and the polymer precipitates at the oil-water interface.[57, 58] A low solubility of the liquid in the continuous phase is required to enable a slow diffusion of the solvent from the droplet.[59] The emulsion solvent evaporation process was previously used for the encapsulation of a broad range of materials. In the solvent evaporation process no chemical reaction is involved. Therefore, it is especially suited for the encapsulation of sensitive molecules, which might lose their activity if they participate in a capsule forming reaction.

2.2.2.3 Interfacial polymerization

In section 2.2.2.1, the interfacial polymerization was mentioned as a possible technique for the preparation of nanocapsules. The nanocapsule formation by interfacial polymerization can be subdivided into three processes depending on the location of the monomer.[58] The first process involves the addition of the monomer to the continuous phase and the polymerization on the droplets surface. An example of this mechanism is the polymerization of oil-soluble cyanoacrylates at the interface of aqueous droplets.[60, 61]

The second approach to interfacial polymerization is the incorporation of monomer and initiator in the dispersed phase.[62] The polymerization can be induced by a temperature change for example. The polymer becomes insoluble in either phase upon polymerization and migrates to the droplet interface. This phase separation process then leads to the nanocapsule formation.[63]

The third approach is a combination of the two previous concepts and is depicted schematically in Figure 2.5. Monomer 1 is dissolved to the aqueous, dispersed phase prior to the emulsification step. Subsequently, a second monomer is added to the continuous phase. Both monomers are insoluble in the opposite phase and can only react and form a polymer at the droplet interface. A cargo can be encapsulated by dissolution in the dispersed phase prior

to ultrasonication. This process was first established for the microcapsule formation and later transferred to nanocapsules.[64, 65] Diisocyanates are reacted with diamines or diols to form polyurea and polyurethane nanocapsules, respectively. The polyaddition reaction is depicted in Figure 2.6. The reaction follows a step growth mechanism. Additionally, the reaction of diisocyanate with water is depicted. The formed amines can react with another isocyanate group to form polyurea. The reaction kinetic of polyurethane formation and the resulting nanocapsule wall composition were studied by Gaudin et al.[66] The side reaction with water can be limited by the choice of an appropriate reaction partner for the diisocyanate. The reactivity with isocyanates is known to increase in the following manner: H_2O < R-OH < R-NH-R < R-NH_2.[67] Even though, the diisocyanate based polyadditon reaction is very unspecific, it is frequently used for the formation of nanocapsules. An important reason is the facile exchange of capsule forming molecules (monomers and polymers) with only minor adjustments in the preparative process, which was pioneered by Crespy et al.[5] Since then, the technique was applied to form a multitude of nanocapsules based on diols,[68] di- and triamines,[69–72] peptides[73] and carbohydrates.[35, 74, 75]

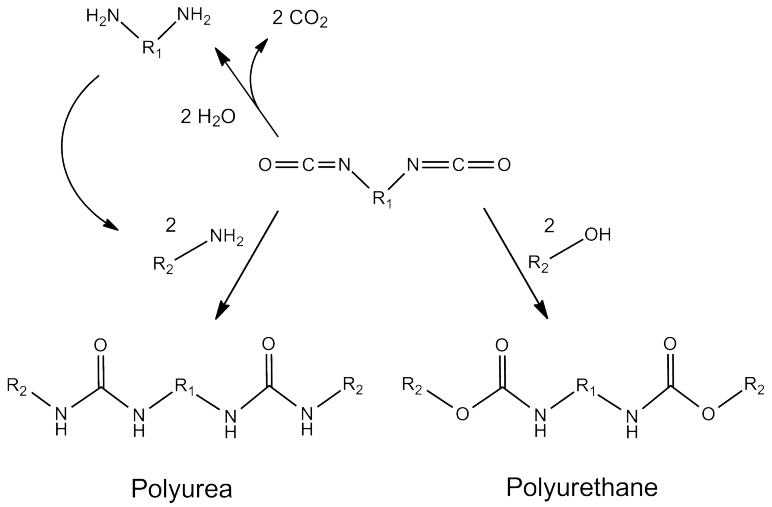

Figure 2.6: Formation of polyurea and polyurethane by reaction of diisocyanate with amines or alcohols. Additionally the side reaction with water is depicted, which also leads to polyurea formation.

The encapsulated molecules should not be affected by the capsule forming reaction. In recent years progress has been made in the development of bio- orthogonal reactions, which can be carried out at ambient conditions without a

cross-sensitivity for functional groups relevant in biomolecules (hydroxyl, amine groups). The progress was initiated by the pioneering work of Sharpless and coworkers on, so-called, click-reactions.[76] Since then, scientists also strive to transfer this concept to the interfacial polymerization. The reactions of azides and alkynes as well as the reactions of thiols and maleimides or olefins (thiolene-click) are referred to as click reactions. The thiol-ene chemistry was reviewed by Hoyle et al. and the application in the formation in dendrimer networks and hydrogel was pointed out.[77, 78] It has also found application in the surface modification of nanoparticles[79, 80] and was used for the formation of a nanocapsule wall by thiolene-click chemistry.[81] An interfacial polymerization by a click reaction at the droplet interface was already demonstrated.[82, 83] The reaction of a water soluble azide with an oil soluble alkyne lead to the formation of nanocapsules with a hydrophilic core. The functionalization of molecules with either azides or alkynes is considered straight forward. However, it has not led to the modification of molecules such as carbohydrates or peptides and their application in interfacial polymerization so far. Scientists still search for reactions combining the versatility of the diisocyanate approach with the mild conditions and specificity of click reactions.

2.2.3 Cargo

The nanocapsules' liquid core enables the facile encapsulation of molecules and makes the nanocapsules a suitable carrier- and delivery-system for the encapsulated molecules. The nanocapsules can be designed to retain or release their cargo (triggered or with time), depending on the application. Molecules that are sensitive to environmental conditions should be retained in the nanocapsules. Dyes for optical application such as upconversion or solar cells, can be protected from oxygen by encapsulation.[84, 85] Besides, the encapsulation of oxygen sensitive dye molecules can also be used as a characterization technique to study the membrane permeability of liposomes.[86] Capsules, which should release their cargo, can be divided in active (triggered) and passive (leakage) release systems. A broad variety of triggers can be used to initiate the release.[87] These include pH,[88, 89] temperature magnetic field, light,[90] electrochemical[91] or mechanical triggers. The triggers can lead to a removal of cross-links in the nanocapsule wall or the production of gases, which induce a pore formation or rupture of the nanostructures.[88, 92, 93]

An example of cargo molecules, which should be released upon stimulus, are the monomers required for self-healing reactions. The triggers used for self-healing application include mechanical stress or change in the redox potential.[94] Self-healing represents an intrinsic repair mechanism of a material. Self-healing is used to avoid further damage or protect materials from corrosion.[95] In self-healing reactions, the release of active components leads to the generation of new material, which seals the damaged area. The principles of self-healing reactions were summarized by Binder.[96] He emphasized the benefit of encapsulating self-healing agents, which makes a multitude of self-healing reactions accessible. The first self-healing microcapsules were composed of polyurethane and contained the monomer for a self-healing reaction based on ring opening metathesis polymerization. The catalyst required for the reaction was distributed in the surrounding polymer matrix.[97] Subsequently, a multicapsule concept evolved, wherein monomer and catalyst were both encapsulated in separate nanostructures.[98] The self-healing concept was transferred to nanoencapsulation by Blaiszik et al.[99]

In biomedical application, the encapsulation of marker molecules can be used to analyze the fate of nanocapsules in the body.[51, 100] Further, drugs are being encapsulated with various intentions as reviewed by Vrignaud and coworkers.[101] The bio-distribution of the drug can be altered by encapsulation. An example is the encapsulation of hydrophobic drugs. These molecules are not soluble in the blood and could not be transported to their target location without their encapsulation.[102–104] Additionally, the encapsulation can increase the stability and the circulation time of a drug in the body and enhance the probability to reach its target.[105, 106] Therefore, nanocapsules are being functionalized with PEG, which exhibits a stealth effect in the human body.[50, 107, 108] Drugs are also encapsulated to reduce their toxicity.[109] Cancer drugs do not only disturb the growth of malign tissue but also affect healthy tissue.[110, 111] An encapsulation should protect healthy parts of the body from the drug and enable a delivery to tumor tissue. Peer and coworkers reviewed nanocarriers as a platform in cancer therapy, with special focus on the possibilities of an active targeting.[112] Two other classes of drugs, which are frequently encapsulated are antimicrobial agents and contrast agents for MRI imaging.[113] Both are of importance in this thesis and will be discussed in detail in sections 2.3 and 2.4, respectively.

2.3 Antimicrobial background

Hospital acquired infections from antibiotic resistant bacteria have become a serious concern over recent years. *Staphylococcus aureus* (*S. aureus*) and *Pseudomonas aeruginosa* are two of the most prevalent bacteria causing hospital acquired infections. *S. aureus* will be discussed in more detail in the following section, due to its importance for this work. Subsequently, the basic principles of biofilm formation will be explained and antimicrobial surface coatings will be discussed.

2.3.1 *S. aureus*

S. aureus has a spherical shape and is gram positive bacteria: it has a phospholipid membrane covered by a thick murein layer (peptidoglycan). This layer is often referred to as cell wall.[114] Molecules of teichoic acid are interwoven in the murein layer. The composition of teichoic acid can vary between strains but in general consists of negatively charged phosphates and sugar units. This makes the surface of *S. aureus* negatively charged.[115] Further, the composition of teichoic acid has been observed to influence the susceptibility of bacteria to antibiotics.[116] Antibiotic resistant strains, like the methicillin resistant *S. aureus* (MRSA), are of special importance in hospital acquired infections. *S. aureus* is commonly found on human skin and nasal soft tissue.[117] However, it grows also under anaerobic conditions, in wounds and under dry conditions.[118] Once colonization is achieved *S. aureus* uses a variety of survival strategies to evade the human immune system.[119] Among them are the inhibition of T cell receptors and the expression of surface proteins to prevent phagocytosis including protein A and Sbi. Besides these very specific processes the excretion of polymers and the formation of a biofilm can protect the bacteria.

2.3.2 Biofilm formation

When planktonic bacteria attach to a surface they are referred to as sessile and can start to form a biofilm. The process of biofilm formation is depicted schematically in Figure 2.7. The bacterial attachment to a surface can be described as a two-step process.[120] The initial step is referred to a reversible attachment and lasts only few hours. Subsequently, the bacteria proliferate on the surface and start to secrete the constituents of the biofilm. The bacteria undergo phenotypic changes as the biofilm forms.[121] A biofilm is mainly comprised

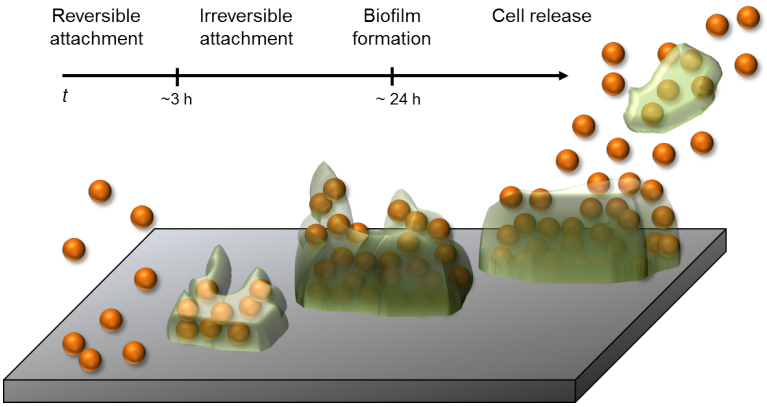

Figure 2.7: Schematic illustration of the biofilm formation upon bacterial surface attachment.

of cell clusters, sugars, teichoic acid and proteins.[122] With time, the biofilm matures and the bacteria start to cross-talk, which is called quorum sensing. The quorum sensing is mediated by the excretion of signaling molecules. In a type of self-regulation the partial detachment of the biofilm can be promoted to colonize new areas. The biofilm acts as a physical protection against mechanical stress (shear). In its function as a chemical barrier, the biofilm can protect the bacteria from acids, toxins and phagocytosis. In conclusion the biofilm is a complex entity, which impedes the effective treatment of infections.

2.3.3 Antimicrobial coatings

Biofilm forming bacteria are most susceptible to treatment in an early stage of infection. Therefore, scientists try to either suppress the initial bacterial attachment to surfaces and/ or kill the bacteria when they approach a surface.[123] There are two broad classes of materials used clinically: those which are in use outside the human body or inside the human body. The first group comes in contact with the body only very briefly like medical devices. The latter group stays inside the body or remains in close contact to tissue for a longer period. This makes cytocompatibility a requirement. Examples are implant materials like catheters or wound dressings.

The surfaces that inhibit the bacterial attachment are so-called anti-fouling surfaces. They inhibit attachment based on their physical properties and do not affect bacterial growth. PEG has been shown to help inhibit protein attachment by retaining water close within its structure. It may inhibit bacterial attachment

since most bacterial attachment is ultimately mediated by a protein-surface interaction. PEG can be attached to surfaces e.g. by grafting methods.[124] Self-assembled monolayers (SAMs) containing oligo(ethylene oxide) groups were found to be anti-fouling as well. The higher density of the SAMs made them competitive to longer chains of loosely grafted PEG.[125] Zwitterionic polymers were also found to be anti-fouling, which was attributed to their hydrophilicity and water binding capacity.[126] Similar effects were observed for surface coatings with hydrophilic polyurethanes.[127] However, all of these anti-fouling materials can only be active as long as they represent the top layer of a surface. When bacteria secrete biomolecules or protein absorption occurs in a wound environment, the anti-fouling surface coatings are being inactivated.

A second group of antimicrobial surface coatings are contact-active materials. Antimicrobial peptides (AMPs) can be excreted by animal and plant cells. The peptides act preferentially on bacterial cell membranes. This is attributed to the presence of negative surfaces charges and the absence of stabilizing cholesterol in bacterial cell membranes.[128] Due to the high antimicrobial activity of AMPs, even at low concentrations, they are well suited for the modification of surfaces. AMPs can be tethered directly or via spacer molecules to surfaces to kill bacteria, which come in contact with the surface. An overview of the existing AMP surface coatings was given by Costa et. al.[129]

Beside AMPs, polycationic polymers also belong to the group of contact-active, non-leaching materials.[130] The hydrophobic part of the polymer enables an interaction with the hydrophobic cell wall of the bacteria. The cations interact with the negatively charged bacterial cell wall (e.g. in teichoic acid) and thus damage the bacterial cell wall. Cationic polymers with quaternary ammonium groups were reviewed by Kenawy et al.[131] The antimicrobial activity was reported to depend on molecular weight and the type of counter ion. Polymers with a molecular weight in the range of 10^4- 10^5 Da were found to have the highest antimicrobial activity. A recent example is the UV-induced formation of hydrogels based on quarternized chitosan.[132] These biocompatible hydrogels showed a broad range antimicrobial activity against gram-positive and gram-negative bacteria, as well as fungi. The contact-active materials need to be directly exposed to the bacteria to be active, similar to the anti-fouling materials. However, the dead bacteria could deposit on the surface and thus block the surfaces after a while. This limits the use of contact-killing materials to medical devices with a short-term usage.

Release systems are the third group of antimicrobial surface coatings. The advantages of local release of antimicrobials have been reviewed by Wu and Grainger.[133] In principle, such systems deliver lower systemic doses and have a lower risk of promoting antimicrobial resistance. The incorporation of common antibiotics into surface coatings and their subsequent release was proven to be effective against bacterial infections.[134] However, bacteria causing hospital acquired infections, like MRSA, are often already resistant against commonly used antibiotics. Therefore, alternatives to common antibiotics are being considered for release systems. Among them are e.g. bacteriophage release systems.[135] Bacteriophages are bacterial viruses, which inject their DNA into host bacteria, where it is used for phage reproduction.[136] The bacterial cells are lysed by lysins produced by the internalized and reproducing bacteriophages. The infection and release cycle proceeds until no host bacteria are present anymore. Bacteriophages are very specific and can only target a single type of bacteria.[137] A cocktail of different bacteriophages would be required to achieve a broad range antimicrobial activity. Additionally, the human body can develop antibodies against the bacteriophages, which could make them ineffective in a second treatment. Therefore, bacteriophages are considered a treatment of last resort.

Another alternative to common antibiotics are metal release systems based on metal ions or metal(oxide) nanoparticles. Many metal ions have broad spectrum antimicrobial activity. In this work zinc metal release systems have been studied. In the literature numerous examples of silver and copper based antimicrobial release systems have been reported.[138–140] These metal ions can interact with thiol groups of proteins and enzymes and thus inhibit the activity of the biomolecules.[141] Mammalian cells have a higher tolerance for zinc ions than bacteria.[142] However, at elevated concentrations zinc ions can be cytotoxic. Zinc has the advantage, over other metal ions, to be required in the metabolism of mammalian cells.[142] Therefore, natural excretion pathways exist and no danger of accumulation in the body is caused by the use of zinc as antimicrobial agent. In addition to metal-ion release systems, a broad range of antimicrobial coatings use zinc oxide nanoparticles.[143, 144] Their mode of action is still not completely understood.[145] However, it is known that zinc oxide nanoparticles can induce the formation of reactive oxygen species.[146] All antimicrobial release systems share a common disadvantage: they can only provide a limited reservoir for antimicrobial compounds. Therefore, they should

either be used for short term applications or the release of the antimicrobial should be triggered by the presence of bacteria.[35, 147, 148]

2.4 Contrast agents for MRI

Magnetic resonance imaging is a non-invasive radiation free method for the visualization of structures in soft tissue. It is based on the principle of nuclear magnetic resonance (NMR) and has evolved from a 2D-imaging technique into a 3D-imaging technique. In the imaging process, one makes use of the tissue specific longitudinal and transversal relaxation rates of protons ($1/T_1$, $1/T_2$). When certain pulse sequences (T_1 or T_2 weighted) are used, the different $1/T_1$ or $1/T_2$ rates can be emphasized, respectively, to generate the desired contrast.[149] An increased signal intensity is obtained in tissues with a high longitudinal relaxation rate by T_1 weighted scans, for example. This results in a bright area in the image, which is referred to as positive contrast. The use of contrast agents to further improve the image contrast is discussed in the following sections. Subsequently, methods for the modifications of contrast agents to improve their properties are highlighted.

2.4.1 Contrast agents

MRI contrast agents are compounds, which can catalytically alter the relaxation times of surrounding protons. Accordingly, they are often crucial to differentiate between tissues with similar relaxation time. MRI contrast agents can be classified either as positive or negative contrast agents. Based on their predominant ability to increase the relaxation rates $1/T_1$ or $1/T_2$ they are referred to as T_1 or T_2 contrast agents. Superparamagnetic iron oxide nanoparticles make up a class of T_2 contrast agents and lead to a lower signal intensity at the respective image regions.[150] Paramagnetic transition and lanthanide ions (Mn^{2+}, Gd^{3+}) lower the relaxation time T_1 of surrounding protons and are used as positive contrast agents.[151, 152] Lanthanide ions can relax proton spins through time-varying magnetic fields by their molecular rotation and relaxation of the electron spin. Gadolinium is ideally suited as contrast agent. It has an electron spin of $7/2$, which means that seven unpaired electrons can couple dipolar to the proton spin and relax it. Contrast agents are characterized by their ability to reduce the relaxation time of surrounding protons which is called relaxivity. The relaxivity is the concentration-dependent change of the measured relaxation rate ($1/T_1$)

or $(1/T_2)$. For the case of Gadolinium it can be described by the following equation:[153–155]

$$\frac{1}{T_{1(measured)}} = \frac{1}{T_{1(Dia)}} + r_1 \cdot c_{Gd} \tag{2.1}$$

Lanthanide ions are toxic to the body and can accumulate in the bone.[156, 157] Therefore, Gd-complexes with very high stability are used as contrast agents. The safety of a contrast agent complex is defined by its complex formation constant. Additionally, no transmetallation should occur. Transmetallation describes the replacement of the paramagnetic ion in the complex by other trace metals like Zn^{2+}, for example. This would lead to the presence of unbound toxic Gd^{3+}, which was reported to cause nephrogenic systemic fibrosis.[158] One differentiates between linear and macrocyclic polyaminocarboxylate ligands. In Figure 2.8 the chemical structures of a linear and macrocylic contrast agent are depicted exemplarily, both have clinical importance. The linear, ionic Gd complex is based on diethylene triamine pentaacetic acid and is referred to as gadopentetate dimegalumin ($[Gd(DTPA)(H_2O)]^{-2}$, Magnevist®). The non-ionic macrocyclic complex gadobutrol (Gd-DO3A-butrol, Gadovist®) can be described chemically as [1,4,7-tris(carboxymethyl)-10-(1-(hydroxymethyl)-2,3-dihydroxypropyl)-1,4,7,10-tetraazacyclododecanato] gadolinium(III).

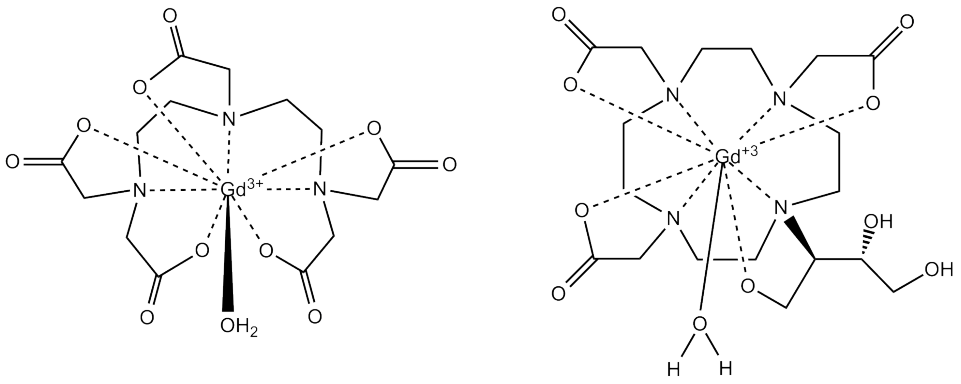

Figure 2.8: Chemical structure of two gadolinium based contrast agents, left:$(Gd(DTPA)(H_2O))^{-2}$ right: Gd-DO3A-butrol.

Beside these two, several other complexes exist, which are mostly derivatives of DTPA or DOTA (the parental molecule of DO3A-butrol). Molecules have been designed to achieve higher relaxivity or to enable an interaction with the surrounding. An example is the complex BOPTA (MultiHance®), a derivative

of DTPA, which can interact with serum albumin due to its phenyl group. However, for the work in this thesis only gadobutrol was used as contrast agent.

The contrast agent complex can differently influence the relaxation rate of water protons in its surrounding. This depends on the interaction of complex and proton, which is a function of the distance between the contrast agent complex and the water molecule. Accordingly, for each type of interaction a relaxivity can be calculated, which contributes to the overall relaxivity. One differentiates between inner sphere contribution (IS), second sphere contribution (SS) and outer sphere contribution (OS). The different interactions are depicted schematically in Figure 2.9. The contribution to the overall relaxivity is as follows:

$$r1 = r1_{IS} + r1_{OS} + r1_{SS} \tag{2.2}$$

Inner sphere contributions originate from protons of the water molecules, which are directly associated to the paramagnetic center of the complex. Depending on the type of contrast agent the number of water molecules is normally either 1 or 2. The more coordination sites are occupied by water molecules the lower is the complex stability. Therefore, in commercially available contrast agents only one water molecule can bind to the gadolinium center. Second sphere contributions arise from protons of water molecules, which are hydrogen bonded to polar groups of the ligand. Protons of water molecules, which are diffusing in proximity of the complex lead to the outer sphere contribution.

Among other parameters the relaxation time of water molecules bound in the inner sphere T_{1m} depends on the correlation time τ_c. Parameters such as the rotational correlation time of the contrast agent τ_r, the electron relaxation time T_{1e}, and the speed of exchange of bound water molecules τ_m influence the correlation time. Among these parameters and at the clinically commonly used field strength of 1.5 T the rotational correlation time τ_r of the complex has the highest impact on IS relaxation. A slower rotation leads to an increasing relaxation rate, up to a certain limit. Accordingly, scientists try to limit the rotation of the complex by various methods. Several approaches will be discussed in the following section. The relaxivity is strongly dependent on the environment and will increase when diffusion and rotation of the complex are reduced.

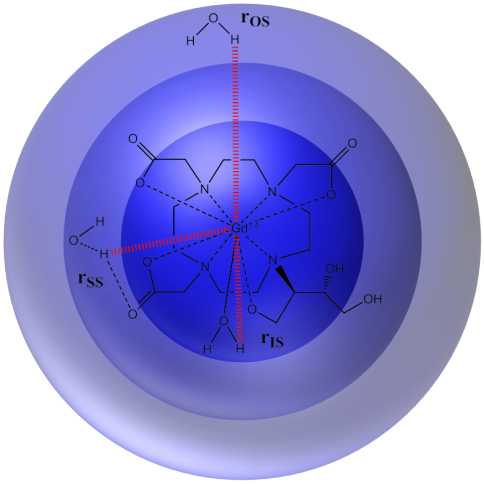

Figure 2.9: Schematic illustration of the interactions of gadobutrol with protons in its surrounding. The contribution of protons to inner, second and outer sphere relaxivity is indicated by colored circles.

2.4.2 Increasing the relaxivity of T_1 contrast agents

For many years, scientists have worked on the confinement of contrast agents or their respective core elements to enhance their relaxivity.[159] Contrast agents were either attached covalently to polymers, micelles, and particles or encapsulated in larger entities like liposomes and capsules. The progress in the use of nanostructures for MRI was recently reviewed by Zhu et al.[160] The polymers used for the attachment of contrast agents include linear or dendritic molecules.[161–166] The resulting multimeric structures were co-functionalized for targeting of blood clot and application in angiography.[167,168] All of these attempts have in common that the number of complexes is limited either by the size of the nanostructure or the number of sites for covalent attachment.[169] Perfluorocarbon nanoparticles were decorated with gadolinium complexes by covalent attachment and yielded a substantial increase in relaxivity (17.9 $s^{-1}{\cdot}mM^{-1}$ 1.5 T).[170–172] Further, poly(lactide-*co*-glycolide) nanoparticles were decorated with a contrast agent and a relaxivity similar to the perfluorcarbon nanoparticles was observed.[173] Cheng et al. combined the immobilization of Gd(III)complexes on dendrimers with the encapsulation in water permeable polymersomes to increase the relaxivity (7.5 $s^{-1}{\cdot}mM^{-1}$, 1.41 T).[174] Even though they could encapsulate larger numbers of gadolinium units, they had to introduce pores into the capsule wall to enable water exchange and enhance the relaxivity. When

the rotational diffusion is sufficiently lowered, the water exchange becomes the limiting factor and can lead to a decreased relaxation rate.[175] Further examples of porous nanostructures include inorganic silica capsules.[176–178] Another approach is the confinement of contrast agents in polymeric nanocapsules. In previous studies a high contrast agent encapsulation efficiency was reported for polyurea/-urethane nanocapsules.[179, 180] However, the relaxivity of the complex did not increase. This correlates well with previous observations for the encapsulation within nanostructures like capsules, particles or liposomes. A high T_1 relaxivity is difficult to achieve due to the limited water access.[181–183] Nevertheless nanocapsules are an interesting carrier system for contrast agents as they provide a potential for postmodification to achieve a targeted delivery. Further the nanocapsules could act as theranostic when drugs are co-encapsulated.[184]

Chapter 3

Characterization methods

In the following sections the characterization techniques of major importance for this thesis are introduced and described on a theoretical level. Experimental details for the measurements are given in chapter 5.

3.1 Inductively-coupled plasma optical emission spectroscopy

Inductively-coupled plasma optical emission spectroscopy[185] (ICP-OES) was developed in the 1970's by Fassel et al. as a trace metal analysis technique. The measurement process can be divided into two stages. In the first stage the samples are ionized/ atomized in the inductively coupled plasma and in the second stage the light emitted by relaxation of elements to the ground state is detected by a spectrometer. A broad range of elements can be detected and quantified at very low concentrations (ppb range). Figure 3.1 shows a simplified schematic of an ICP-OES setup. In a first step, the typically aqueous samples are fed through a nebulizer via a spray chamber (e.g. cyclone chamber) as homogenous ultra-fine droplets into the plasma torch. The torch consists of a glass cylinder surrounded by a coil, where an argon plasma is ignited inductively by a radio frequency generator. The argon plasma has a temperature in the range of 6000 - 9000 K depending on the input power. The elements in the droplet are being atomized and ionized immediately. The excess energy leads to a further excitation of the ions. Upon relaxation intense photon emission occurs at discrete and element characteristic wavelengths in the UV or visible spectrum.

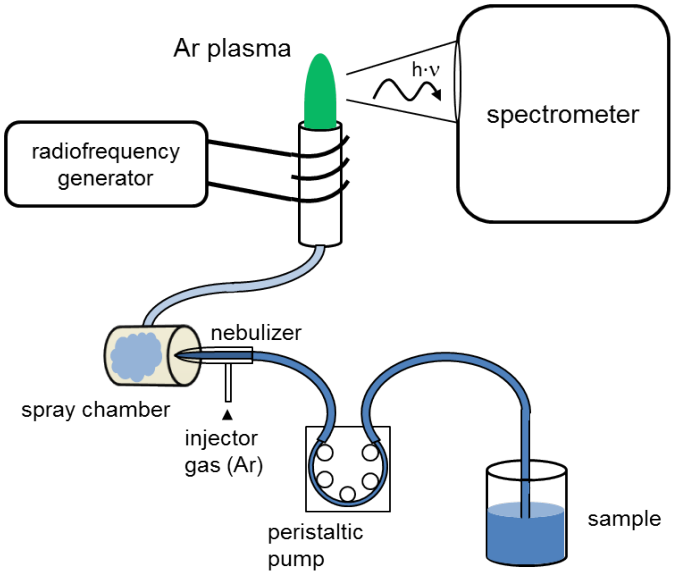

Figure 3.1: Schematic illustration of an ICP-OES setup.

The second step of the measurement process is the optical emission spectroscopy. The emitted light is sent through a diffraction grating and the intensity of a single line is amplified and detected by a photomultiplier. Calibration curves are obtained from aqueous solutions containing the element at a known concentration. With respect to the calibration curve the recorded intensities can be expressed as concentrations ($mg \cdot L^{-1}$). ICP-OES is a sample oriented multi-element technique where several elements can be detected simultaneously.[186] Careful choice of the emission lines allows a detection without cross-sensitivity at the respective wavelength. Therefore, ICP-OES is nowadays employed as a standard quantification technique in environmental analysis or food industry. Calibration solution and sample solution should resemble each other very well to alleviate background effects and achieve a reliable quantification.[187] Dubuisson et al. discussed the influence of especially sodium ions on the droplet formation in the nebulizer.[188] The rare studies of colloidal dispersions have revealed the need for a matrix adaption in the calibration curve. By use of equal surfactant concentrations in calibration solution and dispersion the reliable and quantitative character of ICP-OES can be retained.[189] ICP-OES was used for the quantification of ruthenium, zinc and gadolinium throughout this thesis.

3.2 Scanning electron microscopy

The resolution of optical microscopy is restricted at its lower end by the Abbe diffraction limit (eq.3.1). It defines the minimum distance (d) between two objects that can be resolved at a certain wavelength (λ) in dependence of the numberical aperture (NA). However, for the resolution of nano-sized objects this is not enough. Current electron microscopy techniques make use of the much smaller wavelength of electrons accelerated in an electric field. Scanning and transmission electron microscopes allow a resolution at the lower nanometer scale.

$$d = \frac{\lambda}{2 \cdot NA} \tag{3.1}$$

The first electron microscope was mentioned by Knoll and Rusaka in 1932.[190] Nowadays, scanning electron microscopy (SEM) is a widely used technique for imaging of nanosized structures on solid supports. Beside its superior resolution SEM is superior to optical microscopy due to its large depth of field. In the electron microscope electrons are generated at the electron gun and accelerated to an energy between 0.1 and 30 keV. With decreasing electron energy the method becomes more surface sensitive, as the penetration depth into the sample gets lower. The electron beam is focused by means of lenses and can be scanned over the sample surface with a deflection system. When the electron beam interacts with the surface a variety of processes take place. Characteristic x-rays are emitted, which can be used for an elemental mapping of the surface by energy dispersive x-ray spectroscopy (SEM-EDX). Further, in proximity to the electron beam secondary electrons of low energy are emitted from the sample by interaction with the electron beam. At edges or peaks on the sample surface the emission of secondary electrons is increased. This topographic contrast was already observed by Zworykin et al. in 1942.[191] A part of the beam is back-scattered by interaction with surface atoms based on their atomic number. The emission of secondary and back-scattered electrons varies most as a result of topography changes.[192] Hence, the detection of either type of electrons leads to a 3D-like appearance of the surface. Throughout this thesis SEM was used for the visualization of the prepared nanogels and nanocapsules as well as for the investigation of their morphology.

3.3 Dynamic light scattering

Dynamic light scattering is a commonly used technique to determine the size and size distribution of colloids.[193] The movement of colloids in solution is based on Brownian motion. By means of the Stokes-Einstein-equation (eq. 3.2) the radius (r) of a sphere can be directly related to its self-diffusion. In the equation k_B represents the Boltzmann constant, T the temperature and η the dynamic viscosity of the solvent. The equation allows the determination of the radius of a colloidal sphere by measuring the diffusion coefficient (D_s) in a very dilute dispersion. In principle a reduced particle size leads to an increased diffusion coefficient.

$$D_s = \frac{k_B T}{6\pi\eta r} \tag{3.2}$$

In the measurement setup the sample is irradiated by laser light (coherent). Upon interaction of photons with colloids a part of them is scattered due to the difference of refractive index between colloid and solution. Interference of photons creates a pattern, which can be detected at a defined angle (e.g. 90°). The observed pattern changes overtime as the particles move. The velocity of the change is based on the particles size and their self-diffusion. Accordingly, the measurement of the self-diffusion can be used to determine the particle size. Dynamic light scattering can be limited in its applicability by multiple and back scattering artifacts, which lead to falsification of the measured diffusion coefficients.[194] Hence, the dispersion should be highly diluted. Another limitation is the low scattering intensity of very small particles and the slow diffusion of very large particles. However, it is well suited for the determination of particles and nanocapsules in the size range between 2 and 500 nm. DLS has been used in this work to assess the nanocapsule size and monitor their degradation.

Chapter 4

Results and Discussion

4.1 Polysaccharide based nanocapsules[1]

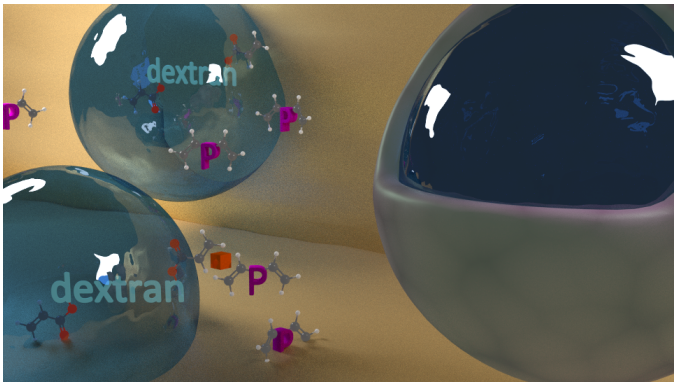

The first synthesis of hollow nanocapsules with an aqueous core via olefin cross metathesis is presented. The reaction was tailored such that it proceeds selectively at the oil-water interface of aqueous nanodroplets in an inverse miniemulsion. The cross metathesis takes place between an acrylated polysaccharide and unsaturated organophosphates under mild conditions. This general protocol allows the synthesis of biocompatible and polyfunctional nanocapsules via bio-orthogonal olefin metathesis, thus generating a highly versatile methodology for the design of future materials for biomedical applications, but also for materials science. Functionalization of the nanocapsules was demonstrated with fluorescent labels, which can be either attached to the pendant phosphoester

[1] This section is based on the publication "Selective Interfacial Olefin Cross Metathesis for the Preparation of Hollow Nanocapsules" by Kerstin Malzahn, Filippo Marsico, Kaloian Koynov, Katharina Landfester, Clemens K. Weiss and Frederik Wurm published in 2014 in Macro Letters, volume 3 on pages 40-43.[195] Reprinted with permission. Copyright 2014 American Chemical Society.

within the crosslinker, exploiting the versatility of the phosphorus chemistry, or via coupling to the capsules' surface.

4.1.1 Motivation

Degradable and renewable polymers are a growing field in modern materials science, because conventional/fossil carbon sources are limited and commodity plastics typically have long half-life times in nature.[196] Moreover, in the biomedical field, e.g. for drug delivery and release, tissue engineering, or to ensure renal clearance of (macro)molecules, degradable polymers are of high interest.[196, 197] Within the field of degradable polymers with biomedical application, polyesters and polysaccharides,[198, 199] such as polylactide or dextran are the most prominent materials.[197, 200] Another, yet rather unexplored class of bio-degradable polymers, are poly(phosphoester)s (PPEs)[201] that are chemically much more versatile than conventional polyesters, because phosphorus can form triesters allowing the inherent functionalization of every ester moiety along a polymer backbone to precisely control their hydrophilicity or functionality.[202, 203]
Heterogeneous polymerization techniques allow the defined generation of (nano)-particles and capsules,[204] which can be loaded in situ with drugs, biomolecules, etc. A well-known example is the formation of polyurethane/ polyurea nanocapsules via a polyaddition reaction of isocyanates and alcohols or amines at the interface of (mini)emulsion droplets.[5, 205] This strategy, however, has only limited use for the encapsulation of pharmaceutically active biomolecules, as nucleophiles of peptides and proteins, especially amines, thiols or alcohols, will participate in the reaction,[73] and might decrease their biomedical activity. Thus, bio-orthogonal reactions are demanded, leaving the biomolecules' functionalities unaltered. Prominent examples are "click" reactions, between thiols and alkene or alkynes and azides which were also successfully used for the formation of nanocapsules.[81, 82, 206–208]
Another example for a bio-orthogonal reaction is olefin metathesis. As metathesis can be performed under mild conditions, tolerating water, oxygen, and a variety of functional groups,[209, 210] it can be easily conducted in aqueous emulsions under ambient conditions. Furthermore, the introduction of olefins into the monomers is a straightforward process and superior to typical azidation reactions as it proceeds in one step avoiding large amounts of activators. Several reports include ring-closing metathesis, acyclic diene metathesis and ring-opening metathesis polymerization that were conducted in emulsion to generate low molec-

ular weight materials, but also polymers and lattices.[209, 211–213] Breitenkamp et al. reported the formation of microcapsules by ring opening polymerization, whereas the reaction takes place in a single phase and the molecules are driven to the interface due to their amphiphilic character.[212]

Instead of relying on the above mentioned assembly process, we go one step further by designing the cross olefin metathesis in such a way that it can only proceed at the oil-water interface. The hydrophilic/hydrophobic character of the respective monomers limits the reaction to the droplets interface of stable miniemulsions. Defined nanocapsules are generated, whereas the potential payload, such as enzymes or peptides, is left unaffected during the reaction. The fast and convenient protocol was used to prepare potentially biodegradable and biocompatible nanocapsules consisting of a hydrophilic core and a shell based on polysaccharides (dextran) and PPEs. Additionally, we use a dye-functionalized organophosphate to underline the convenient introduction of functional groups via the pendant phosphoester. The possibility to create nanocapsules by cross cross-metathesis gives rise to a new quality of nanocapsules in biomedical applications as the hydrophobic catalyst remains in the continuous phase and is easily removed after the reaction. The process generating the shell by cross-metathesis of acrylated dextran (DexA) and an unsaturated organophosphate is schematically shown in Figure 4.1.

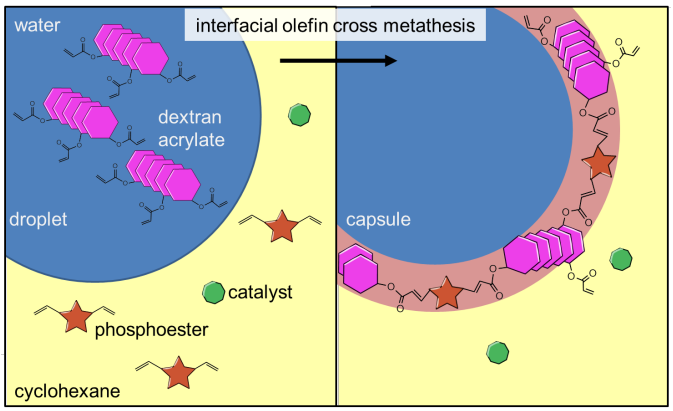

Figure 4.1: Schematic representation of the interfacial olefin cross metathesis at the water-oil interface of a nanodroplet in an inverse miniemulsion process for the formation of stable nanocapsules.

4.1.2 Dextran acrylation

The synthesis of acrylated dextran (DexA) was adapted from Gorodetskaya et al.[214]. The reaction is depicted schematically in in Figure 4.2. The successful modification was confirmed and quantified by ^{1}H NMR spectroscopy (Figure 4.3 a). The integrals of the acrylate peaks (6.5, 6.3, 6.1 ppm) were referenced to the integral of the anomeric proton in the dextran backbone (4.98 ppm) to assess the degree of substitution (DS). Depending on the reaction temperature after addition of acryloyl chloride a resulting DS of 0.13 and 0.55 was obtained for 5 and 10 °C, respectively. The reduced DS obtained by reaction at 5 °C was attributed to reduced solubility of dextran in cold DMF. In addition to NMR spectroscopy, the modification was also confirmed by IR spectroscopy of the freeze-dried dextran. In Figure 4.3 b the spectra of modified dextran were compared to unmodified dextran. All spectra were normalized to the -CH_2 stretch at 2980 cm^{-1}. The characteristic carbonyl stretching of the acrylate was located at 1723 cm^{-1}. This confirmed the successful modification of dextran and gave a qualitative measure for the DS. DexA with a DS of 0.55 was used for all further experiments.

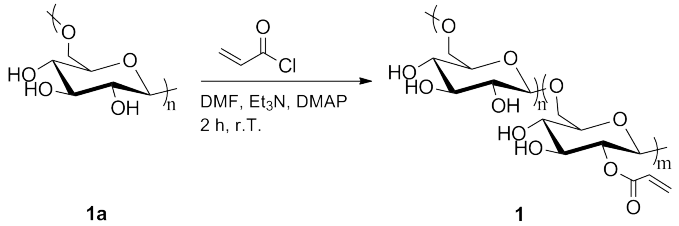

Figure 4.2: Reaction scheme of the modification of dextran (**1a**) with acryloyl chloride.

4.1.3 Nanocapsules obtained by olefin cross metathesis

4.1.3.1 Nanocapsule characterization

The nanocapsules were prepared in an inverse miniemulsion process. An aqueous DexA solution was emulsified in cyclohexane by ultrasonication. Subsequently, the hydrophobic unsaturated organophosphate was added to the emulsion followed by the addition of the oil-soluble catalyst. A Grubbs-Hoyveda 2nd generation catalyst was chosen based on its high tendency to selectively catalyze cross metathesis reactions between type 1 olefins and type 2 olefins,

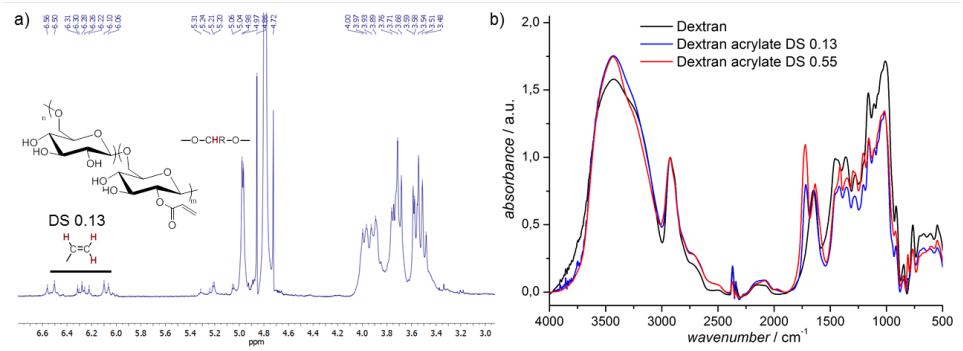

Figure 4.3: Characterization of acrylated dextran by a) ^{1}H NMR spectroscopy, b) infrared spectroscopy of unmodified (black) and modified dextran (blue, red).

i.e. acrylates.[215, 216] The interfacial reaction is depicted schematically in Figure 4.4. Mediated by the catalyst, the cross metathesis takes place at the interface only, crosslinks DexA with biodegradable phosphoesters, and forms a shell surrounding the water droplet. The reaction was allowed to proceed at 40 °C for 16 h. Within 30 min after addition of the catalyst a color change (from green to purple) suggested that the reaction was in progress. Subsequently, the nanocapsules were purified by repetitive centrifugation and washing to remove residual catalyst and monomer from the organic phase. The resulting colorless dispersion was stable for several weeks and the nanocapsules could easily be transferred to an aqueous environment by redispersion in 0.3 wt% SDS solution. This aqueous dispersion was also stable for several weeks. Excess surfactant can be removed by dialysis.

Dynamic light scattering (DLS) was used to determine the average hydrodynamic diameter (d_h) of the nanocapsules in cyclohexane (270 nm +/- 50 nm) which is representative for the droplet size obtained during the miniemulsion process. After redispersion in water the diameter was unchanged (280 nm +/- 50 nm), however a slight increase in size could be attributed to the SDS hydration layer surrounding the nanocapsules after transferring into water, as reported earlier.[35] As the size of the nanocapsules does not change significantly after transfer to an aqueous solution a high degree of crosslinking is assumed to hinder the swelling, which is common for dextran.[217]

To support the DLS results, SEM was used to image the nanocapsules. The image in Figure 4.5 shows nanocapsules with a morphology, which is characteristic for a thin capsule wall. The capsules were partially deflated *in vacuo* during the sample preparation process. The size of the displayed nanocapsules is ca. 300

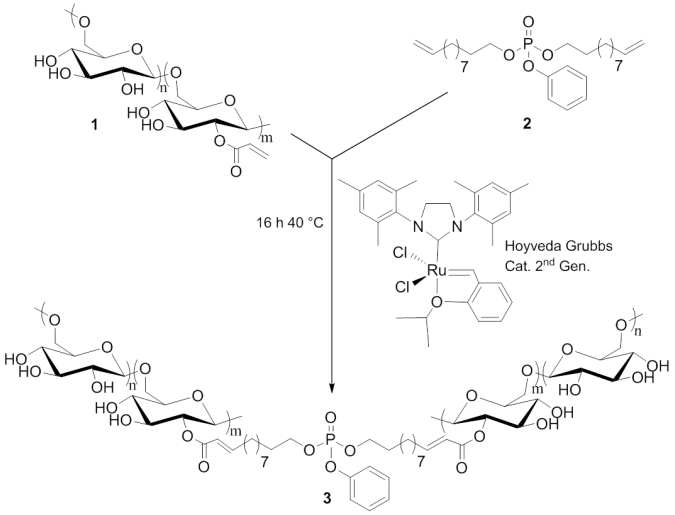

Figure 4.4: Schematic representation of the interfacial reaction between statistically modified dextran acrylate (**1**) and phenyl-di(undec-10-en-1-yl)phosphate (**2**) leading to a crosslinked polymer network (**3**).

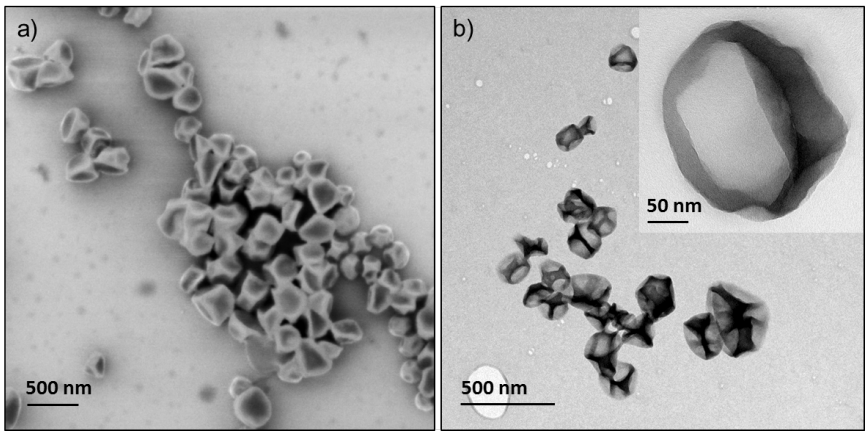

Figure 4.5: a) Scanning electron micrograph and b) transmission electron micrograph of the nanocapsules prepared in a minimulsion process by olefin cross metathesis.

nm, which resembles the results obtained by DLS. Additionally, transmission electron microscopy (TEM) analysis (Figure 4.5 b) confirms the hollow capsule morphology. It was previously mentioned that the catalyst changed its color already within 30 min after its addition. This could imply a rapid start of capsule formation. An additional experiment was performed to investigate when the capsule formation occurred. The capsule formation process was followed qualitatively by SEM imaging of the emulsion in two-hour intervals. Figure 4.6 shows images recorded 2, 4, 6 and 8 h after addition of the catalyst. The nanocapsule formation occured rapidly as indicated by the color change of the catalyst. The nanocapsules were formed within two hours after addition of the catalyst. However, for all further experiments the reaction time over night was maintained.

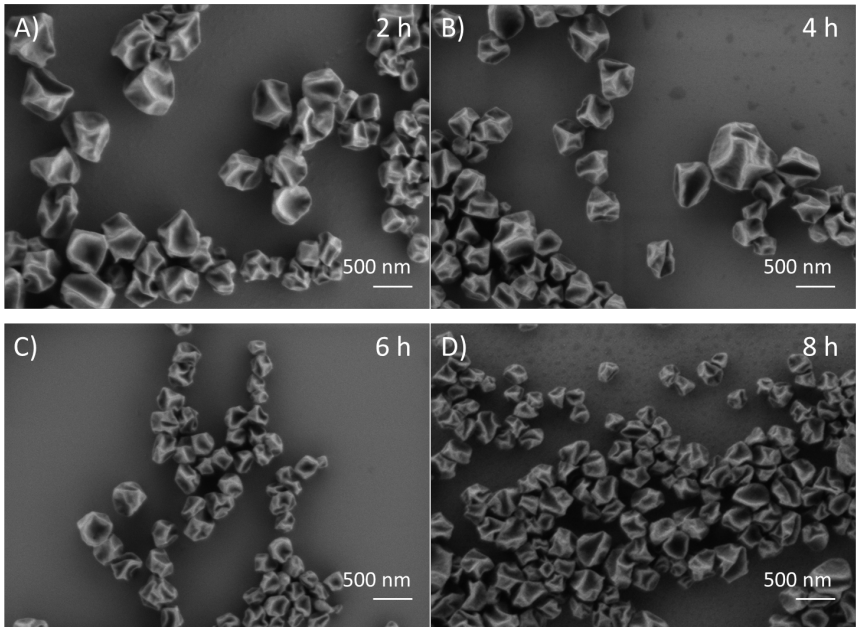

Figure 4.6: Scanning electron micrographs of the nanocapsules during the nanocapsule forming process. Samples have been withdrawn after 2, 4, 6 and 8 h during the reaction. The formed nanocapsules were already observed 2 h after addition of the catalyst.

Additionally, the elemental composition of the capsules was investigated with microanalysis (EDX) after overnight reaction. A peak at 2 keV gave evidence for the presence of the phosphate in the capsule structure. Simultaneously, no ruthenium (Ru) was found in the material by EDX, which indicates that the catalyst was efficiently removed after the reaction as it remained within the

organic phase. Using highly sensitive ICP-OES only trace amounts of Ru were detected in a low ppm regime with respect to the dry weight of the nanocapsules. For further removal of catalyst traces the use of chelating agents and subsequent dialysis is proposed.

4.1.3.2 Investigation of reaction mechanism

The polymer obtained after the capsule formation was insoluble in all common solvents, which indicated that DexA was crosslinked during the reaction, as expected. Accordingly, direct proof that metathesis reaction occurred can only be demonstrated via ^{13}C and ^{31}P solid state NMR. Prior to NMR analysis a soxhlet extraction with methanol and dichloromethane (good solvents for monomer and homopolymer respectively) was performed to purify the capsules from unbound material and residual monomer. No polymeric material was recovered in the organic solvent, which is in good agreement with literature and proves that homopolymerization of the used organophosphate did not occur under these conditions.[216]

The ^{31}P NMR spectrum unambiguously confirmed the incorporation of the phosphate into the cross-linked polymer (Figure 4.7 a) showing a resonance for the phosphoester at -7.7 ppm. The appearance of methylene resonances in the ^{13}C CP-MAS NMR spectrum further proved the incorporation of the organophosphate, while no aliphatic methylene resonances were detected in the reference sample (DexA, Figure 4.7 b). The limited resolution of ^{13}C CP-MAS NMR did not allow quantification of the saccharide to phosphate ratio in the polymer network. Further, the signals originating from the internal post-metathesis double bond and the benzyl group overlap with the signal of the terminal olefin around 128 ppm.

To exclude other reactions than the desired cross metathesis for the capsule formation additional experiments were performed. The miniemulsion process was conducted without the addition of the organophosphate or without catalyst. To confirm that DexA polymerization was not initiated by temperature, light exposure or the catalyst alone an NMR spectrum of the droplets was recorded. All freeze-dried samples of the control reactions were soluble in D_2O, in contrast to the cross-linked nanocapsules. The characteristic peaks for the acrylates (6.5 ppm, 6.25 ppm and 6.1 ppm) remained unchanged after the miniemulsion process (Figure 4.8). This is a direct proof that the nanocapsules were generated by olefin cross metathesis, which could take place only at the interface.

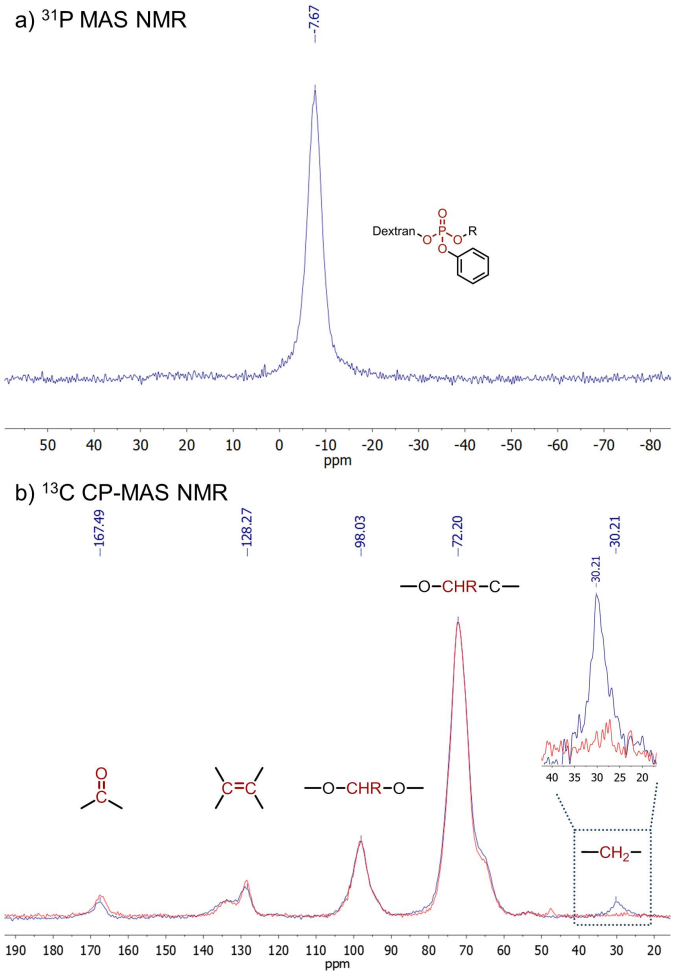

Figure 4.7: ^{31}P (a) and ^{13}C (b) solid state NMR spectra of the nanocapsules (note: (b) shows the superimposed ^{13}C NMR spectra of DexA (red) with the nanocapsules (blue), magnified area high-lighting the methylene resonances stemming from the metathesis reaction with the organophosphate).

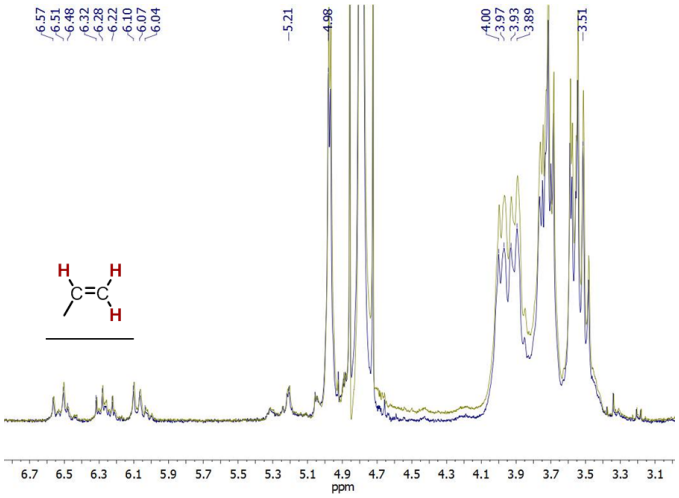

Figure 4.8: ^{1}H NMR spectra of acrylated dextran (**1**, blue) and the reaction product after miniemulsion process (grey) without organophosphate (**2**) and catalyst, demonstrating that the double bonds do not undergo UV/temperature induced polymerization.

4.1.3.3 Fluorescently labeled nanocapsules

In order to demonstrate the potential of the metathesis protocol for modification with functional groups or targeting moieties, a fluorescent marker was chosen as a model. Two possibilities for labeling were investigated: First, in addition to the organophosphate, an unsaturated BODIPY-derivative (λ_{max} = 540 nm, Figure 4.9) was added, which should act as a chain termination agent during the polycondensation and serve as a model for the modification from the "outside". Second, the versatility of the phosphate was exploited and the fluorescent label was attached via the third (pendant) ester into the polymer to act as a model for modification within the shell.[203]

The labeled nanocapsules were studied by various spectroscopic techniques including UV/VIS, fluorescence and fluorescence correlation spectroscopy (FCS). Using UV/VIS and fluorescence spectroscopy well-defined absorption (λ_{max} = 520 nm) and emission peaks (λ_{max} = 540 nm) were obtained at the expected wavelengths (Figure 4.9). This gives a first implication that the dye is bound to the capsules. Further, fluorescence correlation spectroscopy (FCS)[218] measurements were used to prove that the dyes are covalently bound to the nanocapsules. Figure 4.10 shows the fluorescence intensity autocorrelation curves (ACC) recorded of the nanocapsules dispersion. The initial ACC represents fluorescent

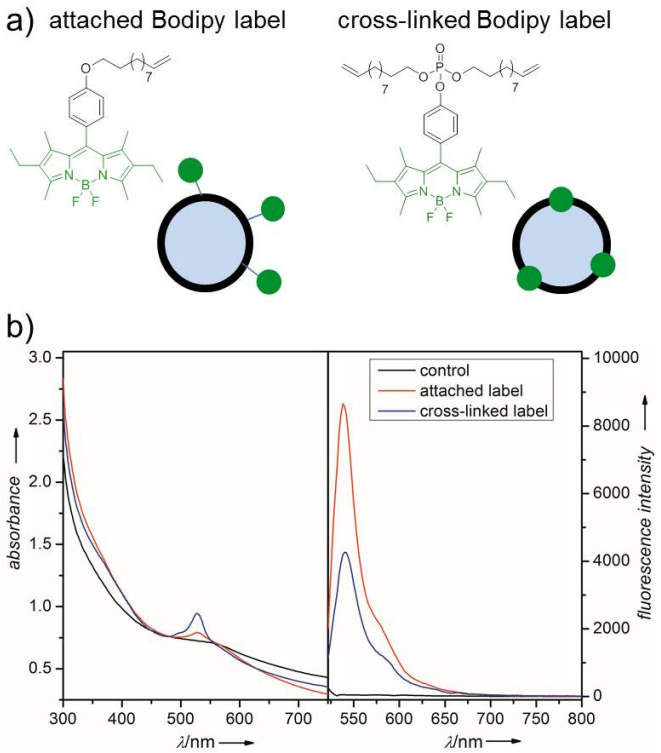

Figure 4.9: Labeling of nanocapsules with BODIPY dyes (λ_{Abs} = 520 nm, λ_{Em} = 540 nm) a) Structure of aliphatic BODIPY-label with terminal olefin and a BODIPY-diolefin phosphoester derivative[203] and the respective schematics of the dye with respect to the capsule wall b) Absorption and Fluorescence scan of the modified nanocapsules in aqueous solution after dialysis.

species with hydrodynamic diameter of ~230 nm (red circles); this value is very close to the hydrodynamic diameters obtained for the capsules by DLS and thus proves incorporation of the dye into the capsule shell.

4.1.3.4 Potential for use in biomedical applications

An important parameter for the biomedical application is the degradation of the nanocapsules for the release of a payload. A potential trigger for degradation can be a reduction in pH. Based on their chemical structure dextran as well as the phosphoester can be degraded by acidic hydrolysis.[219] FCS was previously used to confirm the fluorescent labeling of the nanocapsules. Additionally, it revealed that the nanocapsules were degraded under acidic conditions. A treatment of the nanocapsules with hydrochloric acid during the FCS measurement

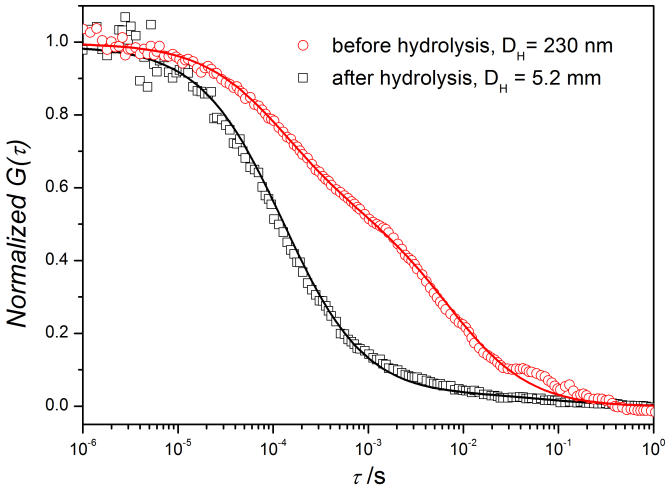

Figure 4.10: Normalized FCS ACC recorded for aqueous dispersions of the fluorescently functionalized nanocapsules before (red circles) and after (black squares) hydrolysis with hydrochloric acid. The solid lines represent the corresponding fits with eq. 5.1.

led to a shift of the corresponding autocorrelation curve (Figure 4.10, black squares) to shorter lag times. This indicated the appearance of smaller fluorescent species with hydrodynamic diameter of approximately 5 nm. This decrease of the hydrodynamic diameter was caused by the hydrolysis of the dextran, or the phosphoesters, thus proving the degradability of the nanocapsules. A further degradation experiment was performed, to ensure that not only the dye was split of the nanocapsules.

The nanocapsules were incubated for 1 h in aqueous solutions of pH 2, 4 and 6.5, for further investigation of the degradation process. This study gave insight in the speed of degradation and the required pH value. The change in hydrodynamic diameter was measured by DLS and the deviation of d_h was taken as measure for the degradation. Figure 4.11 shows the distribution of the nanocapsules hydrodynamic diameter measured after 1 h incubation (black: pH 6.5, red: pH 4, blue: pH 2). The hydrodynamic diameter of the nanocapsules incubated at pH 6.5 was in good agreement with previous DLS measurements as well as with the data obtained by FCS. This can be taken as a measure for the robustness of the measurements and the stability of the nanocapsules at neutral pH values. A deviation from the initial diameter was observed for the nanocapsules incubated at pH 4. The hydrodynamic diameter decreased within 1 h to about 100 nm, which is indicative for a partial degradation of the nanocapsules.

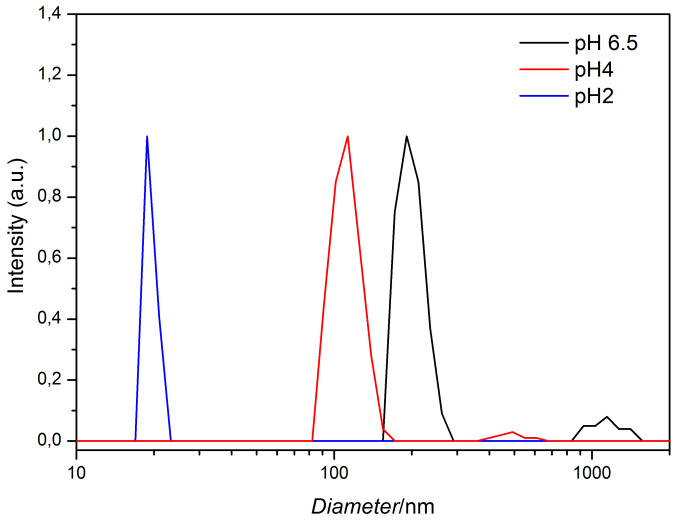

Figure 4.11: Visualization of pH-induced nanocapsule degradation monitored by dynamic light scattering. Starting at neutral pH (black) nearly all capsules have a mean diameter of ca. 200 nm. After incubation for 1 h at pH 4 (red), the apparent size is reduced to ca. 100 nm, while incubation for 1 h at pH 2 (blue) results in total fragmentation of the nanocontainers to 20 nm.

The partial degradation probably led to a collapse of the nanostructure. For the nanocapsules incubated at pH 2 the hydrodynamic diameter was decreased to about 20 nm. This implied that the crosslinks in the capsule wall were almost completely hydrolyzed. The degradation of the phosphoester under acidic pH was clearly observed. Additionally the speed of nanocapsule degradation was faster at lower pH. The beginning degradation of the nanocapsules at pH 4 would be suitable to deliver a cargo via oral ingestion to the digestive tract.

An additional prerequisite for the application of the nanocapsule in biomedical applications is the stability of the nanocapsules in the respective biological surrounding. Therefore, the behavior of the nanocapsules in phosphate buffered saline was studied. When dispersing SDS stabilized nanocapsules in PBS buffer a macroscopic aggregation of the nanocapsules was observed. This is an expected effect, as the stabilization capability of the ionic surfactant is counteracted by the high ionic strength of PBS. When the nanocapsules were stabilized instead with the steric surfactant Lutensol AT50 no macroscopic aggregation was observed. The hydrodynamic diameter was increased slightly, which could be caused by the bulkier structure of Lutensol AT50 compared to SDS.

4.1.4 Conclusion and Outlook

In conclusion, the first nanocapsules with an aqueous core prepared by olefin metathesis are presented. This convenient protocol allows mild bio-orthogonal crosslinking of degradable and biocompatible polymers at the oil-water interface. It combines two materials with high potential for future applications: Poly(phosphoester)s are a currently developing and highly versatile class of biocompatible and degradable polymers,[202, 203, 220, 221] which were combined via olefin metathesis with polysaccharides, here dextran, which are known for their biocompatibility.

Nanocapsules were synthesized by crosslinking acrylated dextran with unsaturated organophosphates in the presence of a metathesis catalyst. They featured defined shell morphology with an aqueous core. Olefin cross metathesis was confirmed as capsule forming reaction by several techniques, such as solid state NMR. Further, the nanocapsules' potential for *in situ* modification with dyes or other functional groups was demonstrated. The transfer to moderately acidic environments (pH 4) was able to trigger a partial degradation within one hour. This may be used for drug delivery in the respective environment. Enzymatic digestion of incorporated dextran should be studied as an additional trigger for degradation.

4.2 Polysaccharide based nanogels and hybrids [2]

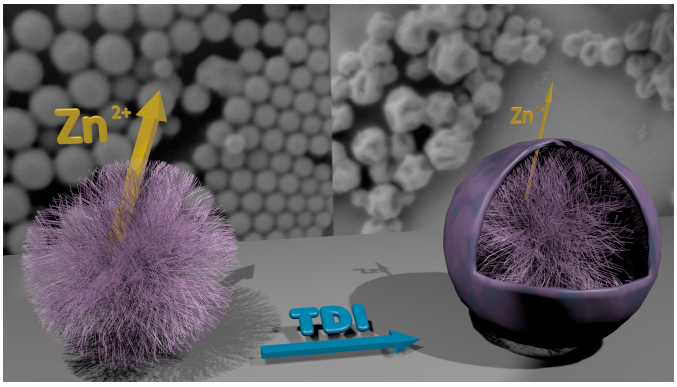

The growth in numbers and severity of hospital acquired infections has increased the need to target bacteria locally and specifically. Consequently, smart drug-delivery systems are being developed for local bactericidal action. The approach takes the concept of nanogels in drug delivery of small molecules to the next level by enclosing them in a shell. Versatile polysaccharide nanogels were loaded with zinc ions as an antibacterial agent in a miniemulsion process, in order to target methicillin resistant strains of *Staphylococcus aureus* (MRSA). The characterization of the nanogels with inductively coupled plasma optical emission spectroscopy (ICP-OES) revealed that zinc ions cannot be retained within without an additional 'shell' layer. The nanogels were surrounded by a dextran-polyurethane shell, which can retain substances by reduction of the water penetration. A delayed zinc release compared to the bare nanogels was confirmed by ICP-OES. Bacterial tests revealed an antibacterial effect of the shell enhanced nanogels against *S. aureus*. The studied nanogel system shows potential in locally addressing bacterial infections. The platform is extremely versatile and can be tailored to application as dextran and $Zn(NO_3)_2$ can be replaced by other polysaccharides (e.g. hyaluronic acid) and antibacterial agents, respectively.

[2] This section is based on the publication "Advanced dextran based nanogels for fighting *Staphylococcus aureus* infection by sustained zinc release" by Kerstin Malzahn, William D. Jamieson, Melanie Dröge, Volker Mailänder, A.Toby A. Jenkins, Clemens K. Weiss and Katharina Landfester published in 2014 in the Journal of Materials Chemistry B, volume 2 on pages 2175-2183.[222] Reproduced by permission of The Royal Society of Chemistry.

4.2.1 Motivation

Hospital acquired infections by multi-drug-resistant bacteria have recently attracted a lot of attention. These infections are difficult to cure due to the resistance to common antibiotics and because infections are often noticed too late when a biofilm already has started to form. Biofilm formation is the second step in the biphasic bacterial attachment process.[223, 224] After the reversible attachment of bacteria within the first few hours the attachment becomes irreversible and a biofilm is formed. A biofilm typically reduces susceptibility to drugs through action as a physical and chemical barrier to antibiotic diffusion, and as a pool of genetic and phenotypic diversity allowing resistance to manifest rapidly.[225] Efficient treatment of bacterial infections should thus be local and immediate.

Smart drug-delivery systems, which can be applied locally (e.g. in wound dressings) and open up specifically in presence of bacteria to release their antibacterial cargo have been developed to address the problem of bacterial attachment and colonization. Recent progress in this field was made by Baier et al.[35] Delivered antibacterial agents at the wound site are, in principle, an alternative to the use of systemic antibiotics when treating wound infection.[226, 227] Metal ions and metal oxides[228] have found applications in advanced antibacterial systems.[229, 230] To encapsulate and release metal salts or oxides, a hydrophilic environment like a hydrogel[143, 231] or a capsule with an aqueous core is more suitable than hydrophobic environments, which require the use of hydrophobic organo-metallic compounds.[232, 233] Additionally, the release into aqueous media requires accessibility by water.

In drug-delivery applications nanogels are considered superior to common bulk hydrogels and were loaded with a variety of cargos.[234, 235] The confinement enables a local, specific release instead of a broad diffuse release. In contrast to bulk hydrogels, nanogels can be modified to target specific parts of the body leading to a cargo release at the desired location.[236] In addition, phospholipid vesicles contained within a hydrogel matrix have been demonstrated as potential antimicrobial delivery vehicles.[237]

Potential opening mechanisms for the drug delivery systems include swelling of hydrogels,[238, 239] environmental pH changes,[240] membrane lytic action of secretion toxins[148, 241, 242] from the infecting bacteria which open phospholipid vesicles or polymer degradation by extracellular enzymes.[73] Accordingly, biodegradable/-compatible materials like polysaccharides seem very promising

for such drug-delivery systems at the nanoscale as they can often be degraded specifically by bacterial enzymes.[8, 243] This is supported by the number of polysaccharide capsules, which are often based on diisocyanate chemistry for the shell forming reaction.[74, 75, 179] The large variety of polysaccharides allows for interchange and fitting to the desired application. Furthermore, the resulting degradation products (saccharides) are typically non-toxic and can be easily excreted by the human body. The dense shell of the nanocapsules leads to good retention of small molecules whilst allowing for full payload release upon opening.

The combination of the benefits of capsule and nanogels in a hybrid gel capsule was realized in a one-pot synthesis utilizing a functionalized dextran for the crosslinking as well as the shell formation. In these hybrids the release can be controlled by the shell density and the swelling of the gel compared to common core-shell hydrogels which only rely on the latter.[244, 245] In this study, the nanogel forming procedure of Klinger et al.[217] was modified to carry zinc ions as an antimicrobial agent. Kobitskaya et al.[246] stated a complexation of zinc ions by polyacrylamide in polymer latexes, which is in agreement with the work of Gromov et al.,[247] and should allow retention of zinc ions in the nanogels. The zinc release from the nanogels was studied and the hydrogels were found to have a release pattern which is too rapid for biomedical applications. Accordingly, the nanogels were enclosed in a shell, thus altering the release pattern and reducing the zinc release rate. Bacterial tests with a methicillin resistant strain of *S. aureus* were performed to study the antimicrobial effect of zinc ion loaded gel capsule hybrids on bacterial growth. Further the effect of the gel capsule hybrids on cell viability was studied to demonstrate applicability in a wound environment.

4.2.2 Nanogel

4.2.2.1 Hydrogel characterization

As described above, the aim of the project was to develop a nanogel system based on polysaccharides, such as dextran. The nanogels shall incorporate zinc nitrate as active antimicrobial agent, which is to be released upon exposure to bacteria. Accordingly, nanogels had to be prepared and the loading and release of zinc from the nanogels had to be studied. Dextran methacrylate (DexMa) served as enzyme degradable crosslinker[217] for polyacrylamide (PAAm) hy-

drogels. The molecular weight of dextran (M_w(Dex) 6000 - 70000) and its crosslinking ability (depending on modification with methacrylate units as characterized by the degree of substitution (DS 0.05-0.2)) was varied. In order to prolong the release of Zn^{2+} for sustained antibacterial action, a shell was introduced to enclose the nanogel and control the zinc elution. The shell was generated by crosslinking the pendant groups with toluene diisocyanate.

The zinc loaded hydrogels were obtained from polymerization of acrylamide (AAm) and crosslinking with DexMa in inverse miniemulsion. The nanogels were characterized with SEM as well as DLS. They can be redispersed in H_2O without the addition of surfactant due to the stabilizing effect of dangling dextran chains.[248] When dispersing the nanogels in water, swelling is expected, the extent of which is inversely proportional to the degree of crosslinking of the nanogels. In Table 4.1 results from DLS measurements in cyclohexane and H_2O are shown exemplarily for the dextran methacrylate with a molecular weight of 6000 g·mol^{-1}. First of all, it can be noted that all nanogels show a similar size in cyclohexane (around 205 nm), which was expected as the same sonication conditions and surfactant concentrations have been used in the miniemulsion process. This is in good agreement with the theory of miniemulsions which states that ideally the droplets, which are created during sonication, turn into single particles without coalescence.[249]

Table 4.1: Results of DLS measurements in cyclohexane and water of Zn^{2+} loaded nanogels prepared from dextran methacrylate (M_w 6000 Da) with various degrees of substitution.

DS	d_h(CH) / nm	d_h(H_2O) / nm
0.05	210 +/- 90	790 +/-120
0.1	205 +/- 65	610 +/- 90
0.2	205 +/- 55	390 +/- 65

Additionally, the size of the nanogels was assessed after redispersion in H_2O to investigate the full extent of swelling of the nanogels. It was expected that the swelling capability of the nanogels decreases when the number of crosslinks increases. An increased DS (of dextran with Ma) enables an increased degree of crosslinking. While nanogels with low crosslinking density (DS = 0.05) exhibit nearly a 4-fold increase of their initial hydrodynamic diameter an increased

crosslinking density (DS = 0.2) only leads to a doubled hydrodynamic diameter of 390 nm. A linear relation between degree of crosslinking and swelling of the nanogels was found for the various M_w(Dex), which were utilized. The micrographs in Figure 4.12 give an overview of the nanogels, which were prepared by variation of M_w(Dex) and DS and dropcast the cyclohexane dispersion onto a silicon wafer. All structures show a spherical morphology and a diameter ranging between 100 and 250 nm. The size estimated from the SEM evaluation of the nanogels is slightly smaller than the values measured by dynamic light scattering from cyclohexane. While the nanogels are completely dried in SEM conditions in cyclohexane dispersion the gels are swollen to some extend limited by the droplet size of the miniemulsion.

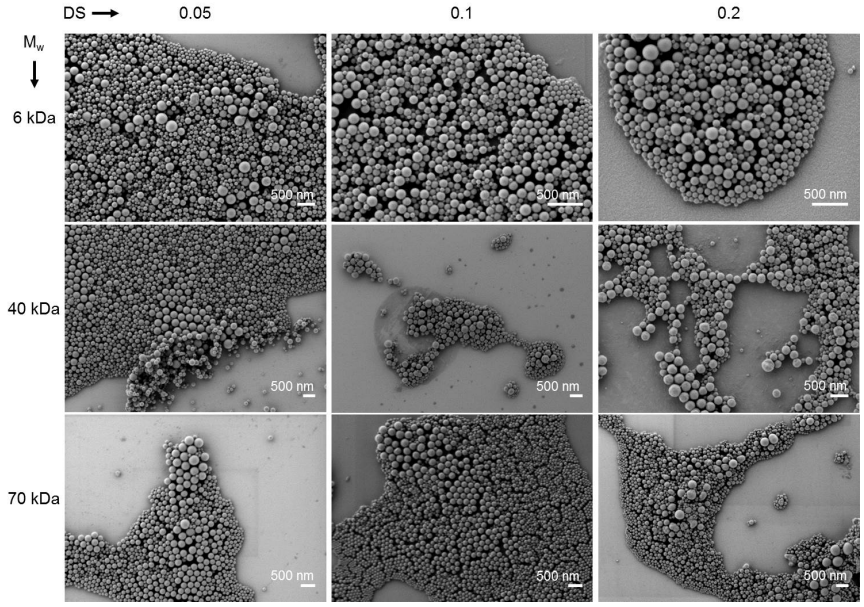

Figure 4.12: Scanning electron micrographs showing zinc loaded dextran-polyacrylamide nanogels dried from cyclohexane.

4.2.2.2 Control of cargo release

In order to evaluate the zinc content of the nanogels, two important parameters had to be studied, namely the zinc loading of the nanogels and the zinc leakage/release from the nanogels over time. In Figure 5.3a) the sampling steps for the respective processes from loading to release are shown. All steps were

investigated by ICP-OES, which is a sensitive technique for elemental analysis in solutions or dispersions.[189]

A theoretical Zn^{2+} content of 2.4 wt% was calculated from the initial amount of zinc nitrate used in the preparation of the nanogels. The total amount of Zn^{2+} in the gels was assessed to determine the encapsulation efficiency. To be able to assess the zinc content in the nanogels while they were dispersed in cyclohexane the samples were freeze dried and degraded by nitric acid prior to ICP-OES measurements. All combinations of M_w(Dex) and DS were assessed. Figure 4.13 shows the zinc content as wt% of dry gel in the respective sample *vs.* DS for the types of dextran. It can be seen that the zinc content in all samples ranges between 2 and 2.5 wt% with respect to the solid content of the aqueous phase. The values, which were calculated from the zinc loading experiment, support the assumption of nearly quantitative incorporation of zinc nitrate, which was drawn from the observation that no precipitate appeared during preparation.

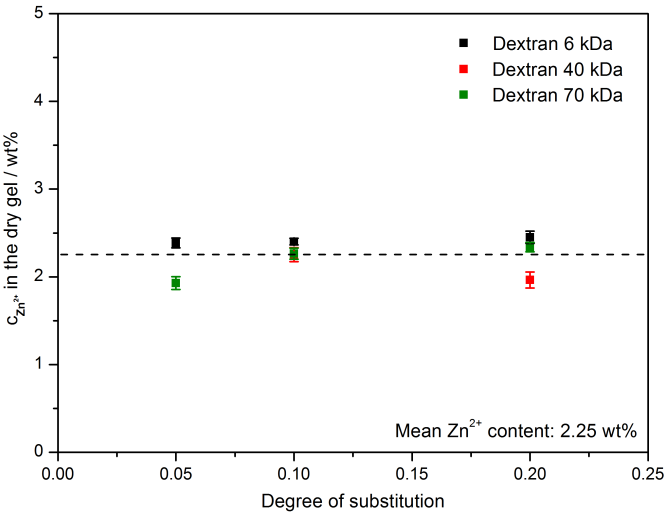

Figure 4.13: Weight percent of zinc with respect to the dry gel is plotted vs. the degree of substitution of dextran (M_w: 6, 40 and 70 kDa). The average zinc loading is noted in the graph.

Additionally, it can be concluded that the incorporation of zinc nitrate is independent of the type of dextran (molecular weight, degree of substitution) and the resulting crosslinking density. This is in good agreement with the principles of miniemulsion[205] and the potential complexation of Zn^{2+} by PAAm.[250, 251] Retention and sustained release of Zn^{2+} in the gels is highly desired in order to

allow redispersion in aqueous phase and long shelf-life time of the gels in aqueous environment. However, the swelling of the nanogels in water suggested that water can penetrate the nanogels, accordingly a leaching can only be avoided by complexation of encapsulated ions. The relative Zn^{2+} content in the nanogels after redispersion was determined by first measuring the dispersion (Figure 4.14, black bars) and then the supernatant subsequent to centrifugation (red bars). Most of the Zn^{2+}, which was found in the dispersion, was already released from the nanogels into the supernatant. This was confirmed by a low Zn^{2+} concentration (blue bars) released from a nanogel pellet within 24 h.

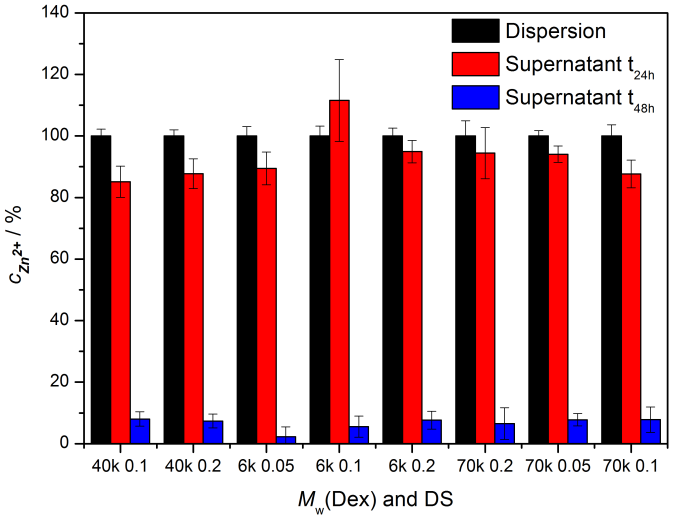

Figure 4.14: Zn^{2+} release from the nanogels with respect to the combination of M_w(Dex) and DS. Zn^{2+} content in the dispersion and in the respective supernatant obtained after centrifugation at 4000 rpm is displayed in black and red, respectively. The blue bars represent the zinc released from the gels after additional 24 h incubation in fresh water.

This implied that during the redispersion process the majority of zinc was already released and only small quantities were retained within the gel. It can be concluded that complexation by PAAm did not provide sufficient retention of Zn^{2+}, which was leached out by a diffusive process during swelling of the hydrogels and water penetration. To guarantee the desired sustained release, the nanogels were modified with a shell, thus creating a unique gel-shell hybrid system. The shell was expected to enhance the Zn^{2+} retention by limiting the water penetration and hindering the swelling of the nanogel.

4.2.3 Core shell hybrid capsules with gel core

4.2.3.1 Hybrid characterzation

The results presented in the previous section revealed that the nanogels had to be modified in order to reduce the Zn^{2+} release rate from the gels. A new gel-shell hybrid system was established by crosslinking the readily available pendant functional groups of the nanogel to form an enclosing shell. The hydroxyl groups and amide groups of dextran and PAAm, respectively were crosslinked with TDI. The successful formation of a shell structure was verified and the effect on the release properties was studied. Following the preparation and purification process, the gel-shell hybrid dispersions in cyclohexane were stable for several weeks. A sterical self-stabilization through the dangling dextran or PAAm chains was reported for the nanogels. For the dispersion of the hybrids a surfactant like SDS (0.3 wt%) was required to avoid aggregation and precipitation. The impact of the shell on the swelling behavior of the nanostructures was studied by DLS measurements in cyclohexane and water after 2,4-toluene diisocyanate (TDI) addition. In cyclohexane, the gel-shell hybrids showed a slightly larger diameter (250 nm) than the pure gels (Table 4.1, 205 nm). The d_h of the gel-shell hybrids was increased to 355 nm after dispersion in water. The increased d_h was caused by the formation of a hydration layer of the surfactant, and a swelling of the nanogel, which is limited by the surrounding shell. The slight swelling further indicated that a certain penetration of the hybrid structure by water was still possible.

The micrographs in Figure 4.15 a) and b) depict the nanogels/hybrids before and after addition of TDI, respectively. The nanogels appear particle-like in SEM imaging, which differed significantly from the results observed after shell formation. The small dried spheres (100 nm) reflect what was observed in Figure 3, while the structures in Figure 4.15 b) rather resemble partially deflated capsules. The observed crumpled morphology is likely to be caused by the drying process and the vacuum conditions during SEM measurement. The inner gel network hinders the shell from complete deflation or rupture as reported by Baier et al.[35]

Figure 4.15 c) and d) show the images of the respective nanostructures as obtained by transmission electron microscopy. The nanogels appear homogeneous throughout the object (Figure 6C magnification), which is expected from homogeneous polymeric particles. After the shell was formed, the nanostructures

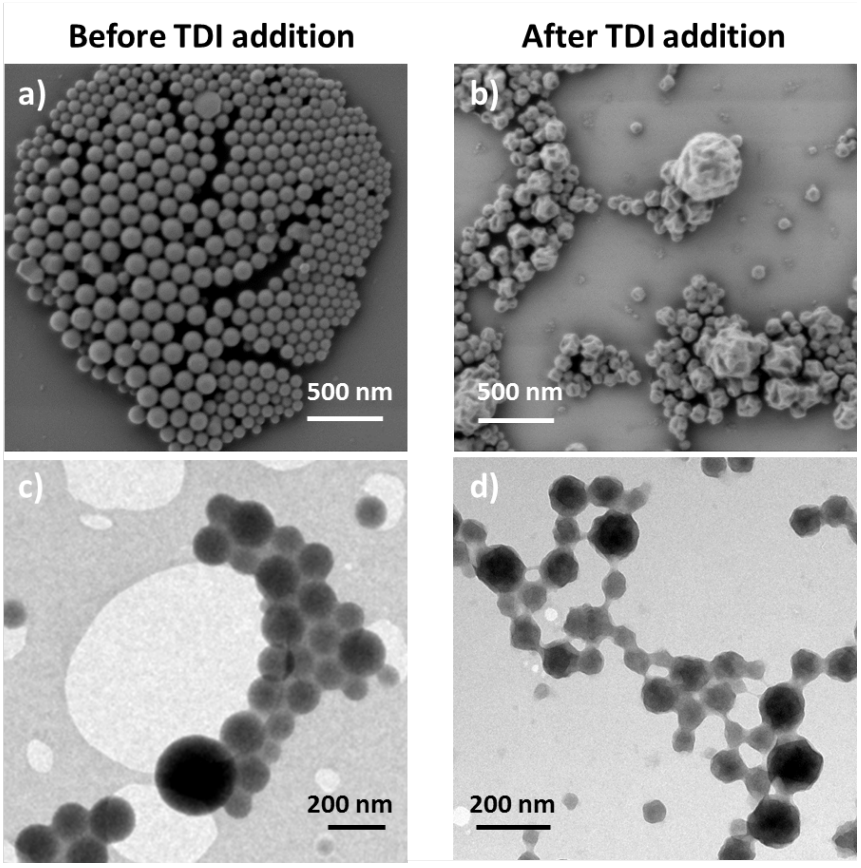

Figure 4.15: Micrographs of dried DexMa-PAAm nanogels a) and c) before TDI addition show spherical morphology, b) and d) Nanogels after shell formation with TDI, nanogels show crumpled morphology caused by water evaporation during drying process in SEM and TEM, respectively.

showed a dark core, which was surrounded by a brighter irregular rim. The dark core corresponded to the collapsed hydrogel inside the structure. The bright rim was attributed to the shell. Additionally, the crumpled morphology observed in SEM, indicating a partial deflation, seemed to be represented by a slightly inhomogeneous contrast of the particles. Bearing in mind that the nanogel/shell hybrids have been prepared in subsequent steps through a miniemulsion process the observations fit well with the expectations. During the miniemulsion process water droplets were formed in the continuous phase and were filled out completely with the swollen nanogel network after polymerization. The dangling chains of the gel can participate in the shell forming reaction, thus being hindered from collapsing during the drying process.

4.2.3.2 Control of cargo release from core-shell hybrids

The nanogels alone were found not to provide a sufficient Zn^{2+} retention ability and are therefore not suitable for application as sustained release system for antimicrobial applications. The nanogels were modified with a shell in order to prevent the leaching of zinc. To investigate the impact of the shell the Zn^{2+} release was measured by ICP-OES. The ratio of TDI to free hydroxyl/amide groups was varied to study the effect of an enhanced crosslinking in the shell. The experiments were conducted as described above for the nanogels. The results are plotted in Figure 4.16 as relative amount of zinc versus the ratio of TDI to hydroxyl groups of dextran. The black bars indicate the zinc content in the dispersion after the redispersion process into aqueous solution and are regarded as 100%. An aliquot of the dispersion was centrifuged and the Zn^{2+} content in the supernatant is shown as red bars relative to the content in the full dispersion. The pellet obtained by centrifugation was resuspended in MilliQ water and the process was repeated twice in 24 h intervals after start of the redispersion (blue and green bars).

The zinc release into the supernatant during the redispersion process as well as in the following 48 h was found to range between 5 and 15% of the total zinc content. This represents a 9-fold reduction in zinc release compared to the bare nanogels without surrounding shell. The deviation in the zinc release over the three days is thought be caused by deviations in sample handling as implied by the similar release pattern of both TDI to OH ratios. The similar release pattern of both TDI to OH/amide ratios implies that both samples have a comparable

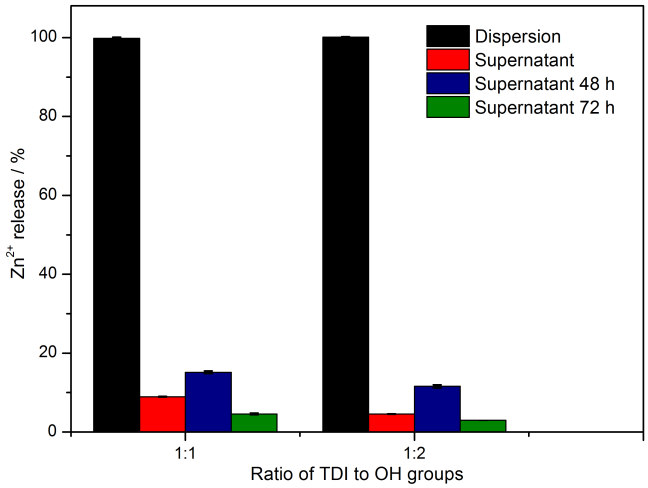

Figure 4.16: Relative zinc release from DexMa-PAAm nanogels with TDI shell is plotted with respect to the amount of TDI used for the shell formation (expressed as the ratio of TDI units to the amount of OH groups available from the dextran). Zn^{2+} content in the supernatant after redispersion (24 h) and in the following two days is displayed relative to the redispersed samples ('Dispersion') which is set to 100% zinc content.

shell structure, which is in good agreement with the literature where no impact of TDI amount on shell thickness was observed.[5]

In conclusion, the nanogel-shell hybrids seem to exhibit a slow and rather steady release which could be described as continuous leakage rather than a boost release as seen for the nanogels. Hereby, it was shown that the hybrid structures allow the encapsulation of small drugs, which makes them superior to common nanogels.

4.2.3.3 Antibacterial efficacy of core-shell hybrids

Having shown enhanced zinc retention in the nanogels after addition of a surrounding shell the antibacterial activity of the system had to be tested on bacteria. Therefore the growth of clinically relevant strains of *S. aureus* (MRSA ST239 μ2, TW20) was monitored as change in optical density (600 nm) for 18 h (Figure 4.17 a) ST239 μ2, b) TW20). The change in absorbance of the positive control (bacteria in TSB medium, black) shows the typical growth pattern consisting of lag-phase, exponential growth and plateau phase. Gel-shell hybrid particles without $Zn(NO_3)_2$ loading were tested (red) and no significant change in absorbance was seen for both bacterial strains in comparison to the positive

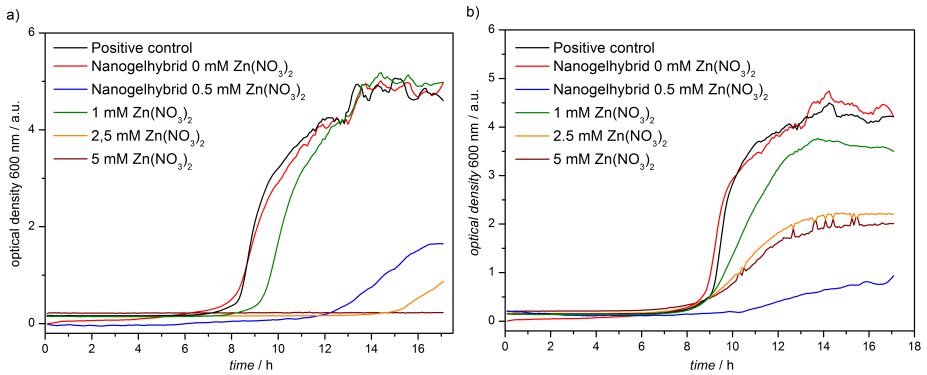

Figure 4.17: Bacterial growth of MRSA ST239 μ2 a) and MRSA TW20 b) in presence of zinc nitrate and dextran nanogels with and without zinc nitrate loading.

control. No growth inhibition of the bacteria caused by gel-shell hybrid particles was observed, thus demonstrating that the carrier material itself has no innate bactericidal activity. To better classify the impact of the zinc loaded gel-shell hybrids bacteria were inoculated with $Zn(NO_3)_2$ containing medium (1, 2.5, 5 mM). Low concentrations (1 mM) of zinc nitrate (green) caused a delay of ST239 μ2 growth indicated by the shifted growth curve (Figure 4.17 a). The TW20 strain did not only show a delayed growth but also a lower maximum absorbance (Figure 4.17 b). Higher concentrations of Zn^{2+} (2.5 mM) further delayed bacterial growth of both strains and the maximum absorbance of the positive control was not reached. Thus the growth of bacteria is limited, while for concentrations of 5 mM (dark blue) no change in absorbance is recorded for ST239 μ2. Accordingly, the concentration where bacterial growth has been completely inhibited (minimum inhibitory concentration, MIC100), is estimated to be about 5 mM $Zn(NO_3)_2$. The value is much higher than reported in literature for zinc acetate (*S. aureus* MSSA 476, 0.7 mM).[252] This deviation may be due to the utilization of an assumedly more resistant strain of *S. aureus*. This is further supported by the fact that for the strain TW20 no complete inhibition of growth could be observed within the concentration range tested, thus showing an even lower susceptibility to zinc than ST239 μ2.

Hybrid gel-shell samples with resulting 0.5 mM Zn^{2+} concentration were used during the bacterial test. This corresponds to 1 mg·L^{-1} dried nanogels. The change of absorbance over time (light blue) shows a strong shift of the growth curve for both bacterial strains, which indicates a strong delay of bacterial

growth. Furthermore, a plateau is reached within 18 h at a comparatively low absorbance, which implies that the bacterial growth is retarded. Hence, the MIC100 for the gel-shell-hybrids seems to be slightly higher than the 0.5 mM Zn^{2+}. Comparing the growth curves of $Zn(NO_3)_2$ and the gel-shell hybrids, the latter appear to be more effective than expected compared with the same concentration of non-encapsulated Zn^{2+}. One explanation of this effect is that the encapsulation of $Zn(NO_3)_2$ and subsequent release leads to a high local concentration of Zn^{2+} in the vicinity of the bacteria. While for chitosan nanoparticles an interaction with *S. aureus* bacteria was observed due to the positive zeta potential,[253] no such effect is expected for dextran, a neutral polysaccharide. The interaction of bacteria and polysaccharides in biofilms is not understood,[9] and an alteration of bacterial metabolism in presence of the presented dextran based hybrid nanogels shell structures cannot be excluded. Nevertheless, the reason for the enhanced antibacterial activity remains unresolved.

4.2.3.4 Tolerance of hybrid capsules by model cell lines

A strongly inhibiting effect of the zinc loaded nanogel shell hybrids on the growth of *S. aureus* was observed. To elucidate the potential for application of such nanogels in wound environments their toxicity has been studied with human derived keratinocytes (HaCaT cells) as a cell line model for human skin. Possible cytotoxic effects of the pure nanogel material on the cell viability have been assessed by incubating the cells with zinc-free nanogel-shell hybrids in various concentrations. Subsequently, the cell viability was monitored in the presence of zinc loaded nanogel shell hybrids. To be able to relate the outcome to the results of the bacterial testing similar nanogel contents were studied. Figure 4.18 shows the relative viability of the cells vs. the concentration of nanogel shell hybrids. The viability of cells which have been grown in medium only was set to 100%. The black line shows the viability for increasing concentrations of zinc free nanogels. Up to the concentration used in bacterial testing (1000 $\mu g \cdot mL^{-1}$, dashed line) the viability remains close to 100%. When further doubling the concentration (2000 $\mu g \cdot mL^{-1}$) the viability of the cells starts to be affected. The LD_{50} is approximated to be around 3000 $\mu g \cdot mL^{-1}$. The effect of the nanogel shell hybrids on the cell viability at high nanocapsules could be attributed to several reasons. These could include e.g. effect of residual surfactant.
The viability of the cells in presence of zinc loaded nanogels was reduced to 75% at the concentration used in bacterial tests (1000 $\mu g \cdot mL^{-1}$). When increasing

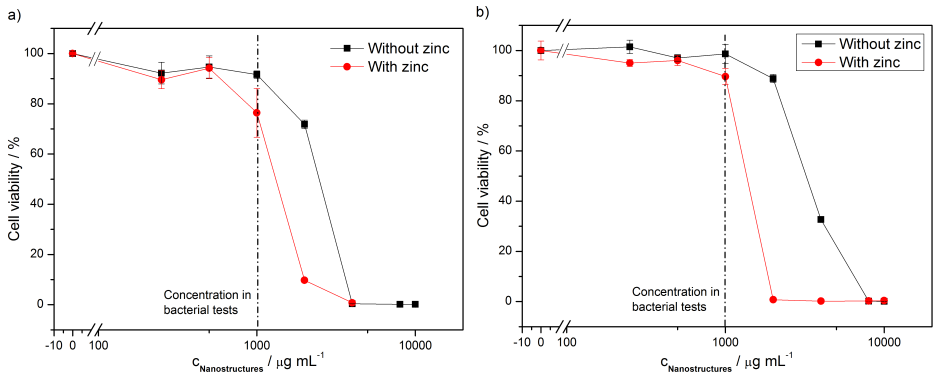

Figure 4.18: Cell viability assay for HaCaT cells. Relative cell viability with respect to untreated cells is plotted against increasing nanogel concentrations. Cell viability in presence of zinc free (black) and zinc loaded (red) nanogels.

the nanogel concentration to 2000 µg·mL^{-1} the viability drops to about 10%. This is probably a cumulative effect of zinc and nanogel concentration (cells with zinc free gels already showed reduced viability). Therefore the LD_{50} is between 1000-2000 µg·mL^{-1}. Additionally, the effect of the nanostructures on HeLa cells was investigated and found to be slightly lower than the effect on HaCaT cells. For 1000 µg·mL^{-1} pure nanogels and zinc loaded nanogels nearly 100% and 90% viability were observed, respectively. A potential application would include the immobilization of the nanogel shell hybrids and thus enhance the viability of the cells, as internalization of the nanogels can thus be avoided.

4.2.4 Conclusion and Outlook

Dextran-crosslinked polyacrylamide nanogels were transferred successfully into a nanocarrier system. Zinc nitrate was incorporated into the nanogels to serve as an antimicrobial agent. When performing zinc release studies deficient zinc retention of the nanogels was observed. Polyacrylamide did not provide sufficient complexation of the zinc ions. The release system was modified to retain the Zn^{2+} over a longer period and be better suited for biomedical application. For this purpose a gel-shell hybrid nanostructure was prepared in consecutive steps based on radical polymerization and polycondensation in inverse miniemulsion. The resulting nanostructures showed an altered morphology as well as a different release pattern compared to the gels. The zinc release was changed from a fast boost release into reduced, but continuous release from the gels, which is more beneficial in biomedical applications.

Polysaccharides are a very versatile group of polymers, accordingly, the nanocarrier concept, here presented with dextran as a model compound is transferable to other polysaccharides to fit the desired application. As a next step the preparation of gels based on methacrylated hyaluronic acid as cross linker is suggested. Several *S. aureus* strains are hyaluronidase positive and could degrade the nanocapsules enzymatically. In order to verify the antimicrobial activity of the nanocarriers, bacterial experiments were conducted with a relevant methicillin resistant strain of *S. aureus*. Growth was delayed and reduced in presence of Zn^{2+} loaded gel-shell hybrids. To further enhance the antibacterial activity Zn^{2+} can easily be replaced by other metals, which are known for an increased antibacterial effect (e.g. silver).
The nanogel shell hybrids show no relevant cytotoxicity on HaCaT cells in the concentration regime required for bacterial inhibition. At the same concentration the zinc loaded nanogel shell hybrids exhibit a slight effect on cell viability, only. To summarize, a drug release system with high potential for application in wound environments was developed, combining strong inhibition of bacterial growth with high biocompatibility.

4.3 Saccharide filled nanocapsules[3]

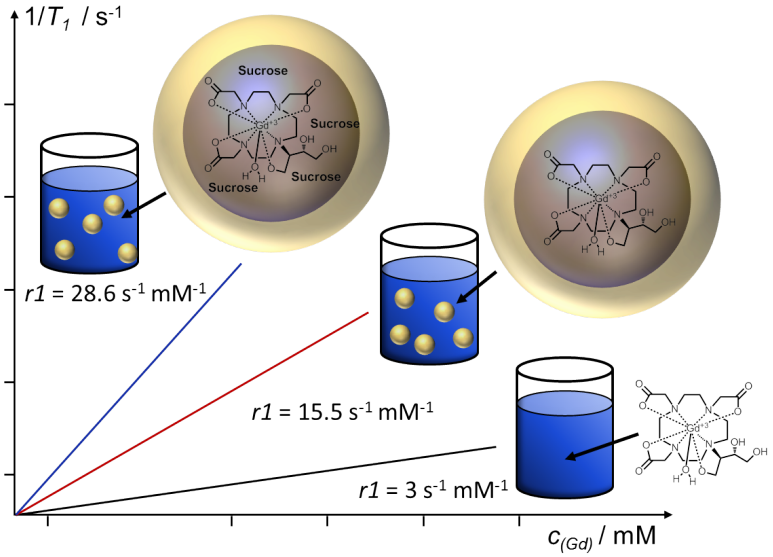

Contrast agents improve the imaging of internal body structures by advanced imaging techniques like MRI or computed tomography. Scientists try to enhance the sensitivity of contrast agents by various techniques. Herein, we present the incorporation the contrast agent Gadovist® in polyurea nanocapsules. In a systematic approach, the influence of monomer type, monomer ratio, and monomer amount on the relaxivity were investigated. Sucrose, dextran, and polyacrylic acid were co-encapsulated to further reduce the mobility of the contrast agent.

4.3.1 Motivation

Magnetic resonance imaging (MRI) is a non-invasive imaging technique, which has evolved since 1952.[254] It can be used to differentiate between soft tissues at a high (submillimeter) spatial resolution.[175, 255] Therefore, it is widely used in clinical diagnosis of cardiovascular diseases as well as for the localization of tumors.[256, 257] Gd-complexes with a very high stability are used as T_1 contrast agents. The ability of a contrast agent to increase the relaxation rate is referred to as relaxivity r_1. The relaxivity is the chelate concentration dependent change of the relaxation rate. Macrocyclic contrast agents have an exceptional inertness, high complex stability and can be used safely at physiological pH values.[59, 258–261] The complex gadobutrol (Gd-DO3A-butrol, Gadovist®)

[3] This section is in preparation for publication. The project was carried out in close cooperation with Sandro Ebert, who was responsible for T_1 measurements and interpretation.

is approved by the Food and Drug Administration (FDA) and of clinical importance. Commonly MRT scanners with a field strength of 1.5 T are used in clinical practice. The rotational diffusion of the complex has the largest influence on the relaxation rate at this field strength.[171, 175] The polymers used for the attachment of contrast agents include linear or dendritic molecules.[161–166] The resulting multimeric structures were co-functionalized for targeting of blood clot and application in angiography.[167, 168] Perfluorocarbon nanoparticles were decorated with gadolinium complexes by covalent attachment and yielded a substantial increase in relaxivity (17.9 $s^{-1}{\cdot}mM^{-1}$, 1.5 T).[170–172] Cheng et al. combined the immobilization of Gd(III)complexes on dendrimers with the encapsulation in water permeable polymersomes to increase the relaxivity (7.5 $s^{-1}{\cdot}mM^{-1}$, 1.41 T).[174] Even though they could encapsulate larger numbers of gadolinium units, they had to introduce pores into the capsule wall to enable water exchange and enhance the relaxivity.
The aim of this work was to elucidate the key parameters in the preparation of high relaxivity nanocapsules. For a high relaxivity and high signal intensity, the reliable encapsulation of the contrast agent is a requirement. The retention of cargo within nanocapsules is often proven by the encapsulation of fluorescent dyes at a low concentration and the monitoring of release by fluorescence spectroscopy.[69, 73] The behavior of the fluorescent dyes might not resemble the behavior of cargo molecules, which have been encapsulated at a higher concentration. In this study, the encapsulation efficiency and gadobutrol retention were monitored by ICP-OES. The co-encapsulation of poly(acrylic acid) (PAA), dextran, and sucrose should further limit the mobility of the complex within the nanocapsules. The relaxivity of gadobutrol after co-encapsulation was compared to the relaxivity of gadobutrol in PAA, dextran, and sucrose bulk solutions.

4.3.2 Optimized gadobutrol retention in nanocapsules

Gadolinium complexes, like gadobutrol, experience a dilution in the blood stream after injection and a fast size-related renal clearance.[258, 262] Thus, an efficient encapsulation of the contrast agent in large entities is necessary to prolong the circulation time in the body, which is available for diagnosis. Additionally, a sufficient water access of the encapsulated contrast agent is relevant for a high relaxivity. In the preparation of polyurea nanocapsules from diamines and diisocyanates, the monomers define the later structure of the nanocapsule wall. To obtain an understanding of the encapsulation efficiency and cargo retention

rather simple monomers were chosen as building blocks. TDI was chosen as diisocyanate because its high reactivity enables a fast formation of the nanocapsules. This study was focused on the use of aliphatic diamines with different chain length, such as 1,4-diamino butane (DAB) and 1,6-diamino hexane (HMDA). They react more rapidly with diisocyanates and are less soluble in the continuous phase than aromatic diamines.

The commercially available contrast agent Gadovist® contains the complex gadobutrol at 1 M concentration. First of all, nanocapsules were prepared from HMDA and TDI (1:1 molar ratio) and loaded with gadobutrol solution (1 M) and dilutions thereof (0.1 M, 0.01 M, 0.001 M) to study the encapsulation efficiency (Figure 4.19). The measured Gd concentrations, after redispersion in aqueous solution, and theoretically expected values were compared. For the calculation of the theoretical Gd concentration, the dilution upon redispersion was considered. The order of magnitude of the measured Gd concentration is in good agreement with the theoretical values. The deviation between measured and theoretical values is largest when $c_{\text{Gdload.}}$ is small (0.001 M).

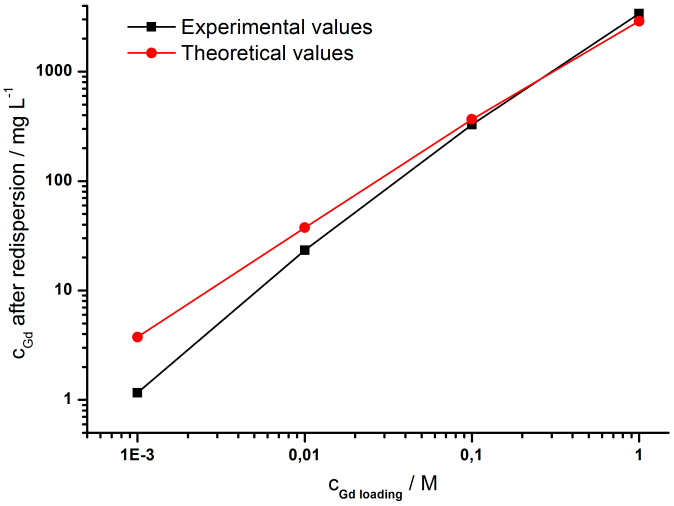

Figure 4.19: Theoretical and experimental Gd concentration after encapsulation for $c_{\text{Gdload.}}$= 0.001 - 1 M measured in aqueous solution.

In a following step, the concentration of Gd retained in the nanocapsules (cGdret.) was assessed by centrifugation and successive ICP-OES measurement. The percentage of Gd retained in the nanocapsules is given by the ratio of Gd in the capsules and the measured total Gd concentration. In Figure 4.20 a) $c_{\text{Gdret.}}$ - both in percent and in mg·L^{-1}, is plotted *vs.* the initial gadobutrol

loading in the dispersed phase ($c_{\text{Gdload.}}$). Two opposite trends can be observed in the graph for the two ordinates. The percentage of Gd retention in the nanocapsules scales approximately linear with the logarithm of $c_{\text{Gdload.}}$. The lower the gadobutrol loading is, the higher the measured retention. The only deviation from this trend is observed for $c_{\text{Gdload.}} = 0.01$ M. The final concentration within the capsule was still higher for increased $c_{\text{Gdload.}}$, even though a larger fraction of Gd was released. These observations were attributed to an increase of the osmotic pressure, which leads to a stronger leakage from the nanocapsules upon redispersion for higher $c_{\text{Gdload.}}$. This assumption is supported by the results shown in Figure 4.20b). 5 days after redispersion for $c_{\text{Gdload.}} = 0.001$ M and 0.01 M, no further release was observed, while the release is continued for the $c_{\text{Gdload.}} = 0.1$ M and 1 M.

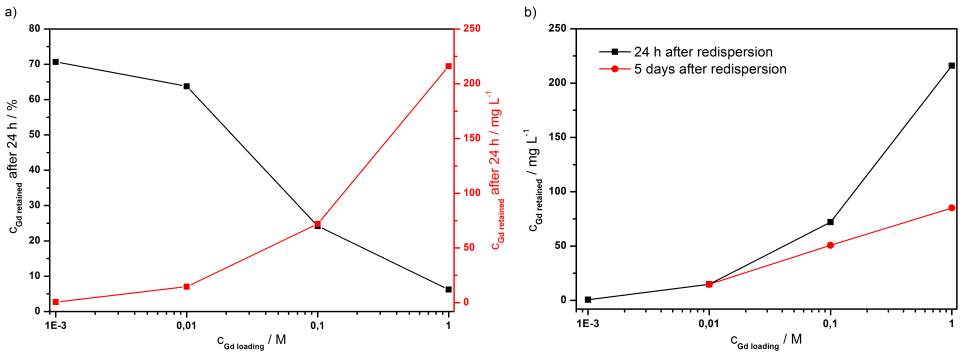

Figure 4.20: Gadobutrol retention in HMDA nanocapsules *vs.* initial gadobutrol loading, a) 24 h after redispersion in % and mg·L^{-1}, b) 5 days after redispersion in %.

The results are in good agreement with previous observations of high dye retention for encapsulation concentrations of less than 1 mM.[69] The obtained results also highlight the necessity of a precise monitoring of $c_{\text{Gdret.}}$ and a purification strategy to remove free gadobutrol. For an increased relaxivity, the confinement of the contrast agent mobility in the nanocapsule environment is a requirement. $c_{\text{Gdret.}}$ feeds directly into the calculation of the relaxivity (equ. 2.1) and could therefore lead to a large error and an underestimation of the relaxivity. For $c_{\text{Gdload.}} = 1$ M, the calculated relaxivity based on the total Gd concentration would be lowered by a factor of 20 as only 6% Gd were retained in the capsules. All further experiments were focused on $c_{\text{Gdload.}} = 0.01$ M and 0.1 M. This is owed to the detection limit of T_1 determination. Additionally,

the osmotic pressure should be limited to create nanocapsules that are stable over long time and retain the gadobutrol reliably.

4.3.2.1 Retention independent of used diamine monomer

First, the influence of the diamine on the gadobutrol retention was studied. Nanocapsules were prepared from HMDA and DAB with varying TDI ratio, respectively. The given ratios always present mM concentrations of the two components in standard experiment with 10 g cyclohexane. For retention in HMDA and DAB nanocapsules a similar trend was observed. The gadobutrol retention in nanocapsules increased when the diamine/TDI ratio was changed from 1:1 to 1:2 for nanocapsules (Figure 4.21). In the nanocapsule formation

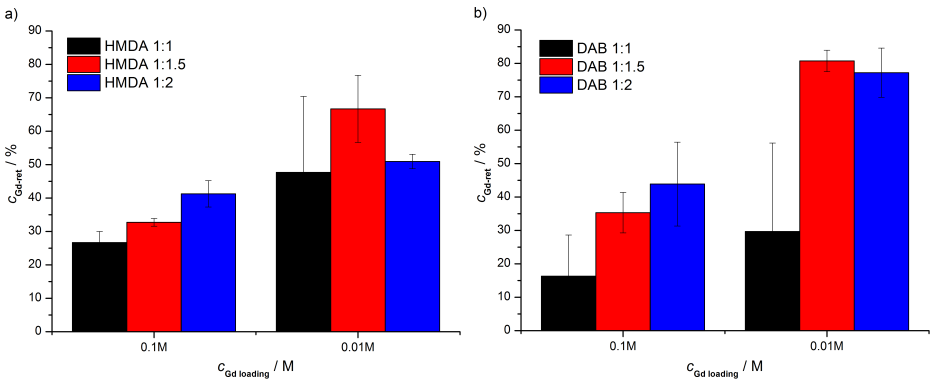

Figure 4.21: Gadobutrol retention in nanocapsules prepared with 0.1 M and 0.01 M gadobutrol solution at different diamine/TDI ratios, a) HMDA nanocapsules, b) DAB nanocapsules.

a number of side reactions can occur. TDI excess was used in the preparation to ensure the complete reaction of the diamines. The observed results were in good agreement with literature. Rosenbauer et al.[69] used a similar amine based surfactant from the same supplier. They reported the incorporation of the surfactant into the capsule wall by reaction with TDI. Additionally, they did not observe nanocapsule formation when an excess of HMDA was used. Several other examples can be found in literature for the use of TDI excess in the preparation of polyurea nanocapsules.[68,69,72,73] The overall gadobutrol retention in the nanocapsule ranged between 25 and 40% with $c_{\text{Gdload.}} = 0.1$ M. A similar change of retention was observed, for the capsules prepared with $c_{\text{Gdload.}} = 0.01$ M compared to $c_{\text{Gdload.}} = 0.1$ M. However, the percentage

of retained gadobutrol was higher with respect to $c_{Gdload.}$. This was expected based on the results of the initial experiments (Figure 4.20).

IR spectroscopy was used to confirm polyurea formation and to investigate changes in nanocapsule shell when the monomer composition was altered.[70] The spectra of the DAB nanocapsules were recorded exemplarily for DAB/TDI ratios ranging from 1:1 to 1.2 after 24 h reaction (Figure 4.22). The peaks at 1642 cm^{-1} and 1548 cm^{-1} correspond to the C=O and C-N stretches of the urea linkage, respectively. The spectra were normalized to the peak at 1649 cm^{-1}. The intensity of the stretching vibrations of the N-H groups (3300 cm^{-1}) and the -CH, -CH_2 and -CH_3 (2950, 2750 cm^{-1}), were equal for all spectra. The most pronounced change between the spectra was observed at 2275 cm^{-1} and was highlighted with a red rectangle. Unreacted isocyanate groups were only found to be still present after 24 h of reaction for a DAB/TDI ratio 1:2 ratio.

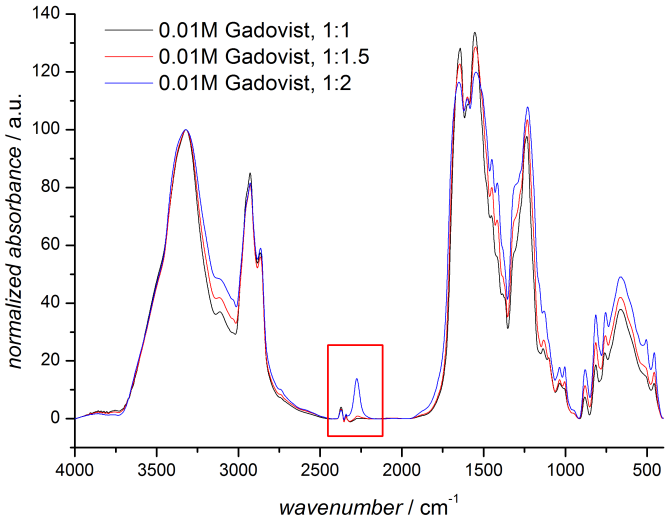

Figure 4.22: IR spectra of DAB nanocapsules synthesized with varying TDI content. Molar DAB/HMDA ratio is changed from 1:1 to 1.2. All spectra were normalized to the polyurea carbonyl peak at 1649 cm^{-1}. The rectangle highlights the position of the -NCO peak at 2250 cm^{-1}.

In the formation of polyurea nanocapsules one cannot easily differentiate between the reaction of TDI with diamine or H_2O. The reaction of water and TDI releases CO_2 and leads to the formation of primary amines, which can further react with TDI to form polyurea.[263] In both cases, polyurea is formed and no additional peak occurs in the IR spectrum. A polyurethane carbonyl peak in

the IR spectrum at 1730 cm^{-1} would have indicated the reaction of TDI with a hydroxyl-group of the gadobutrol complex. The respective peak cannot be identified in the IR spectra but could be overlaid by the prominent urea carbonyl peak. Gadobutrol was present in the dispersed phase at much lower concentration than DAB. Hence, no definitive conclusion can be drawn if the gadobutrol complex is covalently bound to the nanocapsule wall. Additionally, interfacial tension measurements were performed at the water/cyclohexane interface. The interfacial tension of 0.1 M and 0.01 M gadobutrol solutions to cyclohexane was found to be similar as pure water to cyclohexane ($\gamma_{Gd0.1M}$ = 46.6 mN·m^{-1}, $\gamma_{Gd0.01M}$ = 46.8 mN·m^{-1}, γ_{H2O} = 48.4 mN·m^{-1}). This indicated that gadobutrol was not driven to the interface, which would have increased the probability for a reaction with TDI.

So far it was shown, that the type of diamine used in the nanocapsule preparation does not have a large effect on gadobutrol retention. The retention did rather depend on the monomer amount or the monomer ratio. Further, the gadobutrol retention was improved when the amount of gadobutrol used in the preparation process was reduced.

4.3.2.2 Control of the retention with the TDI equivalents

The number of variable parameters in the preparation process was reduced to facilitate the identification of the key paremeters influencing the gadobutrol retention. The further experiments were focused on the encapsulation of 0.01 M gadobutrol solution in nanocapsules prepared from DAB and TDI. Previously, the total monomer content ($n_{\text{diamine}} + n_{\text{TDI}}$) and diamine/TDI ratio were changed simultaneously. Additional experiments were required to differentiate between the effects caused by each parameter. A set of nanocapsules was prepared, where the total monomer content was kept constant for changing DAB/TDI ratios. Nanocapsules were prepared with a varying amount of monomer at a fixed molar DAB/TDI ratio (Figure 4.23). For each studied ratio, three different amounts of monomer were investigated. The samples were grouped based on their DAB/TDI ratio (1:1, 1:1.5 and 1:2). Capsule formation was confirmed by SEM imaging for all investigated DAB/TDI ratios (insets Figure 4.23, enlarged survey images Figure 4.24). However, differences in the appearance of the nanocapsules were observed. The samples with the least amount of monomer (1:1, 0.5:0.75, 0.5:1) showed a strong deviation from a spherical shape. This effect was most pronounced for the sample with 0.5:0.75 ratio and

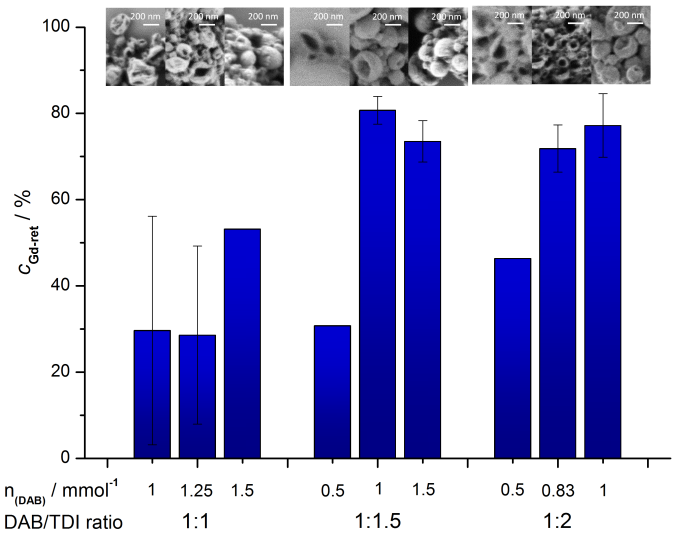

Figure 4.23: Comparison of $c_{Gdret.}$ of nanocapsules prepared with 0.01 M gadobutrol and a fixed DAB/TDI ratio of 1:1, 1:1.5 and 1:2 each with three different amounts of monomer.

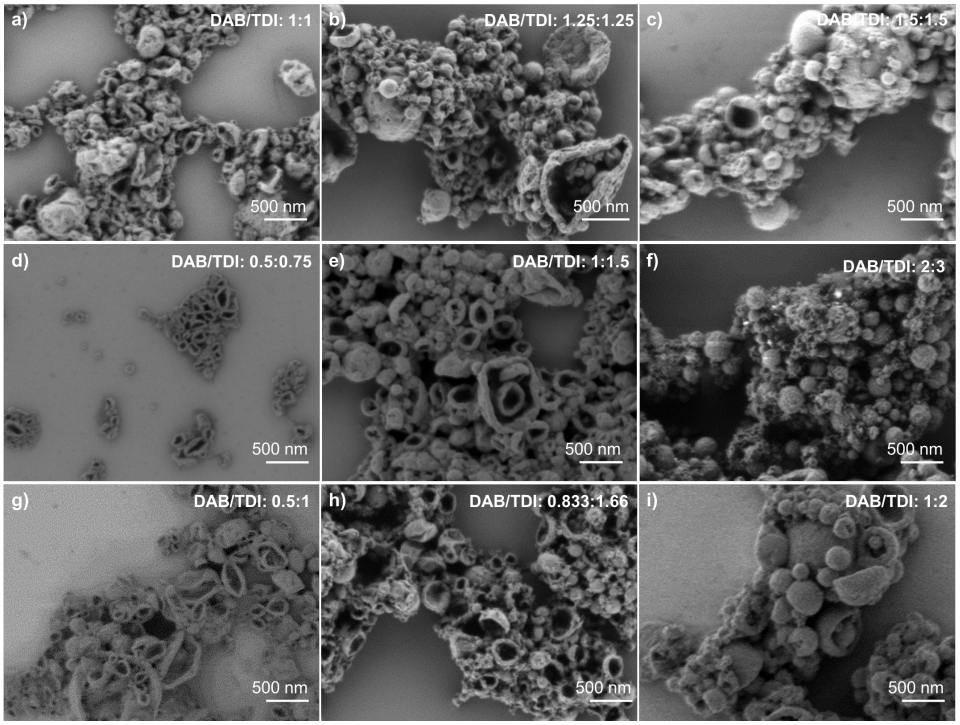

Figure 4.24: Scanning electron micrographs of DAB nanocapsules prepared at fixed DAB/TDI ratios with varying amount of monomer. Top row with 1:1 ratio a) 1:1, b) 1.25:1.25 and c) 1.5:1.5. Middle row with 1:1.5 ratio d) 0.5:0.75, e) 1:1.5, f) 2:3, bottom row with 1:2 ratio g) 0.5:1, h) 0.833:1.666, i) 1:2.

probably indicated a very thin nanocapsule shell. All of these three samples showed the least gadobutrol retention (<45%)among their groups (DAB/TDI ratio). The nanocapsules appeared more cup-like and spherical with increasing amount of monomer for every group of the samples. A bright capsule wall and a dark inner area were observed for most nanocapsules with a low and medium monomer content in every group. The dark area was attributed to the part of the capsule, which was deflated *in vacuo*. This indicated that the capsule wall is still rather flexible. At a high monomer amount, the deflation is only observed for few capsules. This was attributed to a thickening of the nanocapsule wall, resulting from an increased amount of monomer available for capsule formation. These results are in agreement with the previously observed thickening of polyurea nanocapsule walls for increasing amounts of monomer.[5] DLS measurements of the nanocapsules were performed after redispersion in water. For the samples with 1:1 and 1.25:1.25 ratio d_h was around 120 nm. For all other samples d_h was found to be in the range between 150 and 200 nm. Up to 10% of micron-sized nanocapsules were still present in all samples. No correlation between monomer content and capsule size was observed.

The first set of samples (DAB/TDI 1:1) showed low gadobutrol retention around 30% with a high batch-to-batch variation. No batch-to-batch variation was given for the sample with a monomer ratio of 1.5:1.5 because only a single sample was prepared. However, the observed gadobutrol retention was within the error of the other preparations. Reasons for the batch-to-batch variation could be deviations in the preparation process. The speed of TDI addition and the TDI distribution in the continuous phase are crucial steps in the preparation procedure. Secondly, samples with a 1:1.5 ratio were compared. Low gadobutrol retention of around 30% was observed for the sample with a 0.5 mmol DAB. This was already discussed above and attributed to a thin capsule wall based on the low amount of monomer. The long-time stability of this sample will be discussed later-on. For the other preparations (1 mmol, 1.5 mmol DAB), a gadobutrol retention above 70% was observed. The nanocapsules with 1:2 ratio were prepared with 0.5 mmol, 0.833 mmol and 1 mmol DAB. For nanocapsules with 0.5 mmol DAB the retention (45%) was rather low compared to the other two preparations (70%, 75%). This was attributed to the thin shell similar to the sample with a 0.5:0.75 DAB/TDI ratio. The retention was depending on the monomer amount, when the samples were compared among their group. Additionally, the central bars in each group (1.25:1.25, 1:1.5, 0,833:1.66) were

compared. The molar amount of monomer (monomer mass +/- 10%) was constant, only the monomer ratio was changed. The results showed that the monomer ratio influenced the gadobutrol retention. In summary, both, monomer ratio and monomer amount, affect the gadobutrol retention. A DAB/TDI ratio greater than 1:1 was necessary for the stable retention of gadobutrol in the nanocapsules. Further, the retention scaled with the monomer amount for a constant monomer ratio.

A stable encapsulation of gadobutrol is crucial for a prolonged circulation of the drug in the blood stream as well as for a correct determination of the relaxivity. In order to assess the retention of gadobutrol in the nanocapsules two experiments were separately performed (Figure 4.25). In the first experiment, the nanocapsules were isolated from the continuous phase after redispersion in water. The gadobutrol retention in the nanocapsules was monitored over several days. In the second experiment, the nanocapsules were dialyzed for 5 days against an aqueous solution of SDS. The gadobutrol retention during dialysis was monitored to simulate the dilution of a drug in the blood stream. Figure 4.25a) shows the gadobutrol retention in the nanocapsule for a period of 3 days after redispersion. The retention was normalized to the gadobutrol retention after redispersion. This experiment was performed for the samples with 0.5:0.75, 0.5:1 and 1:1.5 molar ratio. While the first two have shown only a low Gd retention after redispersion (30% and 45% respectively), the third sample had the highest retention of about 80% after redispersion. The samples with 0.5:1 and 1:1.5 ratio showed a stable retention over the studied period of time with retention close to 100% of the previously measured value. The sample with the lowest amount of monomer (0.5:0.75) showed a different release pattern. Gadobutrol was released continuously after redispersion until no more gadobutrol was present in the nanocapsules.

In the second step, the gadobutrol retention was studied during dialysis (Figure 4.25b). First, $c_{\mathrm{Gdret.}}$ was assessed after redispersion as previously discussed. Subsequently, the aqueous dispersion was transferred into a dialysis tube and immersed in the 50-fold volume of the dispersion. Samples were withdrawn in 24 h intervals and the gadobutrol content was assessed. Samples with a 1:1.5 DAB/TDI ratio were studied exemplarily for 0.1 M and 0.01 M gadobutrol loading. The value after 24 h corresponds to the concentration determined to be in the nanocapsules after redispersion. The following 5 values (48 h - 144 h) correspond to aliquots withdrawn during dialyis. No significant difference was

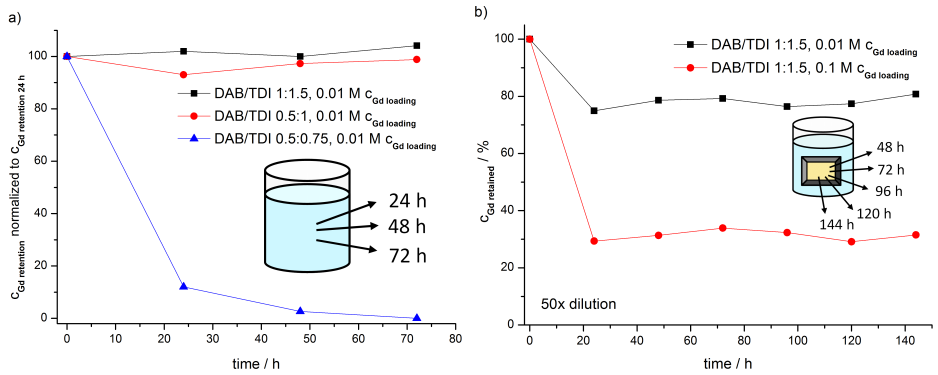

Figure 4.25: Study of gadobutrol retention in DAB nanocapsules a) cGdret over several days after redispersion for samples with DAB/TDI ratio of 0.5:0.75, 0.5:1 and 1:1.5. All curves were normalized to $c_{\text{Gdload.}}$ measured after redispersion, b) $c_{\text{Gdret.}}$ during several days of dialysis.

measured in the content of gadolinium in the capsules after the redispersion and dialysis ($c_{\text{redisp.}} = 0.11$ mM, $c_{\text{dial.}} = 0.12$ mM). The measured loss of gadobutrol compared to the initial amount corresponds hence to gadobutrol that was not encapsulated. These experiments also show that there is no detectable release of complex in aqueous solution even after a large dilution of the nanocapsules dispersion (50×).

4.3.3 Enhanced relaxivity of encapsulated gadobutrol

The relaxivity was defined in chapter 2.4.1 as the concentration dependent change of the relaxation rate. In dilute bulk solution, the relaxivity is independent of the gadobutrol concentration up to at least 50 mM gadobutrol. For nanocapsules, only the gadobutrol molecules within the nanocapsule contribute to an enhanced relaxivity. Therefore, it is crucial to determine the concentration of contrast agent in the nanocapsules. In the previous chapter, a method was introduced for the removal of released gadobutrol and assessment of the remaining gadobutrol concentration in the nanocapsules. The fraction of remaining gadobutrol was referred to as "retention". Diamine type, diamine/TDI ratio and gadobutrol concentration were investigated regarding their influence on the gadobutrol retention. In the following sections, the influence of these parameters on the relaxivity, which was calculated based on the gadobutrol concentration retained in the nanocapsules, will be discussed.

4.3.3.1 Relaxivity increased with use of shorter diamines

Firstly, the influence of the diamine type and Gd concentration on relaxivity were studied. In Figure 4.26 the relaxivity of nanocapsules prepared with HMDA and DAB was compared for 0.1 M and 0.01 M initial Gd loading at a fixed molar diamine/TDI ratio (1:1.5). All samples exceeded the relaxivity of gadobutrol bulk solution ($r_1 = 2.8\ s^{-1}{\cdot}mM^{-1}$). The nanocapsules relaxivity was increased, if less concentrated gadobutrol solutions were encapsulated. This effect was observed for nanocapsules prepared from HMDA ($r_{10.1M} = 4.7\ s^{-1}{\cdot}mM^{-1}$, $r_{10.01M} = 7.6\ s^{-1}{\cdot}mM^{-1}$) and DAB ($r_{10.1M} = 10.9\ s^{-1}{\cdot}mM^{-1}$, $r_{10.01M} = 15.6\ s^{-1}{\cdot}mM^{-1}$). However, independent of the encapsulated gadobutrol concentration the relaxivity was twice as large for DAB nanocapsules compared to HMDA nanocapsules. The gadobutrol retention was similar for both capsules types and cannot be the origin of difference in relaxivity. An equal molar concentration of monomers was used for HMDA and DAB nanocapsules. As a result the total monomer mass was reduced by 7.5% from HMDA to DAB nanocapsules. The change of monomer mass was considered to be too small to largely effect the capsule wall thickness and its properties. Another possible explanation for this observation could be an increased water permeability of the nanocapsule wall.
The deviation in permeability could originate from the difference in hydrophilicity of the diamine monomers. In literature a commonly used measure for the hydrophilicity of a compound is the octanol/water partition coefficient $\log(p_{OW})$.[264] The coefficient reflects the relative solubility of a compound in an octanol and water mixture. For DAB the distribution[265] is shifted in favor of the water phase by a factor of 4.5 compared to HMDA[266]. Cheng et al. observed a relation between pore size of their polymersomes and the relaxivity. They achieved a threefold increased relaxivity when water permeation through pores in the polymersomes was enabled.[174] To further elucidate the reason for the increased relaxivity of DAB nanocapsules diffusion measurements are proposed. In summary the relaxivity of the nanocapsules was influenced by diamine type and encapsulated gadobutrol concentration, whereas the retention did only depend on the latter.

4.3.3.2 Increased relaxivity for higher TDI equivalents

The influence of the monomer amount and the monomer ratio on the nanocapsule relaxivity was studied in more detail for nanocapsules prepared from DAB

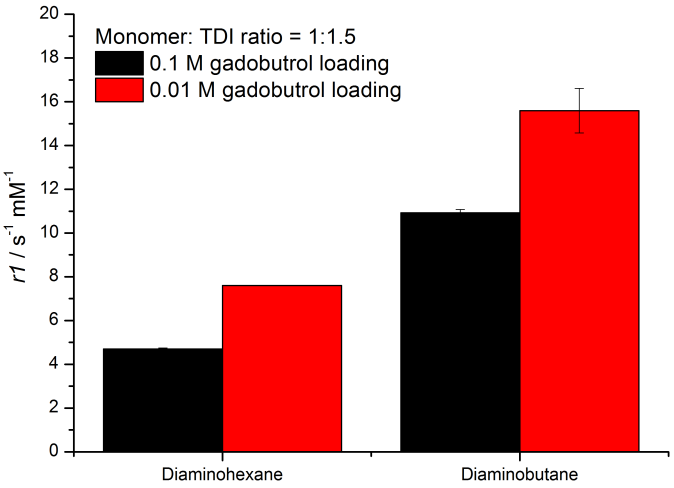

Figure 4.26: Relaxivity of encapsulated gadobutrol in HMDA and DAB nanocapsules with a molar diamine/TDI ratio of 1:1.5.

and TDI. The nanocapsules, which were already studied regarding their gadobutrol retention, were used to assess the relaxivity as well. The samples were again grouped based on their DAB/TDI ratio as shown in Figure 4.27. The samples prepared with a 1:1 DAB/TDI ratio showed a rather high gadobutrol relaxivity above 15 $s^{-1}{\cdot}mM^{-1}$. However, all calculated relaxivity had a large batch-to-batch variation. This was related to the deviation in the gadobutrol retention, as the retained gadobutrol concentration was directly fed into the calculation or r_1. Only one sample was prepared for the 1.5:1.5 ratio as mentioned earlier. The depicted error relates to the standard deviation in the determination of relaxation time. Secondly, the samples with a 1:1.5 ratio were compared. The relaxivity was highest (15.9 $s^{-1}{\cdot}mM^{-1}$) for the sample with 1 mmol DAB. The sample with 0.5:0.75 DAB/TDI ratio showed a relaxivity of 13.9 $s^{-1}{\cdot}mM^{-1}$. However, kinetic release studies for showed a continuous release of gadobutrol from the capsules. Due to the delay of few hours between determination of $c_{\text{Gdret.}}$ and measurement of T_1 the calculation of r_1 would be incorrect. Released and encapsulated gadobutrol have different relaxation times. An average relaxation time would be measured if gadobutrol is present in bulk and in the capsules. This would lead to the misinterpretation of nanocapsules relaxivity. After few days, the relaxivity would be similar to the r_1 of bulk solution, when all gadobutrol has been released.

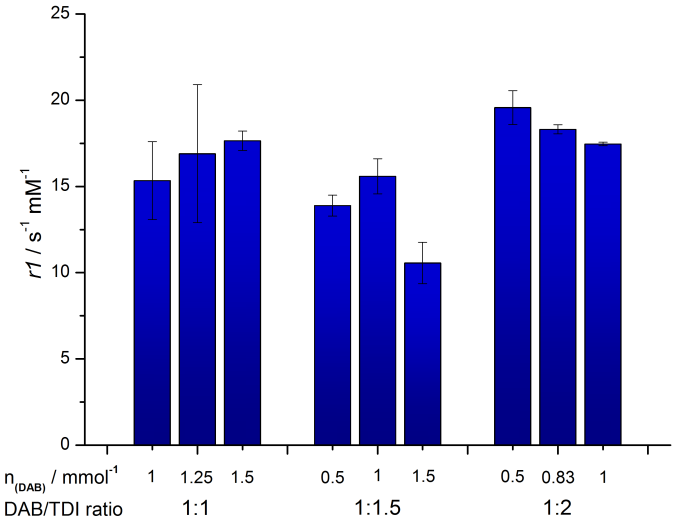

Figure 4.27: Relaxivity of nanocapsules prepared with 0.01 M gadobutrol and a fixed DAB/TDI ratio of 1:1, 1:1.5 and 1:2, each with three different amounts of monomer.

A reduction of r_1 was observed for increasing monomer amounts, when the samples with 1 mmol and 1.5 mmol DAB were compared. A reduced r_1 could originate from a reduced water/proton permeability of the nanocapsule wall. SEM imaging already showed an improved retention of spherical shape with increasing amount of monomer, which indicated the formation of a thicker shell. Accordingly, a reduction of r_1 for increasing monomer amounts fits well with the theoretical expectations. A similar trend was observed for the group of samples with 1:2 ratio. With increasing amount of monomer the relaxivity was reduced from 19.6 to 17.5 $s^{-1}{\cdot}mM^{-1}$. The relaxivity was increased, when the monomer ratio was changed from 1:1.5 to 1:2. This observation was confirmed by comparison of the samples with 1:1.5 and 0.833:1.66 DAB/TDI ratio (same monomer amount).

In summary, the capsule wall composition is a crucial factor in the design of nanocapsules with a high relaxivity. Lower monomer amounts resulting in a thinner capsule shell can enhance the relaxivity. This potential for improvement reaches its limit when the nanocapsule cannot retain the gadobutrol anymore. The preparation of nanocapsules at a 1:2 DAB/TDI ratio allowed the furthest reduction of the monomer amount and yielded the highest relaxivity (0.5:1 ratio, 19.6 $s^{-1}{\cdot}mM^{-1}$). However, it had to be compromised with a lower gadobutrol encapsulation. All further experiments were focused on a 1:1.5 DAB/TDI ratio.

This preparation combined high relaxivity with highest retention. Additionally, no evidence for unreacted isocyanate was identified in the IR spectra.

4.3.4 Superior relaxivity by co-encapsulation

The confinement of gadobutrol in nanocapsules increased the relaxivity. When adjusting the nanocapsule preparation gadobutrol retention and high relaxivity had to be counterbalanced. Beside the influence of the nanocapsule shell also the influence of the nanocapsule core on the relaxivity was investigated. Additional to gadobutrol, molecules such as dextran, sucrose and the sodium salt of poly(acrylic acid) (PAANa), were encapsulated. This is being referred to a co-encapsulation in the following sections. The choice of co-encapsulation agents was made based on the relaxivity of gadobutrol in the respective bulk solutions. The relaxivity in bulk solution will be discussed and compared to the relaxivity of encapsulated gadobutrol later-on.

4.3.4.1 Co-encapsulation limits gadobutrol retention

A co-enapsulation increases the amount of cargo in the nanocapsule. Therefore, the effect of co-encapsulation on gadobutrol retention was studied. The gadobutrol retention was determined as previously established for sole encapsulation of gadobutrol. The insets in Figure 4.28 show magnified images of the nanocapsules obtained by co-encapsulation of 0.01 M gadobutrol (Figure 4.29 survey images). 10 wt% PAA or 20 w% dextran or sucrose were encapsulated additional to gadobutrol. The nanocapsules with PAANa appeared to be deflated, which was previously observed for nanocapsules with the same DAB/TDI ratio of 1:1.5. Additionally, the nanocapsule shell showed a crumpled morphology. This observation was attributed to the presence of polyacrylic acid. PAANa is known to be surface active and its amphiphilic properties could help to stabilize the nanodroplets. This assumption was supported by interfacial tension measurements. For 10 wt% PAANa solution the interfacial tension at the cyclohexane water interface was lowered from 48.4 $mN \cdot m^{-1}$ to 33.6 $mN \cdot m^{-1}$. This implies that PAANa is rather associated to the nanocapsules wall than being distributed in the dispersed phase. The size of the nanocapsules estimated from the SEM images is in agreement with the hydrodynamic diameter of about 125 nm obtained by DLS measurements. The diameter is smaller than previously measured for DAB nanocapsules ($>$150 nm). This could be attributed to the

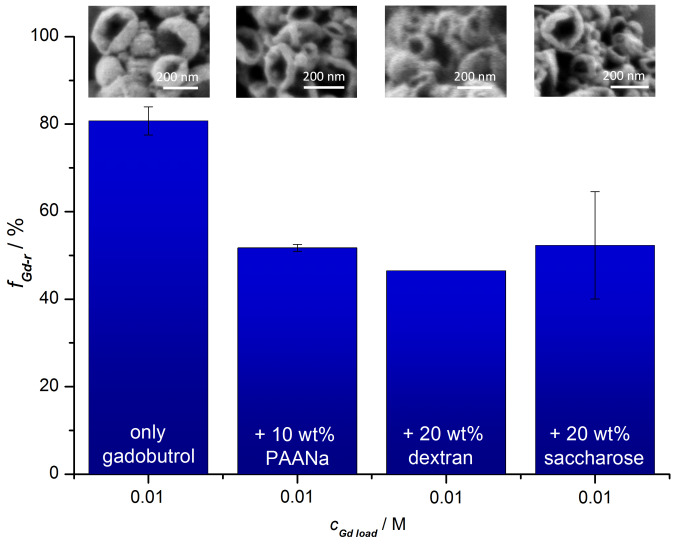

Figure 4.28: Study of gadobutrol retention of DAB nanocapsules with a 1:1.5 DAB/TDI ratio and 0.01 M gadobutrol co-encapsulated with 10 wt% PAANa, 20 wt% dextran and 20 wt% sucrose. Previous data without co-encapsulation were added to facilitate comparison of the data.

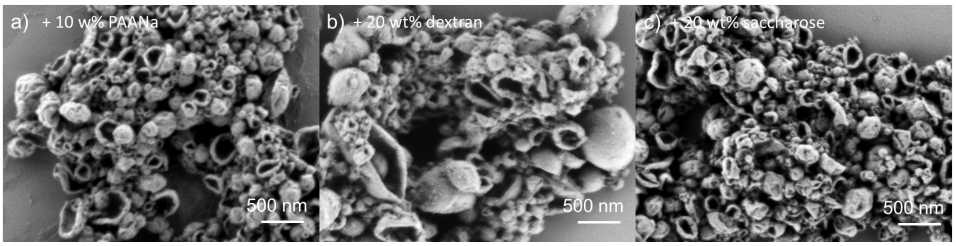

Figure 4.29: Scanning electron micrographs of nanocapsules prepared at DAB/TDI ratio of 1:1.5 with 0.01 M gadobutrol loading and co-encapsulation of a) 10 wt% PAANa b) 20 wt% dextran and c) 20 wt% sucrose.

interfacial activity of PAANA, which could help to stabilize the capsules from within. An increased amount of surfactant leads to the formation of smaller droplets and is therefore expected to result in smaller nanocapsules. No differences in the surface morphology were observed for nanocapsules with dextran and sucrose compared to polyurea nanocapsules. The surface tension of 20 wt% dextran (46.9 $mN \cdot m^{-1}$) solution was measured to be similar to pure water against cyclohexane. This implies, that dextran is rather distributed inside the nanocapsule compared to PAANa. SEM images revealed the increased formation of micron sized capsules when dextran and sucrose were co-encapsulated. DLS measurements were performed to assess the average hydrodynamic diameter of the nanocapsules. Co-encapsulation of 20 wt% dextran and sucrose lead to nanocapsules with about 185 and 160 nm, respectively. The increase of encapsulated sucrose concentration led to the increase of an average nanocapsule size from about 140 nm (10 wt%) to about 210 nm (30 wt%). An increased viscosity of the dispersed phase can hamper the formation of homogeneous droplets during ultrasonication.

Having confirmed successful capsule formation, the capsules were studied regarding their gadobutrol retention. In Figure 4.28 the effect of the co-encapsulation on the gadobutrol retention is directly compared to nanocapsules without co-encapsulation. For nanocapsules prepared with a DAB/TDI ratio of 1:1.5 and 0.01 M gadobutrol loading $c_{Gdret.}$ is reduced from about 80% to 50% for the co-encapsulation of 10 wt% PAANa and 20 wt% dextran or sucrose. The retention appeared to be rather independent of the co-encapsulation agent. The reduced retention could originate from a higher osmotic pressure upon co-encapsulation, which would lead to an increased leakage from the nanocapsules. 20 wt% dextran solution exhibit an osmotic pressure of 1.67 bar.[267] The osmotic pressure of 20 wt% sucrose solution is about 11-fold higher than for 20% dextran due to sucroses higher molar concentration (19 bar).[268] No difference was observed in the retention of gadobutrol, even though both co-encapsulation agents lead to a different osmotic pressure. A possible explanation was found when the nanocapsules were studied by IR spectroscopy (Figure 4.30). The nanocapsules dispersion was compared to a nanocapsules pellet, obtained by centrifugation. Prior to measurement all sample were freeze-dried. For each type of nanocapsule two spectra are shown additional to a reference spectrum of nanocapsules without co-encapsulation. The spectra were recorded subsequent to redispersion and after centrifugation at 4000 rpm (standard speed for capsule purification). All

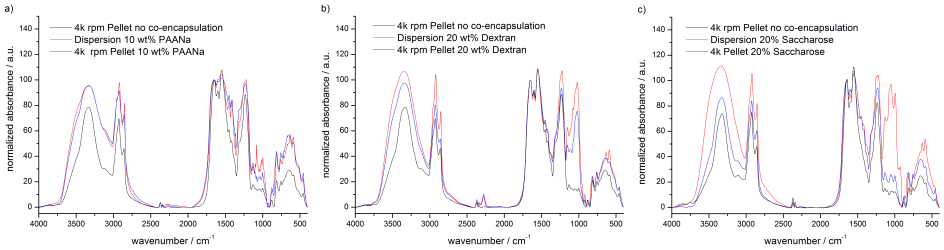

Figure 4.30: IR spectra of DAB nanocapsules prepared with 0.01 M gadobutrol and co-encapsulation of various molecules. For comparison spectra of nanocapsules prepared without co-encapsulation agent were added. Co-encapsulation of a) 10 wt% PAANa, b) 20 wt% dextran and c) 20 wt% sucrose.

spectra have been normalized to the characteristic polyurea peak at 1649 cm^{-1}. For the co-encapsulation agents (PAANa, dextran, and sucrose) a change in the peak intensities between dispersion and pellet after 4000 rpm centrifugation was observed. The changes in the respective peaks (2920, 2850, 1222, 1080 cm^{-1}) can be attributed to SDS, which remained from the redispersion process. No other changes could be observed in the spectra for PAANa co-encapsulation. This indicated that the total amount of PAANa was encapsulated. The intensity of the peaks at 3300 and 1020 cm^{-1} were reduced, additionally, for dextran and sucrose co-encapsulation. These peaks correspond to the hydroxyl groups and the ether moieties characteristically found in carbohydrates.[269] This indicated that also a fraction of dextran and sucrose was removed, which was not encapsulated or already released from the nanocapsules. However, the reduction in the peak intensities was much larger for saccharose co-encapsulation. No evidence for a covalent attachment of dextran or sucrose to the nanocapsule wall was found (polyurethane carbonyl, 1730 cm^{-1}). The spectra revealed that sucrose was only encapsulated partially, while dextran and PAANa remained in the nanocapsules (Figure 4.30). This was attributed to the high osmotic pressure of sucrose solution and could explain why a similar retention was observed for all co-encapsulation experiments. Another reason could be the covalent attachment of the co-encapsulation agent. Polyurethane bonds are formed, when diisocyanates and hydroxyl groups of sugars react. A single polyurethane bond should be sufficient to attach a whole dextran molecule to the nanocapsule. More than 100-fold of polyurethane bonds would be required to attach the same amount of sucrose to the capsule wall. This estimation was made based

on the different molecular weight of dextran and sucrose (40000 g·mol^{-1} vs. 342 g·mol^{-1}).
In another experiment, the gadobutrol retention was found to be independent of the encapsulated sucrose concentration (10, 20, 30 wt%, Figure 4.31). In Figure 4.32 a) and b) the IR spectra of nanocapsules co-encapsulated with 10, 20 and 30 wt% sucrose are shown as obtained from dispersion and nanocapsules pellet, respectively. The peak at 3300 cm^{-1} increased along with the sucrose concentration. A respective trend was observed in the region from 1000 to 1200 cm^{-1}, which is characteristic for carbohydrates. After separation of nanocapsules from the dispersion, changes were observed in the spectra (Figure 4.32b). The characteristic peaks for sucrose (3300 and 1000-1200 cm^{-1}) had a similar intensity in all spectra. This implied that the separated nanocapsules had a similar sucrose content. 50% of gadobutrol were found to remain in the capsules, while only a small percentage of sucrose remained. This implied that sucrose was released preferentially, thus alleviating the osmotic pressure gradient.
The gadobutrol retention was previously found to be stable for several days even under 50-fold dilution for 0.01 M gadobutrol encapsulation. The gadobutrol retention was reduced when molecules such as saccharose were co-encapsulated. Therfore, the kinetic experiments were repeated for sucrose co-encapsulation, to ensure that the measured gadobutrol retention is constant over several days. In Figure 4.33 a) and b) the retention after redispersion and upon dilution (by dialysis) is shown, respectively. For both graphs the total gadobutrol content was set to 100% and the value obtained directly after completing the redispersion process was set 24 h. The retention after redispersion was constant over several days. A similar result was observed in the dialysis experiment (Figure 4.33 b). The gadobutrol retention is stable for at least three days. Deviations in gadobutrol retention were attributed to experimental error in the dialysis process.
In summary, a stable and reliable encapsulation of gadobutrol was obtained with co-encapsulation of PAANa, dextran and sucrose, which is crucial for the application in the biomedical field. This confirms that the measured gadobutrol concentrations were constant until the relaxation time was assessed and beyond.

4.3.4.2 Increased microviscosity enhances relaxivity

To enhance the relaxivity of contrast agents, they have been attached covalently or been confined in nanostructures. In either case the mobility (rotation,

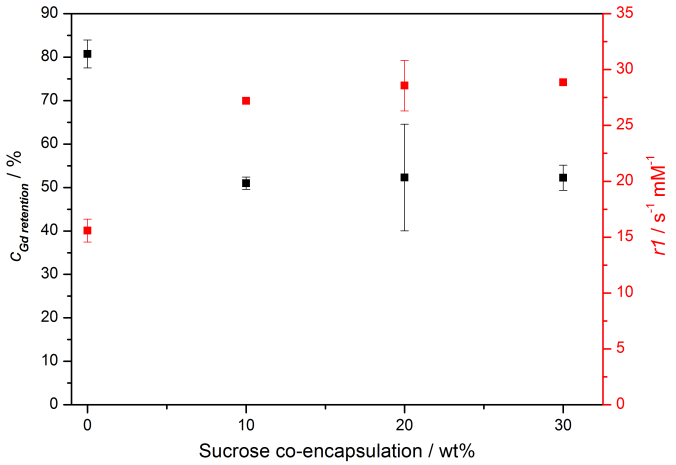

Figure 4.31: a) Gadobutrol retention and relaxivity, of gadobutrol loaded DAB nanocapsules co-encapsulated with 10, 20 and 30 wt% sucrose. All samples were prepared with 1:1.5 DAB/TDI ratio and $c_{\text{Gdload.}} = 0.01$ M.

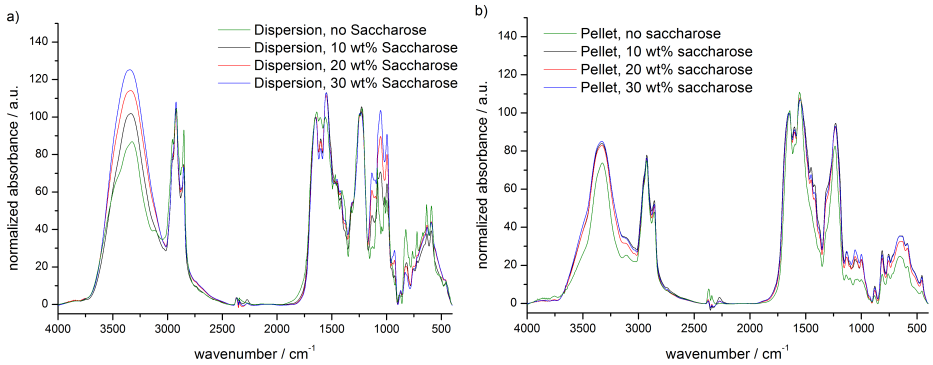

Figure 4.32: IR spectra of DAB nanocapsules prepared with 0.01 M gadobutrol and co-encapsulation of of 10 - 30 wt% sucrose. For comparison spectra of nanocapsules prepared without sucrose were added; a) dispersion, b) nanocapsules separated by centrifugation at 4000 rpm.

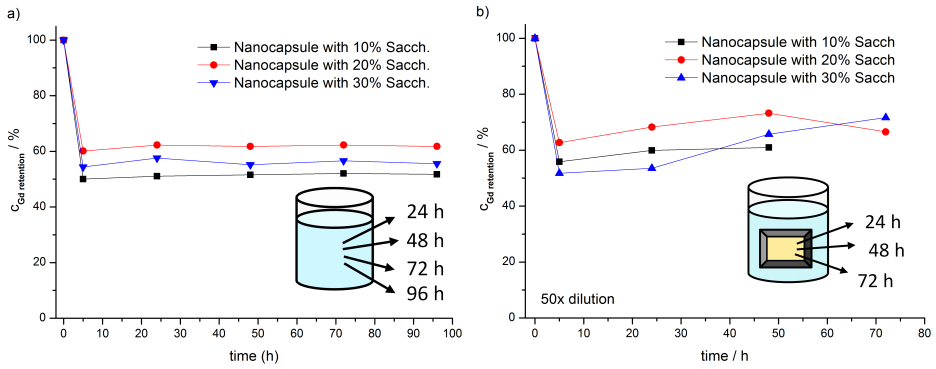

Figure 4.33: Kinetic study of gadobutrol retention in DAB nanocapsules, a) $c_{Gdret.}$ during several days of dialysis, b) $c_{Gdret.}$ after redispersion for co-encapsulation of 10 - 30 wt% sucrose, d) $c_{Gdret.}$ during dialysis for co-encapsulation of 10 - 30 wt% sucrose.

diffusion) of the contrast agent is reduced, which influences the relaxivity of the contrast agent.[270] An increased viscosity in the surrounding of the contrast agent can increase the relaxivity.[153, 271] Sucrose solutions were used to simulate the *in vivo* interaction of contrast agents. Van der Waals interactions between complex and sucrose were considered to alter the rotational behavior of the complex.[272] PAAm and PAA were previously used to increase the viscosity within nanocapsules. An increased relaxivity upon encapsulation was observed.[180] However, this has not been studied systematically so far. In this study, different molecules were investigated regarding their effect on bulk relaxivity, in order to identify suitable candidates for an encapsulation. Polymers such as dextran and PAA were studied regarding their effect on the relaxivity of gadobutrol. PAA is known to bind a large amount of water.[273, 274] Therefore, it was previously thought to be a suitable candidate to enhance the relaxivity. Dextran is a biocompatible material, which is known to yield solutions with a high viscosity at low concentrations. Sucrose has a low molecular weight and is composed of sugar units similar to dextran.

In Figure 4.34, the relaxivity of gadobutrol in 10 wt% PAANa as well as 10, 20 and 30 wt% dextran and in 10, 20 and 30 wt% sucrose solutions is shown. For 10 wt% PAANa the relaxivity was found to be 7.5 $s^{-1}{\cdot}mM^{-1}$, which is a little lower than the value obtained for 30 wt% sucrose (8.7 $s^{-1}{\cdot}mM^{-1}$). The relaxivity increased approximately linear with dextran and sucrose concentrations up to 30 wt%. However, the rate of r_1 increase is higher for sucrose than for dextran. A reason for the high relaxivity of PAA was not yet found. Additional

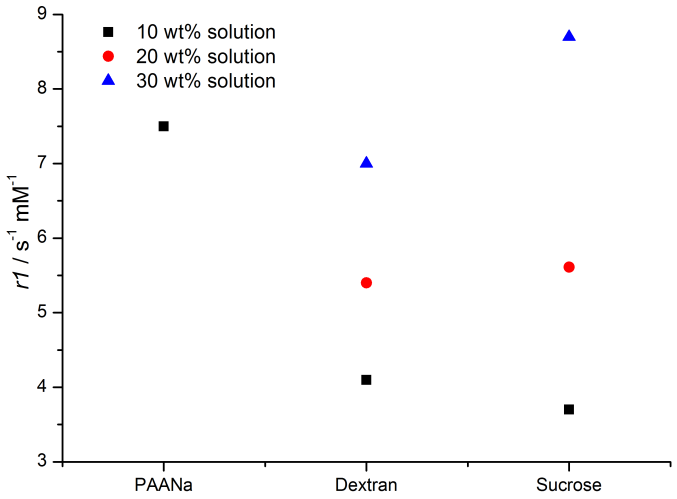

Figure 4.34: Relaxivitiy of gadobutrol in bulk solutions of 10 wt% PAANa and 10 - 30 wt% sucrose and dextran.

experiments have disqualified the molecular weight as the reason. Also, low molecular weight acids (malonic acid) with an equivalent molarity of carboxylate groups did not reach the relaxivity of 10 wt% PAANa. For 20 wt% dextran the relaxivity (5.4 s^{-1}·mM^{-1}) was similar to 20 wt% sucrose (5.6 s^{-1}·mM^{-1}). 20 wt% dextran and 20 wt% sucrose have an approximately equal amount of saccharide units and a rather similar relaxivity in bulk solution. This should enable a direct comparison after co-encapsulation. Additional measurements showed that 20 wt% dextran solution has 8-times the viscosity of 20 wt% sucrose solution (12.6 mPa·s vs. 1.6 mPa·s). Based on the measurement of the macroscopic viscosity a higher r_1 would have been expected for dextran than for sucrose. However, further studies suggested a correlation of the diffusion rather with the microscopic viscosity. The correlation of microviscosity and rotational correlation time (τ_r) was previously reported and supports this observation.[151] The majority of the mentioned bulk solutions were used in the following for co-encapsulation with gadobutrol and the effect on gadobutrol retention as well as relaxivity were studied.

4.3.4.3 Surface tension restricts relaxivity enhancement

In bulk solution the co-encapsulation agents already showed potential to increase the gadobutrol relaxivity. The change of relaxivity by co-encapsulation was studied and compared to the results in bulk solution. Figure 4.35 shows

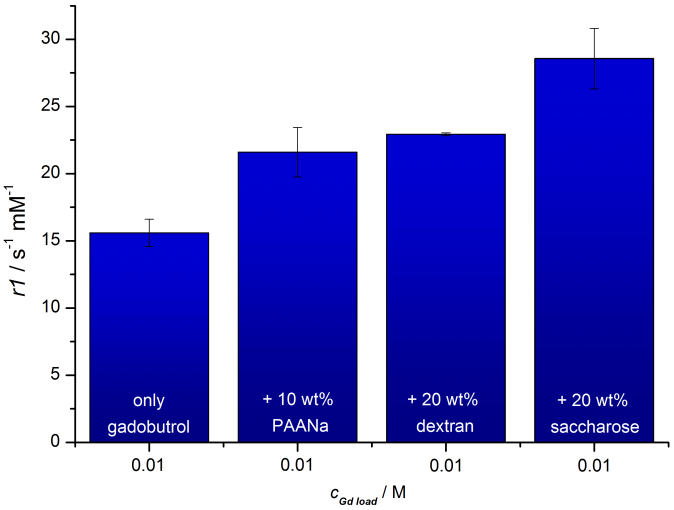

Figure 4.35: Study of relaxivity of DAB nanocapsules with a 1:1.5 DAB/TDI ratio and 0.01 M gadobutrol co-encapsulated with 10 wt% PAANa, 20 wt% dextran and 20 wt% sachcarose. Previous data without co-encapsulation were added to facilitate comparison of the data.

the relaxivities, which were calculated for the co-encapsulation of gadobutrol with 10 wt% PAANa, 20 wt% dextran, and 20 wt% sucrose. The values were compared to the relaxivity of nanocapsules, which contained only gadobutrol. All co-encapsulation agents significantly enhanced the relaxivity. This was previously attributed to a reduced diffusion of water and contrast agent in the nanocapsule.[180] The increase in r_1, achieved by co-encapsulation, was similar for 10 wt% PAANa and 20 wt% dextran. Relaxivities of $r_{1\mathrm{PAANa}} = 21.6$ $\mathrm{s}^{-1}\cdot\mathrm{mM}^{-1}$ and $r_{1\mathrm{Dex}} = 22.9$ $\mathrm{s}^{-1}\cdot\mathrm{mM}^{-1}$ were obtained. These observations contradict the results of the studies in bulk solution. In bulk solution r_1 of 10 wt% PAANa was superior to r_1 of 20 wt% dextran (bulk: $r_{1\mathrm{PAANa}} = 7.5$ $\mathrm{s}^{-1}\cdot\mathrm{mM}^{-1}$, $r_{1\mathrm{Dex}} = 4.5$ $\mathrm{s}^{-1}\cdot\mathrm{mM}^{-1}$). Based on the crumpled morphology observed in the SEM images and interfacial tension measurements it was assumed that PAANa was rather associated to the capsule wall, than being distributed in the nanocapsules volume. This would have reduced the viscosity within the nanocapsule and led to a reduced effect on the rotation of the complex compared to bulk solution. The association of PAANa to the capsule wall could also increase the wall thickness and reduce the water exchange between bulk and capsule volume.

The relaxivity of nanocapsules with $c_{\mathrm{Gdload.}} = 0.01$ M and 20 wt% sucrose was nearly doubled ($r_1 = 28.6$ $\mathrm{s}^{-1}\cdot\mathrm{mM}^{-1}$) compared to the nanocapsules without

sucrose (15.6 $s^{-1}{\cdot}mM^{-1}$). The relaxivity was increased by 25% compared to dextran loaded nanocapsules. Even though, the relaxivity sucrose bulk solution was similar to dextran bulk solution and lower than PAANa bulk solution. A reason could be the incorporation of sucrose in the nanocapsule wall. This would make the capsule wall more hydrophilic. The incorporation of sucrose into the nanocapsule wall would have led to the formation of polyurethane bonds. For the 30 wt% sucrose approximately a 1:1 molar ratio of DAB and sucrose was used in the nanocapsule preparation. However, no peak was detected at the wavenumber characteristic for the polyurethane carbonyl (1730 cm^{-1}). Accordingly, sucrose incorporation into the nanocapsule wall becomes rather improbable. Chen et al. proposed an interaction of the complex with sucrose by hydrogen bonding. He observed change in the rotational behavior of the complex, which led to an increased relaxivity.[272] Additionally, the relaxation rate of the protons at the hydrogen-bonded sucrose molecule could be altered due to the proximity of the contrast agent. This is depicted schematically in Figure 4.36. The interaction can be regarded as a type of second sphere effect. This could be an explanation for the high relaxivity in sucrose loaded nanocapsules. Relaxivities close to 30 $s^{-1}{\cdot}mM^{-1}$ were mostly reported for approaches, which expose the contrast agent to the bulk solution by covalent attachment or confine it in very small entities.[171]

10, 20 and 30 wt% sucrose solutions were encapsulated in an additional experiment. Previously, a similar gadobutrol retention was observed for all three samples. It was studied if the relaxivity of the nanocapsules could be influenced by the amount of co-encapsulation agent. The relaxivity of the nanocapsules was assessed (Figure 4.31) and the obtained r_1 values were found to be independent of the sucrose loading. The amount of sucrose was expected to influence the nanocapsules relaxivity, based on the results in bulk sucrose solution. The experimental results obtained with the nanocapsules do not correlate with the ones obtained from bulk solutions. However, IR spectroscopy revealed that after redispersion the sucrose content was similar in all nanocapsules with sucrose. This would explain the similar relaxivity of all sucrose loaded nanocapsules.

It can be concluded that the co-encapsulation led to the desired and anticipated enhancement of relaxivity. However, only a low amount of sucrose could be retained in the nanocapsules. The retained amount of sucrose was independent of the used sucrose concentrations. This supports the assumption that release of gadobutrol is driven by the osmotic pressure. The enhanced relaxivity was

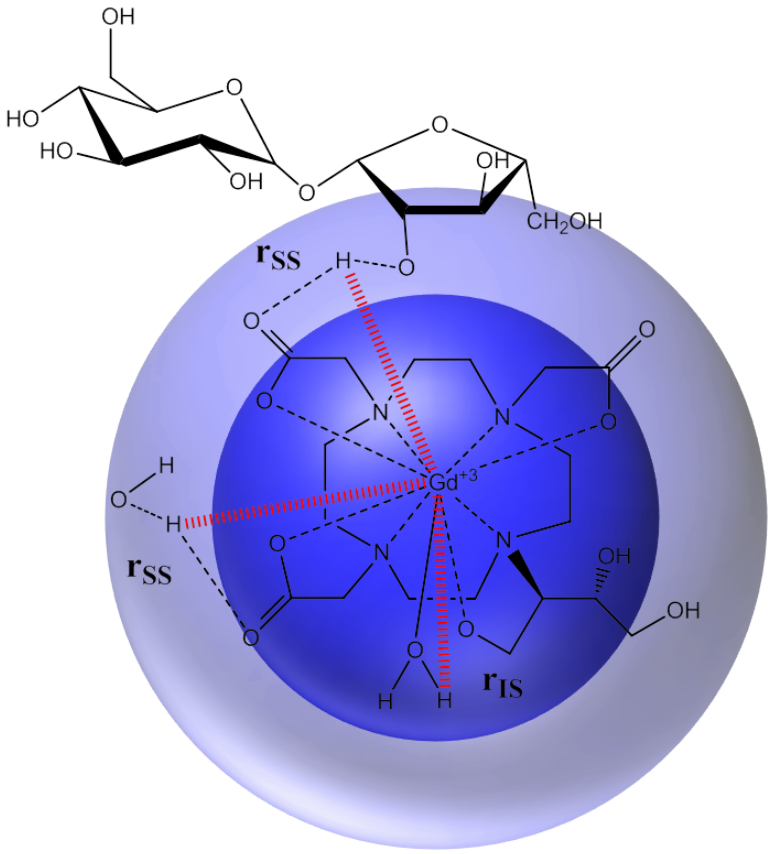

Figure 4.36: Schematic illustration of interaction between sucrose and gadobutrol. Blue sphere shows inner sphere and the proton affected by inner sphere relaxivity r_{IS}. Yellow sphere represents second sphere, wherein the relaxation rate of hydrogen bonded water protons or saccharose protons can be altered (r_{SS}, second sphere effect).

attributed to interactions between the complex and sucrose. Accordingly, it is proposed to study the diffusion through the nanocapsule wall and within the nanocapsules.

4.3.5 Conclusion and Outlook

In this study the commercially available contrast agent Gadovist® was confined in polyurea nanocapsules. The nanocapsules should have high gadobutrol retention and high relaxivity to be used as contrast agent with high signal intensity and signal sensitivity, respectively. The study was focused on the encapsulation of 0.01 M and 0.1 M gadobutrol solutions. The nanocapsule composition was seen to have a large effect on the obtained relaxivity. Nanocapsules prepared from different diamines had similar gadobutrol retention but varied in relaxivity. DAB nanocapsules had twice the relaxivity compared to HMDA nanocapsules prepared at same molarity. A further increase of relaxivity by even shorter diamines could be possible. The monomer amount and monomer ratio did influence the nanocapsules relaxivity. A compromise had to be found between a sufficient retention of the contrast agent in the nanocapsule and a high relaxivity. While nanocapsules with a low monomer amount were beneficial for the relaxivity their contrast agent retention was reduced. A high retention at increased monomer amounts was accompanied by a reduced relaxivity. A DAB/TDI ratio of 1:1.5 mmol in a standard preparation was found to be ideal for the encapsulation of 0.01 M gadobutrol solutions. The obtained relaxivity of 15.6 $s^{-1}{\cdot}mM^{-1}$ is about a 3-fold enhancement compared to gadobutrol bulk solution and previous polyurea/polyurethane nanocapsules.[275] Nanocapsules can be tuned to provide sufficent water access to achieve an enhanced relaxivity. However, the amount of encapsulated contrast agent has to be compromised to maintain capsules stable at a low wall thickness. The relaxivity of the nanocapsules can compete with system such as dendrimers, which are known to provide a good water access.[166, 276] In the first step, the successful design of high relaxivity nanocapsules was demonstrated. In a second step the versatility of nanocapsules was exploited to further enhance the relaxivity. The limitation of the contrast agents' diffusion was known to increase the relaxivity. The relaxivity enhancement in viscous bulk solutions was studied and the respective molecules were co-encapsulated. In bulk, 10 wt% PAANa solution showed a high relaxivity among the tested solutions. The co-encapsulation of dextran and PAANa solutions led to a similar relaxivity of 22.9 $s^{-1}{\cdot}mM^{-1}$and

21.6 $s^{-1} \cdot mM^{-1}$, respectively. The solutions were not expected to have a different influence on relaxivity in bulk solution and in the nanocapsule. A reason could be a stronger interaction of PAANa with the nanocapsule wall instead of a distribution in the nanocapsule core compared to dextran. Results of surface tension measurements supported this assumption. Co-encapsulation of 20 wt% sucrose solution increased the relaxivity to about 28.6 $s^{-1} \cdot mM^{-1}$. The relaxivity obtained by co-encapsulation was nearly doubled compared to the encapsulation of gadobutrol alone. The relaxivity of the nanocapsules exceeded the one reported for perfluorcarbon nanoparticles (25.3 $s^{-1} \cdot mM^{-1}$).[171] Evidence was found in literature that hydrogen-bonding between gadobutrol and sucrose could be the reason for the increased relaxivity of sucrose loaded nanocapsules. Diffusion studies based on NMR could help to differentiate between the diffusion of water molecules or protons through the nanocapsule wall.

Chapter 5

Experimental

5.1 Nanocapsules based on polysaccharides

5.1.1 Materials

10-Undecen-1-ol 98%, phenyl dichlorophosphate $\geq$95%, dextran (35000-40000 g·mol^{-1}), D_2O, dimethyl formamide (DMF), acryloyl chloride (97%, $<$210 ppm MEHQ stabilizer), 4-(dimethylamino)-pyridin (DMAP, $\geq$99%), sodium dodecyl sulfate (SDS) were purchased from Sigma Aldrich. Dichloromethane and triethylamine were dried and stored under argon. Hoveyda-Grubbs catalyst 2^{nd} generation was purchased from Sigma Aldrich and stored under argon. The inhibitor 2,6 Di-tert-butyl-4-methyl phenol (BHT) was purchased from Merck Schuchardt. The oil soluble block copolymer surfactant poly[(ethylene-*co*-butylene)-*b*-(ethylene oxide)] (P(E/B-*b*-EO)) consisting of a poly(ethylene-*co*-butylene) block (M_w = 6800 g·mol^{-1}) and a poly(ethylene oxide) block (M_w = 8000 g·mol^{-1}), was synthesized according to the procedure described in literature.[277] Unless otherwise noted, all chemicals were used as received. Water of MilliQ quality (18 MΩ) was used throughout all experiments.

5.1.2 Modification of dextran

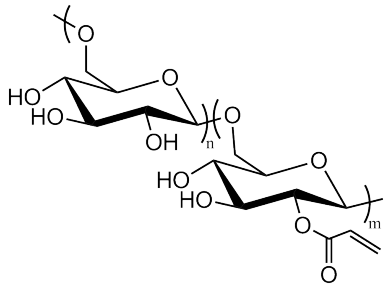

The synthesis of acryloyl dextran (DexA) was adapted from Gorodetskaya et al[214] and is shown in Figure 4.2. The following quantities were used to modify dextran to yield a degree of substitution (DS) of 0.13 at 5 °C. In brief, dextran (with an $M_r \sim$ 40,000, 1 g, 5.55 mmol glucose units) was dissolved in 60 mL of dry DMF containing 4 wt% LiCl (2.28 g, 53 mmol) at 95 °C under an argon atmosphere. Subsequently, the solution was cooled to room temperature and a 0.1 wt% BHT solution in DMF (1 mL) was added, followed by triethylamine (1 mL, 7.2 mmol) that was previously dissolved in a small amount of DMF. Then, acryloyl chloride (0.8 mL, 9.9 mmol) was diluted in DMF and added to the solution through a syringe pump (5 mL·h^{-1}). Afterwards, a catalytic amount of 4-(dimethylamino)pyridine (DMAP 3.9 mg, 0.03 mmol) was added and the reaction was allowed to proceed for two hours.

The modified dextran was precipitated in isopropanol and isolated by centrifugation (10000 rpm). The supernatant was discarded and the pellet was dissolved in MilliQ water followed by repetitive precipitation. The product was dialyzed for 48 h against water (Roth Visking, MWCO 14000 Da), freeze dried and stored until use at 5 °C. The obtained yield was about 70%. The modification was confirmed qualitatively by infrared spectroscopy and quantitatively by ^{1}H NMR spectroscopy (Figure 4.3 a,b). To assess the degree of substitution the integrals of the signals of acryloyl moiety and anomeric proton of the sugar were related. Infrared spectra of pure and modified dextran (DS 0.13 and DS 0.55) were normalized to the band of the asymmetrical CH stretch at 2925 cm^{-1} and compared. All samples show the characteristic dextran bands in the spectra.[278] The peak at 1635 cm^{-1} corresponds to residual water which is tightly bound to dextran even after freeze drying. ^{1}H NMR δ (ppm): 6.56-6.5, 6.31-6.22, 6.1-6.06, 5.31-5.2, 5.06, 4.98, 4-3.89, 3.76-3.68, 3.59-3.48.

5.1.3 Synthesis of phenyl-di(undec-10-en-1-yl)-phosphate

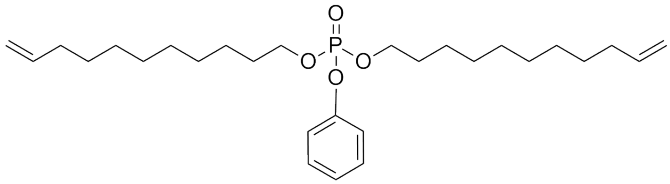

The synthesis and characterization of the phenyl-di(undec-10-en-1-yl)-phosphate was carried out by Filippo Marsico and was already published elsewhere.[220] To a dried three-necked, 250 mL round bottom flask fitted with a dropping funnel, 13.4 mL (0.067 mol, 11.4 g) of 10-undecen-1-ol and 9.3 mL (0.067 mol, 6.8 g) of triethylamine were added under an argon atmosphere and diluted in 70 mL of dry CH_2Cl_2. Then, 5 mL (7.05 g, 0.033 mmol) of phenyl dichlorophosphate dissolved in 20 mL of dry CH_2Cl_2 were added dropwise at 0 °C. After the addition was completed, the mixture was stirred at room temperature for 12 h. Then, the mixture was concentrated under reduced pressure, dissolved in diethyl ether and filtered. The crude product was washed twice with brine. The organic layer was dried over anhydrous sodium sulfate, filtered and concentrated *in vacuo*. The compound is purified by flash chromatography over neutral alumina using dichloromethane as eluent to give a clear oil with a yield of 80%. The structure was determined by ^{1}H NMR, ^{13}C NMR, ^{31}P NMR spectroscopy as well as electrospray ionization mass spectrometry (ESI-MS). ^{1}H NMR δ (ppm) : 7.32 (t, J = 7.7 Hz = 2H), 7.21 (d, J = 7.7 Hz, 2H), 7.16 (t, J = 7.7 Hz, 1H), 5.83-5.77 (ddt, J = 16.8 Hz, J = 10 Hz, J = 3.5 Hz, 2H), 5.00-4.97 (ddt, J = 10Hz, J = 3.5 Hz, J = 1.4 Hz, 2H), 4.93-4.91 (ddt, J = 10Hz, J = 1.4 Hz, 2H), 4.16-4.09 (m, 4H), 2.04-2.01 (m, 2H), 1.69-1.65 (m, 4H), 1.39-1.32 (m, 8H), 1.26 (m, 18H). ^{13}C NMR δ (ppm): 150.98, 150.94, 139.29, 129.77, 125.02, 120.10, 114.27, 68.69, 68.66, 33.93, 30.37, 30.33, 29.55, 29.04. ^{31}P NMR δ (ppm): -6.11. ESI-MS m/z 501.33 $[M+Na]^+$, 979.67 $[2M+Na]^+$, 1458.00 $[3M+Na]^+$ (Calcd for $C_{28}H_{47}O_4P$: 478.32)

5.1.4 Synthesis of nanocapsules by olefin cross metathesis

DexA (50 mg, 0.239 mmol) was dissolved in 500 µL of an aqueous 0.05 M NaCl solution. The resulting solution was added dropwise to 5.6 g cyclohexane containing 30 mg P(E/B-*b*-EO), with P(E/B) 6800 g·mol^{-1} and P(EO) 8000 g·mol^{-1}). A pre-emulsion was formed after stirring for 1 h at 1400 rpm, which was subsequently sonicated under ice-cooling with a 1/2" tip for 2 min

at 90% amplitude (Branson Sonfier W450-Digital). The resulting miniemulsion was sealed in a septum vial purged with argon. Then, the diundecenyl phenyl phosphate (120 mg, 0.25 mmol) was dissolved in cyclohexane (0.4 g) and added dropwise to the emulsion under stirring. Thus, an olefin ratio of nearly 1:4 was obtained between aqueous and cyclohexane phase. In case of labeled nanocapsules, 5 wt% of the phosphate were replaced by the respective labeled monomer. The Grubbs-Hoveyda 2nd generation catalyst (5 mg) was dissolved in toluene and transferred dropwise into the miniemulsion. The temperature was raised to 40 °C and reaction was allowed to proceed overnight. The obtained capsules were purified by centrifugation (5000 rpm, 10 min) to remove excess surfactant, unreacted monomer and catalyst. The capsules were further redispersed into water by stirring overnight in 0.3 wt% SDS solution. To remove excess surfactant the nanocapsules were dialyzed against water overnight.

5.1.5 Analytical tools

Nuclear magnetic resonance (NMR)

The solid state magic angle spinning (MAS) NMR measurements have been recorded with a Bruker Avance II spectrometer operating at 300.23 MHz ^{1}H Larmor frequency using a commercial double resonance probe supporting MAS rotors with 4 mm outer diameter at 10 kHz MAS spinning frequency. Both, the ^{31}P MAS spectrum (121.5 MHz ^{31}P Larmor frequency) and ^{13}C CP-MAS spectra (75.5 MHz ^{13}C Larmor frequency, 1 ms CP contact time) have been acquired with 62.5 kHz ^{1}H nutation frequency high power composite pulse decoupling during acquisition using the SPINAL64 sequence and 5000 transients for each spectrum. The MAS NMR measurements were performed by Robert Graf at the Max Planck Institute for Polymer Research in Mainz.
Further NMR experiments were done with a 5 mm BBI ^{1}H/X z-gradient on a 700 MHz spectrometer with a Bruker Avance III system. For ^{1}H NMR spectra, 128 transients were used with an 11 µs 90° pulse and 12600 Hz spectral width together with a recycling delay of 5 s. The ^{13}C NMR (176 MHz) and ^{31}P NMR (283 MHz) measurements were obtained with an ^{1}H powergate decoupling method using 30° degree flip angle, which had a 14.5 µs 90° pulse for carbon and an 25.5 µs 90° pulse for phosphorous. The spectral widths were 41660 Hz (236 ppm) for ^{13}C and 56818 Hz (200 ppm) for ^{31}P, both nuclei with a relaxation delay of 2 s. For characterization of the diolefin phosphoester, the

proton, carbon and phosphorous spectra were measured in $CDCl_3$ at 298.3 K and the spectra were referenced as follows: for the residual $CHCl_3$ at δ (^{1}H) = 7.26 ppm, $CDCl_3$ δ (^{13}C triplett) = 77.0 ppm and triphenylphosphine (TPP) δ (^{31}P) = -6 ppm. For characterization of acryloyl dextran, the proton spectrum was measured in D_2O and referenced for residual H_2O at δ (^{1}H) = 4.79 ppm. The NMR measurements of the phosphoesters were performed by Filippo Marsico at the Max Planck Institute for Polymer Research in Mainz.

IR spectroscopy

To verify the modification of DexA the polymer was analysed by IR spectroscopy. The sample was freeze dried and 1 mg of powder was pressed with KBr to form a pellet and a spectrum was recorded between 4000 and 500 cm^{-1} using a IFS 113v Bruker spectrometer. The IR measurements were performed by Elke Muth at the Max Planck Institute for Polymer Research in Mainz.

Dynamic light scattering (DLS)

Dynamic light scattering was used to determine the size distribution of the nanocapsules using a PSS Nicomp Particle Sizer 380 (Nicomp Particle Sizing Systems). Measurements were performed with a 90° scattering angle at ambient conditions. The nanocapsules were diluted in the respective solvent to about 0.5 wt% solutions before measurement.

Electron microscopy

A field emission microscope (LEO (Zeiss), 1530 Gemini, Oberkochen, Germany) with an acceleration voltage of 200 V was used to study the capsule morphology by SEM. TEM measurements were performed on a Tecnai F20 (FEI, Germany) at an acceleration voltage of 200 kV. The samples for SEM and TEM were diluted in cyclohexane to about 0.01% solid content, subsequently they were transferred by dropcasting to a silicon wafer or a 300 mesh carbon-coated copper grid, respectively. Energy-dispersive X-ray spectroscopy (EDX) combined with elemental mapping of the nanocapsules was carried out on a Hitachi SU8000 SEM microscope equipped with a Bruker AXS spectrometer with an operation voltage of 5 kV. TEM and EDX measurements were performed at the Max Planck Institute for Polymer Research in Mainz by Katrin Kirchhoff and Gunnar Glasser, respectively.

Inductively coupled optical emission spectroscopy (ICP-OES)

An Activa M spectrometer (Horiba Jobin Yvon, Bernsheim, Germany) equipped with a Meinhardt-type nebulizer and a cyclone chamber was used for ICP-OES measurements. The device was controlled by ACTIVAnalyst 5.4 software. For the measurement the following conditions were chosen: 1250 W forward plasma power, 12 L·min^{-1} Ar flow and 15 rpm pump flow. As a reference line the Ar emission at 404.442 nm was employed. The emission lines chosen for calibration and quantification of Ru were 267.876 nm and 372.803 nm with a 5 s integration time. For the calibration 5 different standard concentrations were used, baseline correction and a dynamic underground correction were provided by the software. Prior to the measurement, the samples were diluted in aqueous 0.3 wt% SDS solution.

Fluorescence spectroscopy

The presence of the dye labeled molecules in the capsules was confirmed by measurements with a plate reader (Infinite M1000, Tecan, Switzerland). Absorbance and fluorescence intensity scans of dialyzed aqueous nanocapsule dispersions were recorded for the sample with attached as well as integrated dye molecule. BODIPY (Ex/Em 520/540 nm) was excited at 515 nm (band width $+/-$ 5 nm).

Fluorescence correlation spectroscopy (FCS)

A commercial setup (Zeiss, Germany) with a ConfoCor2 module and an inverted microscope (Axiovert 200) with water immersion objective (C-Apochromat 40x/ 1.2 W, Zeiss) was used for fluorescence correlation spectroscopy. An argon laser (488 nm) was used to excite the BODIPY dye and the emission was detected after filtering with LP505 or long pass filter. Experiments were performed in an eight-well polystyrene chambered coverglas (Laboratory-Tek, Nalge Nunc International). Prior to the FCS measurements the samples were redispersed in water and filtered. For each dispersion series of 30 measurements with total duration 5 min were performed. In order to determine the diffusion coefficients and hydrodynamic radii of the diffusing fluorescent species compounds, the measured autocorrelation curves were fitted with the model function:[279]

$$G(\tau) = 1 + \frac{1}{N}(\frac{\tau}{\tau_D})^{-1}(1 + \frac{\tau}{S^2\tau_D})^{-1/2} \tag{5.1}$$

where N is the average number of fluorescent species in the observation volume V, τ_D is the lateral diffusion time and $S = z_0/\omega_0$ is the ratio of axial to radial dimension of V. The diffusion coefficient of the fluorescent species D was determined as $D = \omega_0^2/4\tau$ and their hydrodynamic diameter trough $D_H = 2k_BT/6\pi\eta D$ where T is the temperature, k_B the Boltzmann constant and η the viscosity of water. Calibration of the confocal observation volume was done using a reference dye with known diffusion coefficients i.e. Alexa Fluor 488. The FCS measurements were performed by Kaloian Koynov at the Max Planck Institute for Polymer Research in Mainz.

5.2 Nanogel and hybrids based on polysaccharides

5.2.1 Materials

All chemicals were used without further purification. Dextran ($M_r \sim$ 6000, 40000, 70000 Da), dimethyl formamide (DMF), 2,4-toluene diisocyanate (TDI), D_2O, cyclohexane (>99.9%), SDS and acrylamide (AAm, ≥99%) were purchased from Sigma Aldrich. Methacrylic anhydride (94%) and zinc standard for plasma analysis were purchased from Alfa Aesar. Zinc nitrate hexahydrate ($Zn(NO_3)_2 \cdot 6H_2O$) and triethylamine (TEA) were purchased from Fluka. Lubrizol U (poly(isobutylene-succinimide pentamine)) was kindly provided by Lubrizol France. The inhibitor 2,6 di-tert-butyl-4-methyl phenol (BHT) was purchased from Merck Schuchardt. The initiator V-59 (2,2'-azobis(2-methyl-butyronitrile) was a gift from Wako Chemicals. MilliQ water was used throughout the experiments.

5.2.2 Modification of dextran

The synthesis of methacrylated dextran (DexMa) was adapted from Kim et al.[280] In brief, 1 g of dextran ($M_r \sim$ 6000 - 70000 Da) was dissolved in 60 mL 6 wt% LiCl solution (3.4 g, in DMF) at 95 °C under Ar atmosphere. Subsequently, the temperature was reduced to 60 °C and 1 mL of a 0.1 wt% solution of BHT in DMF was added dropwise, followed by 145 µL TEA, which was previously dissolved in a small amount of DMF. Subsequent to the addition of the amine, 156 µL methacrylic anhydride, dissolved in a small amount of DMF, were added dropwise to the solution. Afterwards, the reaction was allowed to proceed for two hours. To stop the reaction and precipitate the modified dextran, the solution was transferred into 2-propanol and the precipitate was isolated by centrifugation (Sigma 3K30, 10000 rpm, 5 min). The supernatant was discarded and the pellet was resuspended in MilliQ water. This procedure was repeated 3 times, always using approx. a water/DMF to isopropanol ratio of 1:4. The resulting DexMa solution was dialyzed (Roth SpectraPor MWCO 3500, Roth Visking MWCO 14000) against water for several days, changing the water daily. The dialyzed product was freeze dried and stored until use. The experimental conditions are given for an exemplarily degree of substitution (DS) of 0.1. The DS was evaluated by ^{1}H-NMR spectroscopy on a Bruker spectrometer (300 MHz) following the method of Aschenbrenner.[281] 2 mg of

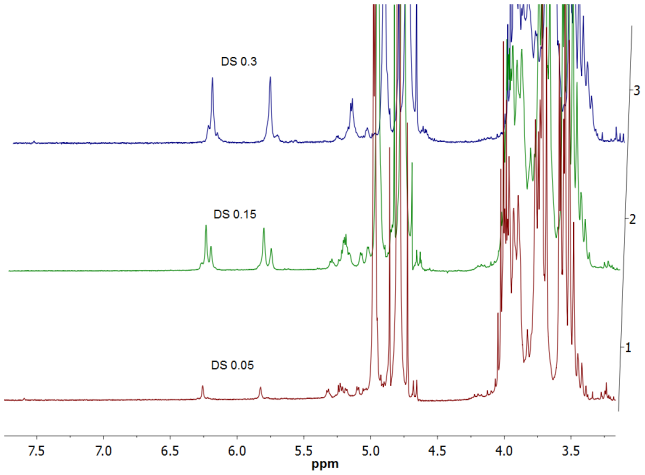

Figure 5.1: NMR spectra of metharylated dextran ($M_r \sim 6$ kDa) with varying degree of substitution.

the dialyzed DexMa were dissolved in D_2O for the analysis. The NMR spectra for DexMa with varying DS are depicted in Figure 5.1

5.2.3 Synthesis of nanogels

The miniemulsion process for the synthesis of the DexMa-poly(acrylamide) (DexMa-PAAm) nanogels follows the procedure of Klinger et al.[217] The dispersed phase was prepared with a 1:1 ratio (wt.) for liquid and solid. 5.8 mmol acrylamide and 0.47 mmol DexMa were dissolved in 500 mg of an aqueous 0.5 M NaCl solution. The resulting solution was added drop wise to 10 g of cyclohexane with 1 wt% Lubrizol U. Afterwards, the mixture (pre-emulsion) was allowed to stir for 2 h at 1750 rpm. Subsequently, the mixture was sonified under ice-cooling with a 1/2" tip for 2 min at 90% amplitude (Branson sonifier 450W-Digital). The vessel was sealed with parafilm and purged with argon to remove oxygen that could affect the radical polymerization. Before increasing the temperature to 60 °C, 10 mg of the initiator (V-59) were dissolved in cyclohexane and added drop wise to the emulsion. When the desired temperature was reached, the reaction was allowed to proceed for 15 h. The steps from two phase system through sonication to hydrogels are shown in Figure 5.2 (I-III). The magnified section for step II depicts the ongoing reactions during polymerization. The multiple methacrylate moieties per DexMa molecule will react with AAm and thus serve as crosslinker. Further steps in the Figure correspond

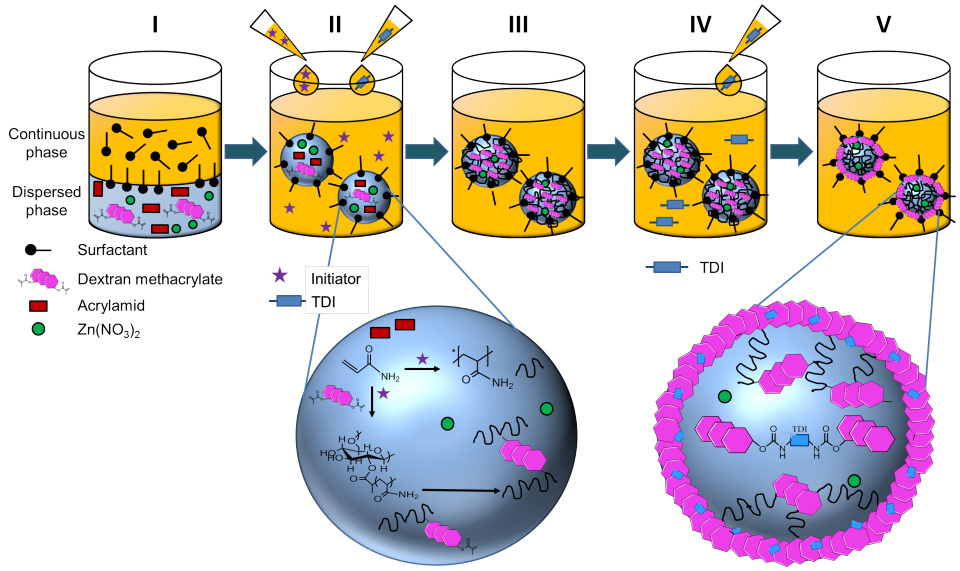

Figure 5.2: Schematic of the modified miniemulsion process, the steps I - V depict the relevant steps to obtain nanogels with a TDI crosslinked dextran shell. The process of polymerization (II) and shell formation (V) is presented in more detail in the enlarged sections.

to the formation of a gel hybrid and will be discussed in the following section. To remove excess surfactant the nanogels were centrifuged at 5000 rpm for 10 min and washed repetitively. The pellet was suspended in cyclohexane and the procedure was repeated two times until the supernatant appeared transparent after centrifugation.

5.2.4 Synthesis of core-shell hybrids

In order to form a shell surrounding the DexMa-PAAm nanogels, TDI was added to crosslink pendant nucleophilic groups of the gel. The process of shell formation directly followed the synthesis for preparation of the nanogels as depicted in Figure 5.2 (IV-V). After 15 h of radical polymerization, as indicated above, TDI dissolved in cyclohexane was added dropwise to the emulsion. The required amounts of TDI were chosen with respect to the free hydroxyl moieties of the DexMa molecules, ratios of 1:1 and 1:2 for TDI and hydroxyl groups were used, respectively.

5.2.5 Zinc release experiments

To assess the total zinc loading of the dispersions in cyclohexane the dispersions were freeze dried and the solid was degraded with nitric acid before being diluted in water for ICP-OES measurements (Figure 5.3b). The zinc leakage during the redispersion process as well as the zinc release in the following 24 h was studied (Figure 5.3c). To ensure that the redispersion process was finished, the first point in time for determination of the zinc leakage was set to 24 h from beginning of the redispersion process. The total zinc content was assessed by a measurement of a diluted dispersion aliquot. Another aliquot was collected and centrifuged for 10 min at 4000 rpm, the supernatant was removed and measured by ICP-OES. To study the further zinc release the supernatant was discarded after centrifugation and the pellet was redispersed in fresh water for 24 h, afterwards the sample was centrifuged again and the zinc concentration in the supernatant was measured.

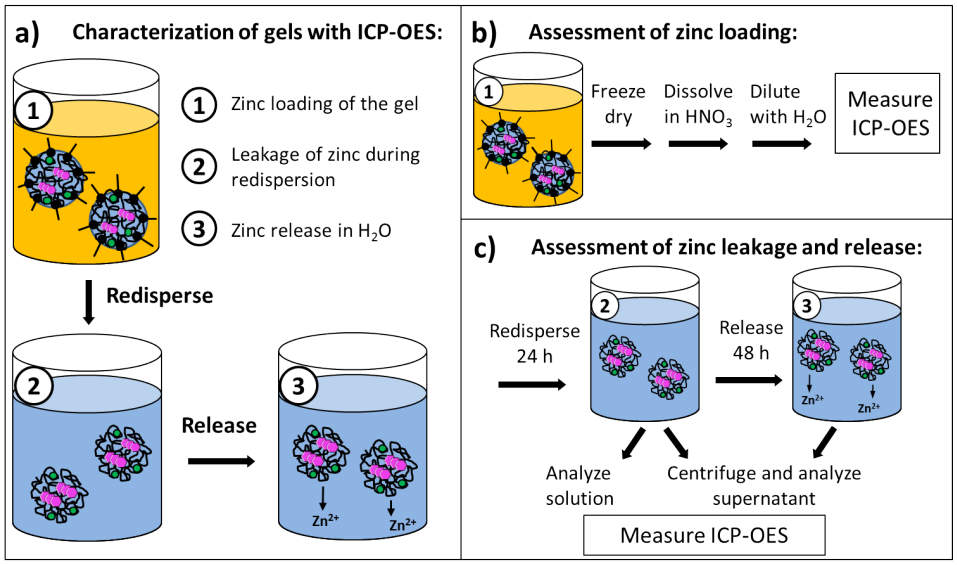

Figure 5.3: a) Scheme showing the three steps of sample characterization by ICP-OES. The steps include the investigation of zinc loading in the gel, of zinc leakage during the redispersion process and the release of zinc during consecutive water immersion. b) Sample collection for assessment of zinc loading. c) Sample collection for assessment of zinc release, additional sampling after 72 h for nanogel-shell hybrids.

5.2.6 Antibacterial testing

To test the expected antibacterial activity of the zinc nanogel-shell hybrids the effect on bacteria, which are relevant in biomedical applications, was studied. For this purpose two methicillin resistant *S. aureus* strains (ST239 μ2, TW20) were exposed to the nanostructures and their growth was studied. Tryptic soy broth (TSB) was prepared with MilliQ water according to the manufacturer's instructions and autoclaved before use in bacterial culture. The bacterial cultures were grown overnight at 37 °C on a shaking incubator. The optical density (OD) was measured at 600 nm and the bacteria were diluted for bacterial testing to an OD of 0.0001. The resulting initial number of colony forming units ($CFU \cdot mL^{-1}$) was determined by conventional plating and colony counting. The adjusted OD corresponded to an initial bacterial concentration of $0.7 \cdot 10^5$ $CFU \cdot mL^{-1}$ and $1.3 \cdot 10^5$ $CFU \cdot mL^{-1}$ for *S. aureus* ST239 μ2 and TW20, respectively. To test the antibacterial activity, the bacteria were inoculated in 96 well plates with the nanogel samples (20 μL) at a total volume of 200 μL per well. The resulting zinc concentration was 0.5 mM $Zn(NO_3)_2$, which corresponds to 1000 $\mu g \cdot mL^{-1}$ nanogels. The change in absorbance at 600 nm was monitored over duration of 18 h in 5 min increments. Each sample was tested in triplicate.

5.2.7 Cytotoxicity assay

To ensure usability of the nanogels in biomedical applications like wound treatment the cytotoxicity of the drug delivery system is studied on human keratinocytes (HaCaT) as a relevant model cell line. The viability of the cells in presence of the nanogel shell hybrids was studied using the CellTiter-Glo® luminescence assay (Promega). The HaCaT cells were received from CLS Cell Service GmbH while the HeLa cells were from DSMZ GmbH. Both were precultured in Dulbeccos modified eagle medium (DMEM) with addition of 10% FCS and 1% penicillin/streptomycin stock solution. To test cell viability in presence of the nanogels shell hybrids the cells were seeded in a 96 well plate at a cell density of 20000 $cells \cdot cm^{-2}$. The nanogels with and without zinc were diluted in cell medium to the desired concentration and 100 μL were added to each well. Nanogels and cells were incubated together for 24 h before 100 μL of CellTiter-Glo® solution were added. The well plate was shaken well for two minutes and the solution was allowed to incubate for 10 min prior to luminescence readout in a plate reader (Tecan) All experiments were performed in triplicate. The

cytotoxicity assay was performed by Melanie Dröge at the Max Planck Institute for Polymer Research in Mainz.

5.2.8 Analytical tools

DLS

The size and size distribution of the nanogels and hybrids was studied by dynamic light scattering (DLS) at 90° scattering angle (20 °C) on a PSS Nicomp Particle Sizer 380 (Nicomp Particle Sizing Systems). After dilution of the samples with the respective solvent the nanocapsules were measured to obtain the hydrodynamic diameter (d_h).

Electron microscopy

The capsule morphology of the nanogel and gel-shell hybrids was investigated by scanning electron microscopy (SEM) on a field emission microscope (LEO (Zeiss), 1530 Gemini, Oberkochen, Germany) with an acceleration voltage of 200 V. TEM measurements were performed on a Tecnai F20 (FEI, Germany) at an acceleration voltage of 200 kV. Prior to SEM and TEM measurements the samples were diluted with cyclohexane to about 0.01% solid content and drop-cast onto a silicon wafer or a 300 mesh carbon-coated copper grid, respectively. TEM measurements were performed by Katrin Kirchhoff at the Max Planck Institute for Polymer Research in Mainz.

ICP-OES

ICP-OES measurements were performed on an ACTIVA M spectrometer (Horiba Jobin Yvon, Bernsheim, Germany) equipped with a Meinhardt-type nebulizer, a cyclone chamber, and controlled by ACTIVAnalyst 5.4 software. The following conditions were applied: 1250 W forward plasma power, 12 L·min^{-1} Ar flow and 15 rpm pump flow. The argon emission line at 404.442 nm was used as reference line. Measurements were performed using four different standard concentrations, two different elemental emission lines and 5 s integration time. As baseline correction, a dynamic underground correction provided by the software was used. The emission lines chosen for the quantification of the Zn were 206.201 nm and 213.857 nm.

5.3 Nanocapsules filled with polysaccharides

5.3.1 Materials

1,6-hexamethylene diamine (HMDA, 98%), 1,4-diamino butane (DAB, 99%), toluene 2,4-diisocyanate (analytical standard), cyclohexane (HPLC grade), dextran (35000-40000 g·mol^{-1}), sucrose (99.5%), poly(acrylic acid sodium salt) (PAANa, average $M_w \sim 5100$ by GPC), poly(acrylic acid) solution (50 wt% $M_w \sim 5000$) and sodium dodecyl sulfate (SDS, 99%) were purchased from Sigma Aldrich. Lubrizol U (poly(isobutylene-succinimide pentamine)) was kindly provided by Lubrizol France. Unless otherwise noted, all chemicals were used as received. Water of MilliQ quality (18 MΩ) was used throughout all experiments.

5.3.2 Synthesis of nanocapsules

For the preparation of gadobutrol loaded nanocapsules by inverse miniemulsion technique, gadobutrol solutions were prepared by diluting the medicinal product Gadovist® (1 M gadobutrol) with MilliQ water to the desired concentration (0.1M, 0.01 M, 0.001 M). The diamine was dissolved in 1.4 g of the respective gadobutrol solution. For the samples prepared with 0.01 M gadobutrol solution additionally 4 mg NaCl were added. The solution was added dropwise to the continuous phase consisting of 7.5 g cyclohexane and 100 mg Lubrizol. The mixture was stirred at 1400 rpm for 1 h in a closed glass vial to obtain a macroemulsion. Subsequently, the emulsion was subjected to ultrasonication with a Branson W450-D sonifier equipped with a 1/2 inch tip under ice-cooling for 3 min pulse-pause regime of 20 s and 10 s, respectively, at 90% amplitude. Afterwards, TDI was dissolved in 2.5 g cyclohexane and added dropwise under stirring to the miniemulsion (900 rpm). The monomers were allowed to react for 24 h. Subsequently, the nanocapsules were redispersed in aqueous solution. 5 g of 0.3 wt% SDS solution were added dropwise to 1 g of dispersion. The mixture was briefly (5 s) shaken in an ultrasonication bath to obtain a fine distribution of oil droplets in the aqueous solution. Subsequently, the mixture was stirred at 800 rpm for 24 h with an open lid to slowly evaporate cyclohexane. All sample compositions are listed in Table 5.1

Table 5.1: Preparation of polyurea nanocapsules from HMDA and DAB. Monomer amounts are given for standard preparations with 1.4 g dispersed phase and 10 g continuous phase; $c_{\text{Gadobutrol}}$ refers to the dispersed phase.

Sample	Monomer/TDI ratio	$c_{\text{Gadobutrol}}$ / M	m_{Diamine} / mg	m_{TDI} / mg	m_{NaCl} / mg	d_{h} / nm
HMDA	1:1	1	116	174	/	185 +/- 130
	1:1	0.1	116	174	/	125 +/- 50
	1:1	0.01	116	174	/	158 +/- 14
	1:1	0.001	116	174	/	380 +/- 250
	1:1.5	0.1	116	262	/	137 +/- 60
	1:1.5	0.01	116	262	2	145 +/- 65
	1:2	0.1	116	348	/	140 +/- 55
	1:2	0.01	116	348	2	134 +/- 25
DAB	0.5:0.75	0.01	44	130	2	186 +/- 21
	0.5:1	0.01	44	174	2	157 +/- 22
	0.833:1.66	0.01	74	290	2	170 +/- 20
	1:1	0.1	88	174	/	125 +/- 10
	1:1	0.01	88	174	2	144 +/- 30
	1:1.5	0.1	88	262	/	166 +/- 20
	1:1.5	0.01	88	262	2	175 +/- 24
	1:2	0.1	88	348	/	155 +/- 35
	1:2	0.01	88	348	2	150 +/- 80
	1.25:1.25	0.01	110	218	2	120 +/- 13
	1.5:1.5	0.01	132	262	2	170 +/- 23
	1.5:2.25	0.01	132	392	2	200 +/- 28
	2:3	0.01	176	524	2	215 +/- 28

5.3.3 Co-encapsulation of gadobutrol

For the preparation of sucrose, dextran or PAANa loaded nanocapsules the synthesis was adjusted slightly. The gadobutrol solution was diluted with 10, 20 or 30 wt% aqueous solutions of the respective co-encapsulation agent (sucrose, PAANa or dextran). All further steps of the preparation were maintained as described in Chapter 5.3.2. The sample compositions are summarized in Table 5.2.

5.3.4 Retention experiments

Retention after redispersion

The aqueous dispersion, obtained by the redispersion process described in Chapter 5.3.2, was sonicated for 30 min at 35 Hz in an ultrasonication bath. The dispersion was first centrifuged at 500 rpm for 5 min to get rid of macroscopic residues from the redispersion process. An aliquot was withdrawn from the supernatant for ICP-OES analysis to assess the total Gd concentration of the sample ($c_{Gdtotal}$). Subsequently, an aliquot of the dispersion was centrifuged at 4000 rpm for 15 min and the Gd content of the supernatant was assessed by ICP-OES ($c_{Gdsupernatant}$). The ratio of the measured values is the percentage of Gd, which was already released from the nanocapsules during the redispersion process. This approach can be described by the following equation:

$$c_{Gdreleased}\% = \frac{c_{Gdsupernatant} \cdot 100}{c_{Gdtotal}} \tag{5.2}$$

Accordingly, the percentage of Gd still retained in the nanocapsules is given by the following equation:

$$c_{Gdretained}\% = 100 - \frac{c_{Gdsupernatant} \cdot 100}{c_{Gdtotal}} \tag{5.3}$$

For several samples additional aliquots were withdrawn over the following days in 24 h intervals in order to assess if the Gd release had reached equilibrium. These samples were centrifuged as well at 4000 rpm for 15 min, the Gd concentrations were measured by ICP-OES and compared to the previous measurements.

Table 5.2: Preparation of polyurea nanocapsules from DAB. Monomer amounts are given for standard preparations with 1.4 g dispersed phase and 10 g continuous phase; $c_{Gadobutrol}$ refers to the dispersed phase.

Sample Monomer/TDI ratio	$c_{Gadobutrol}$ / M	m_{DAB} / mg	m_{TDI} / mg	Load	c_{load} / wt%	m_{NaCl} / mg	d_h / nm
1:1	0.1	88	174	Sucrose	20	/	105 +/- 13
1:1	0.01	88	174	Sucrose	20	2	203 +/- 22
1:1.5	0.1	88	262	Sucrose	20	/	210 +/- 60
1:1.5	0.01	88	262	Sucrose	10	2	143 +/- 100
1:1.5	0.01	88	262	Sucrose	20	2	190 +/- 20
1:1.5	0.01	88	262	Sucrose	30	2	207 +/- 150
1:1.5	0.01	88	262	Dextran	10	2	185 +/- 110
1:1.5	0.1	88	262	PAA	10	/	157 +/- 75
1:1.5	0.01	88	262	PAA	10	2	141 +/- 72
1:1.5	0.1	88	262	PAANa	10	/	134 +/- 80
1:1.5	0.01	88	262	PAANa	10	2	124 +/- 15

Retention during dialysis

To monitor the Gd retention in the nanocapsules while being diluted in a large volume an additional set of experiments was performed. After centrifugation of the dispersion at 500 rpm for 5 min the dispersion was transferred into a dialysis tube (Roth Visking, MWCO 14000 Da) and the dispersion was dialyzed against 50 times its volume for the duration of several days. The sample was dialyzed against a 0.3 wt% SDS solution to prevent a removal of SDS during the dialysis process, which could have led to the aggregation of the nanocapsules. In 24 h intervals aliquots were withdrawn and the Gd concentration was assessed by ICP-OES.

5.3.5 Relaxivity determination

To assess the relaxivity of the nanocapsules they were redispersed and sonicated as described in the previous section. After centrifugation of the nanocapsules at 4000 rpm for 15 min the supernatant was used to assess the concentration of released Gd while the pellet was resuspended in one fifth of the previous volume. The dispersion of the resuspended pellet was provided for relaxivity measurements and an aliquot was withdrawn for analysis by ICP-OES. The relaxation time, T_1, was determined as described in section 5.3.6 and the Gd concentration (mM) obtained by ICP-OES measurements was fed into the calculation of the relaxivity ($s^{-1} \cdot mM^{-1}$). It was attempted to keep the delay between sample preparation/ICP-OES measurement and T_1 determination as short as possible. The average delay was about 3 h and ranged up to 24 h in the worst case.

5.3.6 Analytical tools

Infrared spectroscopy (IR)

To study the nanocapsule composition the capsule material was analyzed by IR spectroscopy. The samples were freeze dried and 1 mg of powder was pressed with KBr to form a pellet and spectra were recorded between 4000 and 500 cm^{-1} using a IFS 113v Bruker spectrometer. The IR measurements were performed by Elke Muth at the Max Planck Institute for Polymer Research in Mainz.

Dynamic light scattering (DLS)

Dynamic light scattering was used to determine the size distribution of the nanocapsules using a PSS Nicomp Particle Sizer 380 (Nicomp Particle Sizing Systems). Measurements were performed with a 90° scattering angle at ambient conditions. The nanocapsules were diluted in the respective solvent to about 0.5 wt% solutions prior to measurement.

Electron microscopy

A field emission microscope (LEO (Zeiss), 1530 Gemini, Oberkochen, Germany) with an acceleration voltage of 200 V was used to study the capsule morphology by SEM. The samples were diluted in cyclohexane to about 0.01% solid content. Subsequently, they were transferred by drop-casting to a silicon wafer .

Inductively coupled optical emission spectroscopy (ICP-OES)

An Activa M spectrometer (Horiba Jobin Yvon, Bernsheim, Germany) equipped with a Meinhardt-type nebulizer and a cyclone chamber was used for ICP-OES measurements. The device was controlled by ACTIVAnalyst 5.4 software. For the measurement the following conditions were chosen: 1250 W forward plasma power, 12 L·min^{-1} Ar flow and 15 rpm pump flow. As a reference line the Ar emission at 404.442 nm was employed. The emission lines chosen for calibration and quantification of Gd were 354.936 nm and 358.496 nm with a 5 s integration time. For the calibration 5 different standard concentrations were used. The calibration standards were prepared by dilution of a commercial standard in 0.3 wt% SDS solution. Baseline correction and a dynamic underground correction were provided by the software. Prior to measurement, the samples were diluted in aqueous 0.3 wt% SDS solution to obtain concentrations with the calibration range.

T_1 quantification

A 1.5 T magnet in vertical design from Bruker (Karlsruhe, Germany) equipped with an Maran DRX spectrometer (Oxford Instruments, Oxfordshire, UK) was used for the measurement of the relaxation time (T_1). Measurements of pre-heated samples were carried-out at 37 °C. In the NMR coil the sample temperature is kept stable by a stream of heated nitrogen gas. A VT-1000 temperature

controller from Bruker (Karlsruhe, Germany) is used in connection with a home-built liquid nitrogen evaporator. Based on an inversion recovery sequence the longitudinal proton relaxation time (^{1}H-T_1) was measured. The relaxation delay was recorded 15 times per T_1 determination and the resulting spectra were integrated. Subsequently, the resulting data points were fitted with a mono exponential curve and T_1 was determined. The relaxivity r_1 of each sample was obtained as the slope of a linear fit from three independently determined relaxation times. All measurements the required data analysis were performed by Sandro Ebert at the Max Planck Institute for Polymer Research in Mainz.

Spinning drop tensiometry

Interfacial tension measurements were performed on a DCAT21 tensiometer (Dataphysics, Filderstadt, Germany) equipped with a DuNoüy ring (ring diameter: 4.85 mm, wire diameter: 0.15 mm). A motor speed of 0.5 mm·s^{-1} was used throughout all measurements. All investigated compounds were dissolved in water at the concentration used in the nanocapsule preparation. The measurements were carried-out at a water cyclohexane interface. The presented values were averaged over 20 measurements. The surface tension measurements were performed by Elke Muth at the Max Planck Institute for Polymer Research in Mainz.

Chapter 6

Summary

In this thesis the diverse benefits of carbohydrates for nanocapsular systems were studied. Three types of nanocapsules were prepared by interfacial polymerization in inverse miniemulsion. It was demonstrated how carbohydrates could either participate in different nanocapsule forming reactions or lead to an improved sensitivity of an encapsulated contrast agent. In the following paragraphs the results of each project are summarized.

A novel interfacial synthesis for nanocapsules was developed and investigated. Dextran acrylate was synthesized as a multifunctional macromonomer for a ruthenium catalyzed interfacial olefin cross-metathesis in inverse miniemulsion. Dextran was modified such that more than every second sugar unit was functionalized with an acrylate moiety (DS = 0.55). An organic phosphoester (phenyl-di(undec-10-en-1-yl)phosphate) was chosen as oil-soluble monomer. The nanocapsule formation was observed to take place within 2 h after addition of the catalyst. NMR spectra confirmed that the nanocapsules were indeed synthesized by olefin cross-metathesis. Dextran acrylate alone did not polymerize under the used reaction conditions, no capsule formation was observed. The catalyst was removed effectively after the reaction, only trace amounts (low ppm regime) of the catalyst were found to remain in the nanocapsules dispersion. Like polysaccharides, phosphoester belong to a biocompatible and biodegradable class of materials. In comparison to conventional esters, phosphoesters offer an additional opportunity for chemical functionalization. This was demonstrated by the incorporation of fluorescently labeled phosphoesters. The fluorescent label was used study the pH-triggered degradation of the nanocapsules by fluorescence correlation spectroscopy. The modular synthesis is expected to be easily

adaptable to other water-soluble acrylates. Next studies should determine the encapsulation efficiency and confirm the biocompatible character of the nanocapsules by cytotoxicity studies. The development of a purification strategy for the further removal of the catalyst is suggested.

The second project aimed at the treatment of hospital acquired infections by antibiotic resistant bacteria with drug-delivery systems. Dextran methacrylate cross-linked polyacrylamide nanogels were synthesized. Zinc nitrate was encapsulated in the nanogels as an alternative to common antibiotics. Due to the swelling of the nanogels zinc nitrate could not be retained in the nanogels. The swelling increased the hydrodynamic diameter up to 400% of the initial droplet size depending on the DS of dextran methacrylate. The nanogels were modified to control the swelling and improve the retention of zinc ions. Subsequent to hydrogel formation by radical polymerization, pendant nucleophilic groups were reacted with toluene diisocyanate (TDI). Thus, the nanogels were enclosed in a shell. The change towards a capsule morphology was confirmed by SEM and TEM. The capsule formation limited the swelling capability to less than 50%. Simultaneously, the Zn^{2+} release was reduced to 10% per day. The obtained core-shell hybrids were able to inhibit and delay the growth of two different strains of methicillin resistant *S. aureus*. The core-shell hybrids may be applied as coating of wound dressings. The growth of bacteria could then be inhibited locally at the infection site in an early stage of infection. Therefore the viability of a dermal model cell line was tested in presence the nanostructures. The concentrations of nanostructures used in antibacterial testing, had only a small effect on the viability of the investigated model cell line. In future, investigating the cross-linking of gel core and capsule wall could be help to estimate the drug encapsulation efficiency in advance.

A high relaxivity/signal sensitivity of the contrast agent is important for MRI, this can be achieved by a limitation of the contrast agents mobility. In both previous projects the carbohydrates served as monomer in the nanocapsule preparation. The aim of this work was to investigate the parameters for the synthesis of nanocapsules with high relaxivity for MRI. Gadobutrol was chosen as contrast agent for the encapsulation due to its high stability and clinical relevance. The contrast agent was encapsulated in polyurea nanocapsules, which were prepared in an inverse miniemulsion process. In this project the carbohydrates were not used as a monomer but as a agent to alte the nanocapsules properties. The

retention was rather independent of the diamine used in the capsule preparation (1,4-diamino butane: DAB, 1,6-diamino hexane: HMDA). The retention of gadobutrol was increased by the use of excess TDI and diluted gadobutrol solution (0.01 M) in the nanocapsule preparation. The use of DAB as monomer led to a stronger increase of the relaxivity. A reason could be an influence of the more hydrophilic DAB on the capsule preparation process. The lower the amount of monomer used for the capsule formation, the higher the relaxivity. This was probably caused by a reduction of capsule wall thickness. Additionally, the use of excess TDI in the capsule preparation increased the relaxivity. A covalent attachment of gadobutrol to the capsule wall could be a reason for the increased relaxivity but could not be confirmed, yet. The nanocapsules can be tuned to provide either high relaxivity or high signal intensity (retention), depending on the need for the respective MRI measurement.
The relaxivity of the contrast agent is increased in viscous solutions. Molecules such as sucrose, dextran and poly(acrylic acid) sodium salt were co-encapsulated with gadobutrol to increase the viscosity of the nanocapsules core. All co-encapsulation agents led to an increased relaxivity compared to the encapsulation of gadobutrol alone. The co-encapsulation of sucrose doubled the relaxivity of the nanocapsules. This was attributed to a second sphere effect of sucrose, an interaction of contrast agent and sucrose based on hydrogen bonding.

In conclusion, these three projects provided an insight into the manifold ways how carbohydrates can be used for the synthesis and improved performance of nanocarrier systems. An understanding of the underlying physical processes is of importance, especially for the efficient encapsulation and the subsequent release of drugs. In future, the diffusion of drugs and water within and through the nanocapsule wall will require detailed investigations and simulations.

Chapter 7

Zusammenfassung

In dieser Arbeit wurde der vielfältige Nutzen von Kohlenhydraten in Nanokapsel Systemen untersucht. Drei verschiedene Nanokapsel-Typen wurden durch Reaktion an der Grenzfläche von inversen Miniemulsionen hergestellt. Es wurde gezeigt, dass die Kohlenhydrate nach Modifizierung als Monomer an der Kapselbildung teilnehmen können, oder zur Erhöhung der Sensitivität eines verkapselten Kontrastmittels beitragen können. Im Folgenden werden die Ergebnisse der einzelnen Projekte zusammengefasst.

Eine neuartige Grenzflächen-Synthese zur Herstellung von Nanokapseln wurde entwickelt und untersucht. Bei der Reaktion handelt es sich um eine Ruthenium katalysierte Olefin-Kreuzmetathese, welche für die Reaktion an der Grenzfläche angepasst wurde. Als wasserlösliches Macromonomer wurde Dextranacrylat mit einem Subsitutionsgrad von 50% der Zuckereinheiten synthetisiert. Bei dem Reaktionspartner handelte es sich um ein öl-löslichen Phosphoester (Phenyldi(undec-10-en-1-yl)phosphat). Die Kapselbildung konnte bereits zwei Stunden nach Zugabe des Katalysators zur Miniemulsion nachgewiesen werden. Anhand von NMR-Spektren wurde gezeigt, dass die Kapselbildung auf Olefin Kreuzmetathese beruht. Dextranacrylat allein polymerisierte nicht unter den Reaktionsbedingungen, so dass keine Kapseln gebildet wurden. Der Katalysator konnte nach der Reaktion effektiv entfernt werden, so dass davon nur noch Spuren im niedrigen ppm-Bereich nachgewiesen wurden. Sowohl Polysaccharide als auch Phosphoester sind biokompatible und bioabbaubare Moleküle. Im Vergleich zu konventionellen Estern haben Phosphorester eine weitere Möglichkeit zur chemischen Funktionalisierung. Dies wurde exemplarisch durch die Verwendung von fluoreszenzmarkierten Phosphoestern gezeigt. Die Markierung

wurde verwendet, um die pH-induzierte Abbaubarkeit der Nanokapseln mittels Fluoreszenz-Korrelations-Spektroskopie zu beobachten. Die modulare Synthese sollte auch auf andere wasserlösliche Acrylate übertragbar sein. Die nächsten Schritte beinhalten die Untersuchung der Verkapselungseffizienz sowie der Biokompatibilität anhand von Zytotoxizitätsstudien. Die Entfernung des Katalysators könnte durch eine Aufreinigungs-Strategie verbessert werden.

Ziel des zweiten Projekts war es, Nanostrukturen zu entwickeln, um Infektionen mit Antibiotika-resistenten Bakterien lokal zu behandeln. Dazu wurden mit Dextranmethacrylat vernetzte Poly(acrylamid) basierte Nanogele synthetisiert und Zinknitrat als Alternative zu herkömmlichen Antibiotika zugesetzt. Auf Grund des Quellens der Nanogele, konnten die Zinkionen nicht in den Nanogelen gehalten werden. Eine Erhöhung des Nanogeldurchmessers auf 200-400% wurde in Abhängigkeit vom Substitutionsgrad des Dextranmethacrylat beobachtet. Daraufhin wurde die Synthese der Nanogele erweitert, um durch Vernetzung freier Alkoholgruppen mit Toluoldiisocyanat eine Kapselschale zu erhalten. Die Schalenbildung konnte morphologisch mittels Elektronenmikroskopie nachgewiesen werden und spiegelte sich auch in einer geringeren Quellbarkeit der Gel-Schale-Hybride wieder (<50%). Gleichzeitig wurde die Zinkfreisetzung auf 10% pro Tag verringert. Die erhaltenen Gel-Schale-Hybride waren in der Lage das Wachstum von zwei Methicillin-resistenten Bakterienstämmen (*S. aureus*) zu unterdrücken und verzögern. Die synthetisierten Hybridstrukturen könnten in der Beschichtung von Wundauflagen Verwendung finden, um bakterielle Infektionen lokal und direkt nach Ausbruch zu behandeln. Deswegen wurde die Zell-Viabilität einer dermalen Modell Zell-Linie in Gegenwart der Nanostrukturen untersucht. Die in den Bakterien-Tests verwendeten Konzentrationen an Nanostrukturen beeinflussten die Viabilität der untersuchten Zellen nur geringfügig. Eine Untersuchung der Vernetzung von Gel und Schale könnte es ermöglichen, die Verkapselungseffizienz des Wirkstoffes im Vorhinein abzuschätzen.

Eine hohe Relaxivität/Signalsensitivität des Kontrastmittels ist von großer Bedeutung für die Bildgebung mittels MRI, dies kann durch die Begrenzung der Mobilität des Kontrastmittels erreicht werden. Ziel des Projektes war es, die wichtigen Parameter in der Herstellung von Nanokapseln mit hoher Sensitivität zu identifizieren. Aufgrund seiner hohen Komplexstabilität und seiner klinischen Bedeutung wurde das Kontrastmittel Gadobutrol für die Verkapselung verwendet. Das Kontrastmittel wurde in Polyharnstoff-Kapseln eingeschlossen,

die durch einen inversen Miniemulsion-Prozess hergestellt wurden. In diesem Projekt wurden die Kohlenhydrate nicht als Monomer-Baustein für die Kapselbildung verwendet, sondern als Agens im Inneren der Nanokapseln, um deren Eigenschaften zu verändern. Es wurde kein Einfluss der für die Kapselbildung verwendeten Diamine (1,4-Diaminobutan: DAB, 1,6-Diaminohexan: HMDA) auf die Verkapselungseffizienz beobachtet. Der Einsatz von Diisocyanat im Überschuss und die Verwendung von verdünnten Gadobutrol-Lösungen (0.01 M) verbesserten die Verkapselungseffizienz. Bei Verwendung von DAB als Monomer wurde eine größere Steigerung der Relaxivität erreicht. Dies könnte durch die stärkere Hydrophilie des kürzerkettigen Diamines begründet sein. Während mit steigender Monomermenge die Relaxivität reduziert wurde, wird sie durch die Verwendung eines größeren Diisocyanate Überschusses erhöht. Die Relaxivität wird vermutlich durch die Kapselwanddicke und eine kovalente Anbindung des Kontrastmittels an die Kapselwand beeinflusst, dies konnte jedoch noch nicht nachgewiesen werden. Die Synthesebedingungen können je nach Bedarf angepasst werden um Nanokapseln mit hoher Verkapselungseffizienz oder mit hoher Relaxivität herzustellen.
Die Relaxivität des Kontrastmittels ist erhöht in viskosen Lösungen. Um die Viskosität im Inneren der Nanokapsel zu erhöhen, wurden zusätzlich Saccharose, Dextran und Polyacrylsäure verkapselt. In Gegenwart aller drei Verbindungen wurde die Relaxivität im Vergleich zur Verkapselung von Gadobutrol allein weiter erhöht. In Gegenwart von Saccharose konnte die Relaxivität verdoppelt werden. Dies gründet sich vermutlich auf einem "Second-sphere" Effekt der Saccharose, einer auf Wasserstoffbrückenbindungen beruhende Interaktion von Kontrastmittel und Saccharose.

Anhand der hier vorgestellten Projekte, konnte die vielfältige Einsetzbarkeit von Kohlenhydraten in der Synthese und Optimierung von Nanotransportern gezeigt werden. Für die effiziente Verkapselung und kontrollierte Freisetzung von Wirkstoffen ist ein Verständnis der zugrundeliegenden physikalischen Prozesse von besonderer Bedeutung. In Zukunft sollten durch Simulation und experimentelle Untersuchung die Diffusion von Wirkstoffen und Wasser innerhalb und durch die Kapselwand aufgeklärt werden.

Literature

[1] G. Harris, *Seeking Sustainability in an Age of Complexity*, Cambridge University Press, **2007**.

[2] T. M. S. Chang, *Science* **1964**, *146*(3643), 524–525.

[3] J. Ugelstad, M. S. El-Aasser, J. W. Vanderhoff, *J. Polym. Sci. Pol. Lett.* **1973**, *11*(8), 503–513.

[4] K. Landfester, M. Willert, M. Antonietti, *Macromolecules* **2000**, *33*(7), 2370–2376.

[5] D. Crespy, M. Stark, C. Hoffmann-Richter, U. Ziener, K. Landfester, *Macromolecules* **2007**, *40*(9), 3122–3135.

[6] K. J. Whittlesey, L. D. Shea, *Exp. Neurol.* **2004**, *190*(1), 1–16.

[7] A. Lehninger, D. Nelson, M. Cox, *Lehninger Principles of Biochemistry*, W. H. Freeman, **2005**.

[8] V. R. Sinha, R. Kumria, *Int. J. Pharm.* **2001**, *224*(1-2), 19–38.

[9] I. W. Sutherland, *Microbiology+* **2001**, *147*(1), 3–9.

[10] L. Pasteur, *Bull. Soc. Chim.* **1861**, 30.

[11] M. Naessens, A. Cerdobbel, W. Soetaert, E. J. Vandamme, *J. Chem. Technol. Biotechnol.* **2005**, *80*(8), 845–860.

[12] T. Heinze, T. Liebert, B. Heublein, S. Hornig, in *Polysaccharides II*, Bd. 205 von *Advances in Polymer Science*, (Herausgegeben von D. Klemm), Springer Berlin Heidelberg, **2006**, 199–291.

[13] E. Braswell, A. Goodman, K. G. Stern, *J Polym Sci* **1962**, *61*(171), 143–154.

[14] K. A. Granath, P. Flodin, *Makromol. Chem.* **1961**, *48*(1), 160–171.

[15] M. Zief, G. Brunner, J. Metzendorf, *Ind. Eng. Chem.* **1956**, *48*(1), 119–121.

[16] I. A. Wolff, C. L. Mehltretter, R. L. Mellies, P. R. Watson, B. T. Hofreiter, P. L. Patrick, C. E. Rist, *Ind. Eng. Chem.* **1954**, *46*(2), 370–377.

[17] A. DeBelder, in *Amersham bioscience*, **2003**.

[18] T. D. Leathers, *Dextran*, Wiley-VCH Verlag GmbH & Co. KGaA, Kap. 12, **2005**, 299–321.

[19] F. Chaubet, R. Huynh, J. Champion, J. Jozefonvicz, D. Letourneur, *Polym. Int.* **1999**, *48*(4), 313–319.

[20] T. Sato, J. Nishimura-Uemura, T. Shimosato, Y. Kawai, H. Kitazawa, T. Saito, *J Food Protect* **2004**, *67*(8), 1719–1724.

[21] F. Arranz, M. Sanchez-Chaves, J. C. Ramirez, *Angew. Makromol. Chem.* **1992**, *194*(1), 79–89.

[22] R. Mehvar, *J. Control. Release* **2000**, *69*(1), 1–25.

[23] C. Larsen, *Adv. Drug Delivery Reviews* **1989**, *3*(1), 103–154, prodrugs for Improved Drug Delivery.

[24] A. de Belder, *Medical application of dextran and its derivatives*, CRC Press, Kap. 12, **1996**, 505–525.

[25] J. Zhang, R. Pelton, L. Wagberg, *Colloid Polym. Sci.* **1998**, *276*(6), 476–482.

[26] M. Beesh, P. Majewska, F. Vandamme, *Int. J. Drug Delivery* **2011**, *2*(1), 22–31.

[27] S.-H. Kim, C.-Y. Won, C.-C. Chu, *J. Biomed. Mater. Res.* **1999**, *46*(2), 160–170.

[28] L. Chen, J. Dong, Y. Ding, W. Han, *J. Appl. Polym. Sci.* **2005**, *96*(6), 2435–2439.

[29] L. M. Landoll, *J. Polym. Sci. Pol. Chem.* **1982**, *20*(2), 443–455.

[30] C. Rouzes, R. Gref, M. Leonard, A. De Sousa Delgado, E. Dellacherie, *J. Biomed. Mater. Res.* **2000**, *50*(4), 557–565.

[31] A. de Belder, B. Norrman, *Carbohyd. Res.* **1969**, *10*(3), 391–394.

[32] J. Robyt, in *Essentials of Carbohydrate Chemistry*, Springer New York, Springer Advanced Texts in Chemistry, **1998**, 328–344.

[33] L. Zevenhuizen, *Carbohyd. Res.* **1968**, *6*(3), 310–318.

[34] J. F. Robyt, R. J. Ackerman, *Arch. Biochem. Biophys.* **1971**, *145*(1), 105–114.

[35] G. Baier, A. Cavallaro, K. Vasilev, V. Mailänder, A. Musyanovych, K. Landfester, *Biomacromolecules* **2013**, *14*(4), 1103–1112.

[36] X. Huang, D. Appelhans, P. Formanek, F. Simon, B. Voit, *Macromolecules* **2011**, *44*(21), 8351–8360.

[37] A. D. Price, A. P. Johnston, G. K. Such, F. Caruso, in *Modern Techniques for Nano- and Microreactors/-reactions*, Bd. 229 von *Advances in Polymer Science*, (Herausgegeben von F. Caruso), Springer Berlin Heidelberg, **2010**, 155–179.

[38] K. Landfester, *Macromol. Rapid Comm.* **2001**, *22*(12), 896–936.

[39] H. Bader, H. Ringsdorf, B. Schmidt, *Angew. Makromol. Chem.* **1984**, *123*(1), 457–485.

[40] F. Chécot, J. Rodríguez-Hernández, Y. Gnanou, S. Lecommandoux, *Biomol. Eng.* **2007**, *24*(1), 81–85.

[41] G. Riess, *Prog. Polym. Sci.* **2003**, *28*(7), 1107–1170.

[42] M. Yokoyama, S. Inoue, K. Kataoka, N. Yui, Y. Sakurai, *Makromol. Chem., Rapid Commun.* **1987**, *8*(9), 431–435.

[43] A. S. Narang, D. Delmarre, D. Gao, *Int. J. Pharm.* **2007**, *345*(1-2), 9–25.

[44] M. Massignani, H. Lomas, G. Battaglia, in *Modern Techniques for Nano- and Microreactors/-reactions*, Bd. 229 von *Advances in Polymer Science*, (Herausgegeben von F. Caruso), Springer Berlin Heidelberg, **2010**, 115–154.

[45] C. LoPresti, H. Lomas, M. Massignani, T. Smart, G. Battaglia, *J. Mater. Chem.* **2009**, *19*(22), 3576–3590.

[46] B. M. Discher, Y.-Y. Won, D. S. Ege, J. C.-M. Lee, F. S. Bates, D. E. Discher, D. A. Hammer, *Int. S. Techn. Pol. Inn.* **1999**, *284*(5417), 1143–1146.

[47] B. M. Discher, D. A. Hammer, F. S. Bates, D. E. Discher, *Curr. Opin. Colloid In.* **2000**, *5*(1-2), 125–131.

[48] F. Meng, C. Hiemstra, G. H. M. Engbers, J. Feijen, *Macromolecules* **2003**, *36*(9), 3004–3006.

[49] O. Onaca, R. Enea, D. W. Hughes, W. Meier, *Macromol. Biosci.* **2009**, *9*(2), 129–139.

[50] J. S. Lee, J. Feijen, *J. Control. Release* **2012**, *161*(2), 473–483, drug Delivery Research in Europe.

[51] K. Landfester, A. Musyanovych, V. Mailänder, *J. Polym. Sci. Pol. Chem.* **2010**, *48*(3), 493–515.

[52] K. Landfester, *Angew. Chem. Int. Edit.* **2009**, *48*(25), 4488–4507.

[53] K. Landfester, *Macromol. Symp.* **2000**, *150*(1), 171–178.

[54] H.-D. Dörfler, *Grenzflächen und kolloid-disperse Systeme: Physik und Chemie*, Springer, **2002**.

[55] P. Taylor, *Adv. Colloid Interfac.* **1998**, *75*(2), 107–163.

[56] G. W. Burton, C. P. O'Farrell, *J Elastom Plast* **1977**, *9*(1), 94–101.

[57] J. P. Rao, K. E. Geckeler, *Prog. Polym. Sci.* **2011**, *36*(7), 887–913.

[58] N. Anton, J.-P. Benoit, P. Saulnier, *J. Control. Release* **2008**, *128*(3), 185–199.

[59] X. Wang, T. Jin, V. Comblin, A. Lopez-Mut, E. Merciny, J. F. Desreux, *Inorg. Chem.* **1992**, *31*(6), 1095–1099.

[60] G. Lambert, E. Fattal, H. Pinto-Alphandary, A. Gulik, P. Couvreur, *Pharmaceut. Res.* **2000**, *17*(6), 707–714.

[61] A. Musyanovych, K. Landfester, in *Surface and Interfacial Forces - From Fundamentals to Applications*, Bd. 134 von *Progress in Colloid and Polymer Science*, (Herausgegeben von G. Auernhammer, H.-J. Butt, D. Vollmer), Springer Berlin Heidelberg, **2008**, 120–127.

[62] F. Tiarks, K. Landfester, M. Antonietti, *Langmuir* **2001**, *17*(3), 908–918.

[63] A. J. van Zyl, R. F. Bosch, J. B. McLeary, R. D. Sanderson, B. Klumperman, *Polymer* **2005**, *46*(11), 3607–3615.

[64] S. K. Yadav, N. Ron, D. Chandrasekharam, K. C. Khilar, A. K. Suresh, V. M. Nadkarni, *J. Macromol. Sci. B* **1996**, *35*(5), 807–827.

[65] C. Ramarao, S. V. Ley, S. C. Smith, I. M. Shirley, N. DeAlmeida, *Chem. Commun.* **2002**, (10), 1132–1133.

[66] F. Gaudin, N. Sintes-Zydowicz, *Colloids and Surfaces A: Physicochem. Eng. Aspects* **2012**, *415*(0), 328–342.

[67] E. Sharmin, F. Zafar, *Polyurethane: An Introduction*, InTech, Kap. 1, **2012**, 3–16.

[68] U. Paiphansiri, J. Dausend, A. Musyanovych, V. Mailänder, K. Landfester, *Macromol. Biosci.* **2009**, *9*(6), 575–584.

[69] E.-M. Rosenbauer, K. Landfester, A. Musyanovych, *Langmuir* **2009**, *25*(20), 12084–12091, pMID: 19618925.

[70] M. Takasu, H. Kawaguchi, *Colloid Polym. Sci.* **2005**, *283*(7), 805–811.

[71] I. Montasser, S. Briançon, H. Fessi, *Int. J. Pharm.* **2007**, *335*(1-2), 176–179.

[72] L. Spernath, S. Magdassi, *Polym. Advan. Technol.* **2011**, *22*(12), 2469–2473.

[73] J. Andrieu, N. Kotman, M. Maier, V. Mailänder, W. S. L. Strauss, C. K. Weiss, K. Landfester, *Macromol. Rapid Comm.* **2012**, *33*(3), 248–253.

[74] G. Baier, A. Musyanovych, M. Dass, S. Theisinger, K. Landfester, *Biomacromolecules* **2010**, *11*(4), 960–968.

[75] G. Baier, D. Baumann, J. M. Siebert, A. Musyanovych, V. Mailänder, K. Landfester, *Biomacromolecules* **2012**, *13*(9), 2704–2715.

[76] H. C. Kolb, M. G. Finn, K. B. Sharpless, *Angew. Chem. Int. Edit.* **2001**, *40*(11), 2004–2021.

[77] C. E. Hoyle, C. N. Bowman, *Angew. Chem. Int. Edit.* **2010**, *49*(9), 1540–1573.

[78] M. P. Lutolf, N. Tirelli, S. Cerritelli, L. Cavalli, J. A. Hubbell, *Bioconjugate Chem* **2001**, *12*(6), 1051–1056.

[79] H. Kakwere, S. Perrier, *J. Am. Chem. Soc.* **2009**, *131*(5), 1889–1895.

[80] M. Heggli, N. Tirelli, A. Zisch, J. A. Hubbell, *Bioconjugate Chem* **2003**, *14*(5), 967–973.

[81] J. Zou, C. C. Hew, E. Themistou, Y. Li, C.-K. Chen, P. Alexandridis, C. Cheng, *Adv Mater* **2011**, *23*(37), 4274–4277.

[82] J. M. Siebert, G. Baier, A. Musyanovych, K. Landfester, *Chem. Commun.* **2012**, *48*(44), 5470–5472.

[83] S. Kai, M. Ashaduzzaman, S. Uemura, M. Kunitake, *Chem. Lett.* **2011**, *40*(3), 270–272.

[84] C. Wohnhaas, K. Friedemann, D. Busko, K. Landfester, S. Baluschev, D. Crespy, A. Turshatov, *ACS Macro Letters* **2013**, *2*(5), 446–450.

[85] M. Han, E. Lee, E. Kim, *Optical Materials* **2003**, *21*(1-3), 579–583.

[86] K. P. McNamara, Z. Rosenzweig, *Anal. Chem.* **1998**, *70*(22), 4853–4859.

[87] A. P. Esser-Kahn, S. A. Odom, N. R. Sottos, S. R. White, J. S. Moore, *Macromolecules* **2011**, *44*(14), 5539–5553.

[88] C.-J. Ke, T.-Y. Su, H.-L. Chen, H.-L. Liu, W.-L. Chiang, P.-C. Chu, Y. Xia, H.-W. Sung, *Angew. Chem. Int. Edit.* **2011**, *50*(35), 8086–8089.

[89] K. E. Broaders, S. J. Pastine, S. Grandhe, J. M. J. Frechet, *Chem. Commun.* **2011**, *47*, 665–667.

[90] X. Yuan, K. Fischer, W. Schärtl, *Langmuir* **2005**, *21*(20), 9374–9380.

[91] W. Ong, Y. Yang, A. C. Cruciano, R. L. McCarley, *J. Am. Chem. Soc.* **2008**, *130*(44), 14739–14744.

[92] M. Volz, P. Walther, U. Ziener, K. Landfester, *Macromol. Mater. Eng.* **2007**, *292*(12), 1237–1244.

[93] M. Bannwarth, Dissertation, Johannes Gutenberg-Universität, **2014**.

[94] A. Vimalanandan, L.-P. Lv, T. H. Tran, K. Landfester, D. Crespy, M. Rohwerder, *Adv. Mater.* **2013**, *25*(48), 6980–6984.

[95] D. G. Shchukin, M. Zheludkevich, K. Yasakau, S. Lamaka, M. G. S. Ferreira, H. Möhwald, *Advanced Materials* **2006**, *18*(13), 1672–1678.

[96] W. Binder, *Self-Healing Polymers: From Principles to Applications*, Wiley, **2013**.

[97] S. R. White, N. R. Sottos, P. H. Geubelle, J. S. Moore, M. R. Kessler, S. R. Sriram, E. N. Brown, S. Viswanathan, *Nature* **2001**, *409*(6822), 794–797.

[98] M. Keller, S. White, N. Sottos, *Adv. Funct. Mater.* **2007**, *17*(14), 2399–2404.

[99] B. Blaiszik, N. Sottos, S. White, *Composites Science and Technology* **2008**, *68*(3-4), 978–986.

[100] J. Dausend, A. Musyanovych, M. Dass, P. Walther, H. Schrezenmeier, K. Landfester, V. Mailänder, *Macromol. Biosci.* **2008**, *8*(12), 1135–1143.

[101] S. Vrignaud, J.-P. Benoit, P. Saulnier, *Biomaterials* **2011**, *32*(33), 8593–8604.

[102] R. Nagarajan, in *Solvents and Self-Organization of Polymers*, Bd. 327 von *NATO ASI Series*, (Herausgegeben von S. Webber, P. Munk, Z. Tuzar), Springer Netherlands, **1996**, 121–165.

[103] K. Kataoka, A. Harada, Y. Nagasaki, *Adv. Drug Deliver. Rev.* **2001**, *47*(1), 113–131.

[104] V. Torchilin, *J. Control. Release* **2001**, *73*(2-3), 137–172.

[105] S. C. Yadav, A. Kumari, R. Yadav, *Peptides* **2011**, *32*(1), 173–187.

[106] C. P. Reis, R. J. Neufeld, A. J. Ribeiro, F. Veiga, *Nanomed-Nanotechnol* **2006**, *2*(2), 53–65.

[107] M. A. Dobrovolskaia, S. E. McNeil, *Nat. Nano.* **2007**, *2*(8), 469–478.

[108] C. P. Reis, R. J. Neufeld, A. J. Ribeiro, , F. Veiga, *Nanomed-Nanotechnol.* **2006**, *2*(1), 8–21.

[109] M. Goldberg, R. Langer, J. Xinqiao, *J. Biomat. Sci.-Polym. E.* **2007**, *18*(3), 241–268.

[110] D. Kalaria, G. Sharma, V. Beniwal, M. Ravi Kumar, *Pharmaceut Res* **2009**, *26*(3), 492–501.

[111] G. Lambert, J. R. Bertrand, E. Fattal, F. Subra, H. Pinto-Alphandary, C. Malvy, C. Auclair, P. Couvreur, *Biochem. Bioph. Res. Co.* **2000**, *279*(2), 401–406.

[112] D. Peer, J. M. Karp, S. Hong, O. C. Farokhzad, R. Margalit, R. Langer, *Nat. Nano.* **2007**, *2*(12), 751–760.

[113] V. P. Torchilin, *Nat. Rev. Drug Discov.* **2005**, *4*(2), 145–160.

[114] S. Cavalieri, A. S. for Microbiology, *Manual of Antimicrobial Susceptibility Testing*, American Society for Microbiology, **2009**.

[115] M. Gross, S. E. Cramton, F. Götz, A. Peschel, *Infect. Immun.* **2001**, *69*(5), 3423–3426.

[116] A. Peschel, C. Vuong, M. Otto, F. Götz, *Antimicrob. Agents Chemother.* **2000**, *44*(10), 2845–2847.

[117] C. von Eiff, K. Becker, K. Machka, H. Stammer, G. Peters, *N. Engl. J. Med.* **2001**, *344*(1), 11–16, pMID: 11136954.

[118] S. E. Cramton, M. Ulrich, F. Götz, G. Döring, *Infect. Immun.* **2001**, *69*(6), 4079–4085.

[119] G. Y. Liu, *Pediatr. Res.* **2009**, *65*(5 Part 2), 71R–77R.

[120] C. von Eiff, C. Heilmann, G. Peters, *Eur. J. Clin. Microbiol. Infect. Dis.* **1999**, *18*(12), 843–846.

[121] D. Pavithra, M. Doble, *Biomed Mater* **2008**, *3*(3).

[122] M. Hussain, M. Wilcox, P. White, *FEMS Microbiol. Rev.* **1993**, *10*(3-4), 191–207.

[123] K. Page, M. Wilson, I. P. Parkin, *J. Mater. Chem.* **2009**, *19*, 3819–3831.

[124] I. Banerjee, R. C. Pangule, R. S. Kane, *Advanced Materials* **2011**, *23*(6), 690–718.

[125] K. Prime, G. Whitesides, *Science* **1991**, *252*(5009), 1164–1167.

[126] G. Cheng, Z. Zhang, S. Chen, J. D. Bryers, S. Jiang, *Biomaterials* **2007**, *28*(29), 4192–4199.

[127] J. A. Nagel, R. B. Dickinson, S. L. Cooper, *J. Biomater. Sci. Polym. Ed.* **1996**, *7*(9), 769–780.

[128] M. Zasloff, *Nature* **2002**, *415*(6870), 389–395.

[129] F. Costa, I. F. Carvalho, R. C. Montelaro, P. Gomes, M. C. L. Martins, *Acta Biomater.* **2011**, *7*(4), 1431–1440.

[130] L. Ferreira, A. Zumbuehl, *J. Mater. Chem.* **2009**, *19*(42), 7796–7806.

[131] E.-R. Kenawy, S. D. Worley, R. Broughton, *Biomacromolecules* **2007**, *8*(5), 1359–1384.

[132] P. Li, Y. F. Poon, W. Li, H.-Y. Zhu, S. H. Yeap, Y. Cao, X. Qi, C. Zhou, M. Lamrani, R. W. Beuerman, E.-T. Kang, Y. Mu, C. M. Li, M. W. Chang, S. S. Jan Leong, M. B. Chan-Park, *Nat. Mater.* **2011**, *10*(2), 149–156.

[133] P. Wu, D. W. Grainger, *Biomaterials* **2006**, *27*(11), 2450–2467.

[134] E. M. Hetrick, M. H. Schoenfisch, *Chem. Soc. Rev.* **2006**, *35*, 780–789.

[135] J. J. Curtin, R. M. Donlan, *Antimicrob. Agents Chemother.* **2006**, *50*(4), 1268–1275.

[136] A. Sulakvelidze, Z. Alavidze, J. G. Morris, *Antimicrob. Agents Chemother.* **2001**, *45*(3), 649–659.

[137] G. W. Hanlon, *Int. J. Antimicrob. Agents* **2007**, *30*(2), 118–128.

[138] R. Kumar, H. Münstedt, *Biomaterials* **2005**, *26*(14), 2081–2088.

[139] C. Marambio-Jones, E. M. Hoek, *J. Nanopart. Res.* **2010**, *12*(5), 1531–1551.

[140] M. Li, L. Zhu, D. Lin, *Environ. Sci. Technol.* **2011**, *45*(5), 1977–1983.

[141] P. Gajjar, B. Pettee, D. Britt, W. Huang, W. Johnson, A. Anderson, *J. Biol. Eng.* **2009**, *3*(1), 9–22.

[142] B. Sugarman, *Rev. Infect. Dis.* **1983**, *5*(1), 137–147.

[143] V. B. Schwartz, F. Thétiot, S. Ritz, S. Pütz, L. Choritz, A. Lappas, R. Förch, K. Landfester, U. Jonas, *Adv. Funct. Mater.* **2012**, *22*(11), 2376–2386.

[144] R. Rajendra, C. Balakumar, H. Ahammed, S. Jayakumar, K. Vaideki, E. Rajesh, *Int. J. Eng. Sci. Technol.* **2010**, *2*(1), 202–208.

[145] L. Zhang, Y. Jiang, Y. Ding, N. Daskalakis, L. Jeuken, M. Povey, A. J. O'Neill, D. W. York, *J. Nanopart. Res.* **2010**, *12*(5), 1625–1636.

[146] N. Padmavathy, R. Vijayaraghavan, *Sci. Technol. Adv. Mat.* **2008**, *9*(3), 035004.

[147] V. V. Komnatnyy, W.-C. Chiang, T. Tolker-Nielsen, M. Givskov, T. E. Nielsen, *Angew. Chem. Int. Edit.* **2014**, *53*(2), 439–441.

[148] J. Zhou, A. L. Loftus, G. Mulley, A. T. A. Jenkins, *J. Am. Chem. Soc.* **2010**, *132*(18), 6566–6570.

[149] P. Caravan, J. J. Ellison, T. J. McMurry, R. B. Lauffer, *Chem. Rev.* **1999**, *99*(9), 2293–2352.

[150] B.-T. Doan, S. Meme, J.-C. Beloeil, *General Principles of MRI*, John Wiley & Sons, Ltd, Kap. 1, **2013**, 1–23.

[151] v. Tóth, L. Helm, A. Merbach, in *Contrast Agents I*, Bd. 221 von *Topics in Current Chemistry*, (Herausgegeben von W. Krause), Springer Berlin Heidelberg, **2002**, 61–101.

[152] v. Tóth, L. Helm, A. Merbach, *Relaxivity of Gadolinium(III) Complexes: Theory and Mechanism*, John Wiley & Sons, Ltd, Kap. 2, **2013**, 25–81.

[153] R. B. Lauffer, *Chem. Rev.* **1987**, *87*(5), 901–927.

[154] E. Werner, A. Datta, C. Jocher, K. Raymond, *Angew. Chem. Int. Edit.* **2008**, *47*(45), 8568–8580.

[155] S. Aime, M. Fasano, E. Terreno, *Chem. Soc. Rev.* **1998**, *27*, 19–29.

[156] P. Wedeking, K. Kumar, M. Tweedle, *Magn. Reson. Imaging* **1992**, *10*(4), 641–648.

[157] F. Franano, W. Edwards, M. J. Welch, M. W. Brechbiel, O. A. Gansow, J. R. Duncan, *Magn. Reson. Imaging* **1995**, *13*(2), 201–214.

[158] P. Marckmann, L. Skov, K. Rossen, A. Dupont, M. B. Damholt, J. G. Heaf, H. S. Thomsen, *J. Am. Soc. Nephrol.* **2006**, *17*(9), 2359–2362.

[159] E. Terreno, D. D. Castelli, A. Viale, S. Aime, *Chem. Rev.* **2010**, *110*(5), 3019–3042.

[160] D. Zhu, F. Liu, L. Ma, D. Liu, Z. Wang, *Int. J. Mol. Sci.* **2013**, *14*(5), 10591–10607.

[161] M. G. Duarte, M. H. Gil, J. A. Peters, J. M. Colet, L. V. Elst, R. N. Muller, C. F. G. C. Geraldes, *Bioconjugate Chem.* **2001**, *12*(2), 170–177.

[162] V. Torchilin, *Curr Pharm Biotechno* **2000**, *1*(2), 183–215.

[163] M. Rohrer, H. Bauer, J. Mintorovitch, M. Requardt, H.-J. Weinmann, *Invest. Radiol.* **2005**, *40*(11), 715–724.

[164] C. Casali, M. Janier, E. Canet, J. Obadia, S. Benderbous, C. Corot, D. Revel, *Acad. Radiol.* **1998**, *5*(1), S214–S218.

[165] J. L. Turner, D. Pan, R. Plummer, Z. Chen, A. K. Whittaker, K. L. Wooley, *Adv. Funct. Mater.* **2005**, *15*(8), 1248–1254.

[166] Z. Cheng, D. L. J. Thorek, A. Tsourkas, *Angew. Chem. Int. Edit.* **2010**, *49*(2), 346–350.

[167] Z. Zhang, M. T. Greenfield, M. Spiller, T. J. McMurry, R. B. Lauffer, P. Caravan, *Angew. Chem. Int. Edit.* **2005**, *44*(41), 6766–6769.

[168] E. Spuentrup, A. Buecker, M. Katoh, A. J. Wiethoff, E. C. Parsons, R. M. Botnar, R. M. Weisskoff, P. B. Graham, W. J. Manning, R. W. Günther, *Circulation* **2005**, *111*(11), 1377–1382.

[169] W. J. M. Mulder, G. J. Strijkers, A. W. Griffioen, L. van Bloois, G. Molema, G. Storm, G. A. Koning, K. Nicolay, *Bioconjugate Chem* **2004**, *15*(4), 799–806.

[170] S. Flacke, S. Fischer, M. J. Scott, R. J. Fuhrhop, J. S. Allen, M. McLean, P. Winter, G. A. Sicard, P. J. Gaffney, S. A. Wickline, G. M. Lanza, *Circulation* **2001**, *104*(11), 1280–1285.

[171] A. M. Morawski, P. M. Winter, K. C. Crowder, S. D. Caruthers, R. W. Fuhrhop, M. J. Scott, J. D. Robertson, D. R. Abendschein, G. M. Lanza, S. A. Wickline, *Magn. Reson. Med.* **2004**, *51*(3), 480–486.

[172] P. M. Winter, S. D. Caruthers, X. Yu, S.-K. Song, J. Chen, B. Miller, J. W. Bulte, J. D. Robertson, P. J. Gaffney, S. A. Wickline, G. M. Lanza, *Magn. Reson. Med.* **2003**, *50*(2), 411–416.

[173] G. Ratzinger, P. Agrawal, W. Körner, J. Lonkai, H. d. Sanders, E. Terreno, M. Wirth, G. Strijkers, K. Nicolay, F. Gabor, *Biomaterials* **2010**, *31*(33), 8716–8723.

[174] Z. Cheng, D. L. J. Thorek, A. Tsourkas, *Adv. Funct. Mater.* **2009**, *19*(23), 3753–3759.

[175] P. Caravan, *Chem. Soc. Rev.* **2006**, *35*, 512–523.

[176] J. S. Ananta, B. Godin, R. Sethi, L. Moriggi, X. Liu, R. E. Serda, R. Krishnamurthy, R. Muthupillai, R. D. Bolskar, L. Helm, M. Ferrari, L. J. Wilson, P. Decuzzi, *Nat. Nano.* **2010**, *5*(11), 815–821.

[177] S. Santra, R. P. Bagwe, D. Dutta, J. T. Stanley, G. A. Walter, W. Tan, B. M. Moudgil, R. A. Mericle, *Adv Mater* **2005**, *17*(18), 2165–2169.

[178] Y.-S. Lin, Y. Hung, J.-K. Su, R. Lee, C. Chang, M.-L. Lin, C.-Y. Mou, *J. Phys. Chem. B* **2004**, *108*(40), 15608–15611.

[179] N. Jagielski, S. Sharma, V. Hombach, V. Mailänder, V. Rasche, K. Landfester, *Macromol. Chem. Physic* **2007**, *208*(19-20), 2229–2241.

[180] S. Sharma, Dissertation, University of Ulm, **2009**.

[181] Y. Liu, N. Zhang, *Biomaterials* **2012**, *33*(21), 5363–5375.

[182] C. Tilcock, E. Unger, P. Cullis, P. MacDougall, *Radiology* **1989**, *171*(1), 77–80.

[183] S. Hak, H. M. Sanders, P. Agrawal, S. Langereis, H. Grüll, H. M. Keizer, F. Arena, E. Terreno, G. J. Strijkers, K. Nicolay, *Eur. J. Pharm. Biopharm.* **2009**, *72*(2), 397–404.

[184] M. S. Bhojani, M. Van Dort, A. Rehemtulla, B. D. Ross, *Mol. Pharmaceut.* **2010**, *7*(6), 1921–1929.

[185] S. Greenfield, I. L. Jones, C. T. Berry, *Analyst* **1964**, *89*, 713–720.

[186] J. Nölte, *ICP Emission Spectrometry: A Practical Guide*, Wiley, **2003**.

[187] J. W. Olesik, *Anal. Chem.* **1991**, *63*(1), 12A–21A.

[188] C. Dubuisson, E. Poussel, J. Todoli, J. Mermet, *Spectrochim. Acta B* **1998**, *53*(4), 593–600.

[189] N. Vogel, C. P. Hauser, K. Schuller, K. Landfester, C. K. Weiss, *Macromol. Chem. Physic* **2010**, *211*(12), 1355–1368.

[190] M. Knoll, E. Rusaka, *Z. Tech. Phys.* **1932**, *78*, 318–339.

[191] V. Zworykin, J. Hillier, R. Snyder, *ASTM Bull.* **1942**, *117*, 15–23.

[192] J. Goldstein, *Scanning Electron Microscopy and X-ray Microanalysis: Third Edition*, Springer US, **2003**.

[193] W. Schaertl, in *Light Scattering from Polymer Solutions and Nanoparticle Dispersions*, Springer Berlin Heidelberg, Springer Laboratory, **2007**, 1–24.

[194] M. Schmidt, W. Burchard, N. C. Ford, *Macromolecules* **1978**, *11*(3), 452–454.

[195] K. Malzahn, F. Marsico, K. Koynov, K. Landfester, C. K. Weiss, F. R. Wurm, *ACS Macro Letters* **2014**, *3*(1), 40–43.

[196] A. A. Shah, F. Hasan, A. Hameed, S. Ahmed, *Biotechnol Adv* **2008**, *26*(3), 246–265.

[197] L. S. Nair, C. T. Laurencin, *Prog. Polym. Sci.* **2007**, *32*(8-9), 762–798.

[198] C. K. Williams, *Chem. Soc. Rev.* **2007**, *36*(10), 1573–1580.

[199] S. Mizrahy, D. Peer, *Chem. Soc. Rev.* **2012**, *41*(7), 2623–2640.

[200] R. Mehta, V. Kumar, H. Bhunia, S. N. Upadhyay, *J. Macromol. Sci. C* **2005**, *45*(4), 325–349.

[201] Y.-C. Wang, Y.-Y. Yuan, J.-Z. Du, X.-Z. Yang, J. Wang, *Macromol. Biosci.* **2009**, *9*(12), 1154–1164.

[202] T. Steinbach, E. M. Alexandrino, F. R. Wurm, *Polymer Chemistry* **2013**, *4*(13), 3800–3806.

[203] F. Marsico, A. Turshatov, K. Weber, F. R. Wurm, *Org. Lett.* **2013**, *15*(15), 3844–3847.

[204] S. Yang, H. Liu, Z. Zhang, *J. Polym. Sci. Pol. Chem.* **2008**, *46*(12), 3900–3910.

[205] K. Landfester, C. Weiss, in *Modern Techniques for Nano- and Microreactors/-reactions*, Bd. 229 von *Advances in Polymer Science*, (Herausgegeben von F. Caruso), Springer Berlin Heidelberg, **2010**, 1–49.

[206] C.-K. Chen, W.-C. Law, R. Aalinkeel, Y. Yu, B. Nair, J. Wu, S. Mahajan, J. L. Reynolds, Y. Li, C. K. Lai, E. S. Tzanakakis, S. A. Schwartz, P. N. Prasad, C. Cheng, *Nanoscale* **2014**, *6*(3), 1567–1572.

[207] J. E. Moses, A. D. Moorhouse, *Chem. Soc. Rev.* **2007**, *36*(8), 1249–1262.

[208] C. A. DeForest, B. D. Polizzotti, K. S. Anseth, *Nat. Mater.* **2009**, *8*(8), 659–664.

[209] D. Burtscher, K. Grela, *Angew. Chem. Int. Edit.* **2009**, *48*(3), 442–454.

[210] M. Schuster, S. Blechert, *Angew. Chem. Int. Ed. Engl.* **1997**, *36*(19), 2036–2056.

[211] A. Chemtob, V. Héroguez, Y. Gnanou, *J. Polym. Sci. Pol. Chem.* **2004**, *42*(5), 1154–1163.

[212] K. Breitenkamp, T. Emrick, *J. Am. Chem. Soc.* **2003**, *125*(40), 12070–12071.

[213] L. Gulajski, P. Sledz, A. Lupa, K. Grela, *Green Chem* **2008**, *10*(3), 271–274.

[214] I. A. Gorodetskaya, T.-L. Choi, R. H. Grubbs, *J. Am. Chem. Soc.* **2007**, *129*(42), 12672–12673.

[215] A. H. Hoveyda, D. G. Gillingham, J. J. Van Veldhuizen, O. Kataoka, S. B. Garber, J. S. Kingsbury, J. P. A. Harrity, *Org. Biomol. Chem.* **2004**, *2*(1), 8–23.

[216] S. Demel, C. Slugovc, F. Stelzer, K. Fodor-Csorba, G. Galli, *Macromol. Rapid Comm.* **2003**, *24*(10), 636–641.

[217] D. Klinger, E. M. Aschenbrenner, C. K. Weiss, K. Landfester, *Polymer Chemistry* **2012**, *3*(1), 204–216.

[218] K. Koynov, H.-J. Butt, *Curr. Opin. Colloid In.* **2012**, *17*(6), 377–387.

[219] A. M. Basedow, K. H. Ebert, H. J. Ederer, *Macromolecules* **1978**, *11*(4), 774–781.

[220] F. Marsico, M. Wagner, K. Landfester, F. R. Wurm, *Macromolecules* **2012**, *45*(21), 8511–8518.

[221] T. Steinbach, R. Schroder, S. Ritz, F. R. Wurm, *Polym. Chem.* **2013**, *4*, 4469–4479.

[222] K. Malzahn, W. D. Jamieson, M. Dröge, V. Mailänder, A. T. A. Jenkins, C. K. Weiss, K. Landfester, *J. Mater. Chem. B* **2014**, *2*, 2175–2183.

[223] P. Tenke, C. R. Riedl, G. L. Jones, G. J. Williams, D. Stickler, E. Nagy, *Int J Antimicrob Ag* **2004**, *23*, S67–S74.

[224] M. Katsikogianni, Y. F. Missirlis, *Eur. Cell Mater.* **2004**, *8*, 37–57.

[225] C. A. Fux, J. W. Costerton, P. S. Stewart, P. Stoodley, *Trends Microbiol.* **2005**, *13*(1), 34–40.

[226] A. Dubin, P. Mak, G. Dubin, M. Rzychon, J. Stec-Niemczyk, B. Wladyka, K. Maziarka, D. Chmiel, *Acta Biochim. Pol.* **2005**, *52*(3), 633–638.

[227] T. Koburger, N.-O. Hübner, M. Braun, J. Siebert, A. Kramer, *J. Antimicrob. Chemoth.* **2010**, *65*(8), 1712–1719.

[228] M. L. Kääriäinen, C. K. Weiss, S. Ritz, S. Pütz, D. C. Cameron, V. Mailänder, K. Landfester, *Appl. Surf. Sci.* **2013**, *287*(0), 375–380.

[229] C. James, A. L. Johnson, A. T. A. Jenkins, *Chem. Commun.* **2011**, *47*(48), 12777–12779.

[230] C. James, T. Pugh, A. L. Johnson, A. T. A. Jenkins, *Eur. Polym. J.* **2011**, *47*(6), 1338–1345.

[231] V. Thomas, M. Namdeo, Y. Murali Mohan, S. K. Bajpai, M. Bajpai, *J. Macromol. Sci. A* **2007**, *45*(1), 107–119.

[232] C. P. Hauser, D. T. Thielemann, M. Adlung, C. Wickleder, P. W. Roesky, C. K. Weiss, K. Landfester, *Macromol. Chem. Physic* **2011**, *212*(3), 286–296.

[233] A. Manzke, N. Vogel, C. K. Weiss, U. Ziener, A. Plettl, K. Landfester, P. Ziemann, *Nanoscale* **2011**, *3*(6), 2523–2528.

[234] L. Messager, N. Portecop, E. Hachet, V. Lapeyre, I. Pignot-Paintrand, B. Catargi, R. Auzely-Velty, V. Ravaine, *J. Mater. Chem. B* **2013**, *1*(27), 3369–3379.

[235] R. T. Chacko, J. Ventura, J. Zhuang, S. Thayumanavan, *Adv. Drug Deliver. Rev.* **2012**, *64*(9), 836–851.

[236] S. V. Vinogradov, T. K. Bronich, A. V. Kabanov, *Adv. Drug Deliver. Rev.* **2002**, *54*(1), 135–147.

[237] S. E. Marshall, S.-H. Hong, N. T. Thet, A. T. A. Jenkins, *Langmuir* **2013**, *29*(23), 6989–6995.

[238] J. K. Oh, R. Drumright, D. J. Siegwart, K. Matyjaszewski, *Prog. Polym. Sci.* **2008**, *33*(4), 448–477.

[239] M. Karg, T. Hellweg, *Curr. Opin. Colloid In.* **2009**, *14*(6), 438–450.

[240] L. Zhang, D. Pornpattananangkul, C. M. J. Hu, C. M. Huang, *Curr. Med. Chem.* **2010**, *17*(6), 585–594.

[241] S. Tamilvanan, N. Venkateshan, A. Ludwig, *J. Control. Release* **2008**, *128*(1), 2–22.

[242] M. Laabei, A. Young, A. T. A. Jenkins, *Pediatr. Infect. Dis. J.* **2012**, *31*(5), e73–e77.

[243] K. Raemdonck, J. Demeester, S. De Smedt, *Soft Matter* **2009**, *5*(4), 707–715.

[244] D. Suzuki, T. Yamagata, M. Murai, *Langmuir* **2013**, *29*(33), 10579–10585.

[245] C. D. Jones, L. A. Lyon, *Macromolecules* **2000**, *33*(22), 8301–8306.

[246] E. Kobitskaya, D. Ekinci, A. Manzke, A. Plettl, U. Wiedwald, P. Ziemann, J. Biskupek, U. Kaiser, U. Ziener, K. Landfester, *Macromolecules* **2010**, *43*(7), 3294–3305.

[247] V. F. Gromov, *Usp Khim+* **1995**, *64*(1), 93–104.

[248] D. Klinger, K. Landfester, *Polymer* **2012**, *53*(23), 5209–5231.

[249] F. J. Schork, Y. Luo, W. Smulders, J. Russum, A. Butté, K. Fontenot, in *Polymer Particles*, Bd. 175 von *Advances in Polymer Science*, (Herausgegeben von M. Okubo), Springer Berlin Heidelberg, **2005**, 129–255.

[250] G. Dzhardimalieva, A. Pomogailo, V. Volpert, *J Inorg Organomet P* **2002**, *12*(1-2), 1–21.

[251] K. B. Girma, V. Lorenz, S. Blaurock, F. T. Edelmann, *Coordin Chem Rev* **2005**, *249*(11-12), 1283–1293.

[252] N. Poulter, M. Donaldson, G. Mulley, L. Duque, N. Waterfield, A. G. Shard, S. Spencer, A. T. A. Jenkins, A. L. Johnson, *New J. Chem.* **2011**, *35*(7), 1477–1484.

[253] L. Qi, Z. Xu, X. Jiang, C. Hu, X. Zou, *Carbohyd Res* **2004**, *339*(16), 2693–2700.

[254] H. Y. Carr, *Phys Today* **2004**, *57*(7), 83–83.

[255] P. Rinck, *Magnetic Resonance in Medicine*, Wiley, **2001**.

[256] C. B. Marcu, A. M. Beek, A. C. van Rossum, *Can. Med. Assoc. J.* **2006**, *175*(8), 911–917.

[257] D. Benaron, *Cancer Metast Rev* **2002**, *21*(1), 45–78.

[258] S. Morcos, *Eur. J. Radiol.* **2008**, *66*(2), 175–179.

[259] K. P. Pulukkody, T. J. Norman, D. Parker, L. Royle, C. J. Broan, *J. Chem. Soc., Perkin Trans. 2* **1993**, 605–620.

[260] K. Kumar, M. F. Tweedle, *Inorg. Chem.* **1993**, *32*(20), 4193–4199.

[261] E. Brucher, A. D. Sherry, *Inorg. Chem.* **1990**, *29*(8), 1555–1559.

[262] M.-F. Bellin, *Eur. J. Radiol.* **2006**, *60*(3), 314–323.

[263] J. M. Borsus, R. Jérôme, P. Teyssié, *J. Appl. Polym. Sci.* **1981**, *26*(9), 3027–3043.

[264] A. Leo, C. Hansch, D. Elkins, *Chem. Rev.* **1971**, *71*(6), 525–616.

[265] 1,4-Diamino-butan, MSDS No. 51799 (Online), **2014**, sigma Aldrich: Steinheim, Germany, http://www.sigmaaldrich.com/catalog/product/fluka/ 51799?lang=de&region=DE, (accessed Feb 17, 2014).

[266] 1,6-Diamino-hexan, MSDS No. H11696 (Online), **2012**, sigma Aldrich: Steinheim, Germany, http://www.sigmaaldrich.com/catalog/product/aldrich/ h11696?lang=de&region=DE, (accessed Feb 17, 2014).

[267] H. Vink, *Eur. Polym. J.* **1971**, *7*(10), 1411–1419.

[268] R. Earle, in *Unit Operations in Food Processing (Second Edition)*, (Herausgegeben von R. EARLE), second edition Aufl., Pergamon, Amsterdam, Kap. 9, **1983**, 116 – 142.

[269] R. S. Tipson, *Infrared spectroscopy of carbohydrates : a review of the literature / [by] R. Stuart Tipson*, Washington : U.S. Dept. of Commerce, National Bureau of Standards; for sale by the Supt. of Docs., U.S. Govt. Print. Off, **1968**, bibliography: p. 20-21.

[270] C. C. Lester, R. G. Bryant, *Magn. Reson. Med.* **1992**, *24*(2), 236–242.

[271] D. Schwert, J. Davies, N. Richardson, in *Contrast Agents I*, Bd. 221 von *Topics in Current Chemistry*, (Herausgegeben von W. Krause), Springer Berlin Heidelberg, **2002**, 165–199.

[272] J. W. Chen, R. B. Clarkson, R. L. Belford, *J. Phys. Chem.* **1996**, *100*(20), 8093–8100.

[273] J. E. Elliott, M. Macdonald, J. Nie, C. N. Bowman, *Polymer* **2004**, *45*(5), 1503–1510.

[274] F. Buchholz, in *Absorbent Polymer Technology*, Bd. 8 von *Studies in Polymer Science*, (Herausgegeben von L. Brannon-Peppas, R. S. Harland), Elsevier, **1990**, 23 – 44.

[275] S. Sharma, U. Paiphansiri, V. Hombach, V. Mailänder, O. Zimmermann, K. Landfester, V. Rasche, *Contrast Media Mol. I.* **2010**, *5*(2), 59–69.

[276] S. Langereis, Q. G. de Lussanet, M. H. P. van Genderen, E. W. Meijer, R. G. H. Beets-Tan, A. W. Griffioen, J. M. A. van Engelshoven, W. H. Backes, *NMR Biomed.* **2006**, *19*(1), 133–141.

[277] H. Schlaad, H. Kukula, J. Rudloff, I. Below, *Macromolecules* **2001**, *34*(13), 4302–4304.

[278] A. N. J. Heyn, *Biopolymers* **1974**, *13*(3), 475–506.

[279] R. Rigler, E. Elson, *Fluorescence correlation spectroscopy: theory and applications*, Bd. 65, Springer Verlag, **2001**.

[280] S.-H. Kim, C.-C. Chu, *J. Biomed. Mater. Res.* **2000**, *49*(4), 517–527.

[281] E. Aschenbrenner, K. Bley, K. Koynov, M. Makowski, M. Kappl, K. Landfester, C. K. Weiss, *Langmuir* **2013**, *29*(28), 8845–8855.

Appendix

Abbreviations

ACC	Autocorrelation curves
AAm	acrylamide
a.u.	arbitrary units
BHT	2,6 di-tert-butyl-4-methyl phenol
CFU	colony forming units
$c_{\text{Gdret.}}$	concentration of retained Gd
$c_{\text{Gdload.}}$	initial gadobutrol loading concentration
CH	cyclohexane
DAB	1,4-diamino butane
DexA	dextran acrylate
DexMa	dextran methacrylate
d_h	hydrodynamic diameter
DLS	dynamic light scattering
DMSO	dimethyl sulfoxide
DS	degree of substitution
ESI-MS	electrospray ionization mass spectrometry
FCS	fluorescence correlation spectroscopy
Gd	Gadolinium
HaCaT	human derived keratinocytes
HeLa	human derived epithelial cancer cell line
HMDA	1,6-diamino hexane
ICP-OES	inductively-coupled-plasma optical emission spectroscopy
IR	infra-red
λ_{Abs}	maximum absorption wavelength
λ_{Abs}	maximum emission wavelength
LD50	dose lethal to 50% of a population
MIC100	minimum inhbitory concentration, 100% inhibition
MRI	magnetic resonance imaging
MRSA	methicillin resistant *Staphylococcus aureus*
M_w	molecular weight
NMR	nuclear magnetic resonance
PAA	polyacrylic acid

PAANa	polyacrylic acid sodium salt
PAAm	polyacrylamide
P(E/B-*b*-EO)	Poly[(ethylene-*co*-butylene)-*b*-(ethylene oxide)]
PPE	poly(phosphoester)
ppm	parts per million
r1	change of longitudinal relaxation rate per Gd concentration
rpm	rotations per minute
SEM	scanning electron microscopy
TDI	2,4-toluene diisocyanate
T_1	longitudinal relaxation time
T_2	transversal relaxation time
TEA	triethylamine
TEM	transmission electron microscopy

List of Figures

Acknowledgments

Curriculum Vitae

Scientific Contribution

Publications

K. Malzahn, W.D. Jamieson, M. Dröge, V. Mailänder, A.T.A. Jenkins, Clemens K. Weiss, K. Landfester,
Advanced dextran based nanogels for fighting Staphylococcus aureus infections by sustained zinc release, J. Mater. Chem. B, 2014, 2, 2175.

K. Malzahn, F. Marsico, K. Koynov, K. Landfester, C. K. Weiss, F. R. Wurm
Selective Interfacial Olefin Cross Metathesis for the Preparation of Hollow Nanocapsules, Macro Lett., 2014, 3, 40.

K. Malzahn, L. Duque, P. Ciernak, S. Wiesenmüller, K. Bender, R. Förch,
Antimicrobioal activity and cyto-compatibility of plasma polymerizd zinc acetylacetonate thin films, Plasma Process. Polym., 2013, 10, 243.

K. Malzahn, J.R. Windmiller, G.Valdés Ramirez, J. Wang,
Wearable electrochemical sensors for in-situ analysis in marine environments, Analyst, 2011, 136, 2912.

A. Poghossian, **K. Malzahn**, M.H. Abouzar, P. Mehndiratta, E. Katz, M.J. Schöning,
Integration of biomolecular logic gates with field-effect transducers, Electrochim. Acta, 2010, 56, 9661.

Conference contributions

K. Malzahn, C. Weiss, K. Landfester
Dextran nanogels as delivery-system for release of zinc as antibacterial agent (Oral contribution),
ESB 2013, 25th European conference on biomaterials, Madrid - Spain.

K. Malzahn, L. Duque, P. Ciernak, S. Wiesenmüller, K. Bender, K. Landfester, R. Förch
Applicability of zinc releasing thin films with antimicrobial properties in cell culture (Oral and poster contribution)
EnFi 2012, Engineering Functional Interfaces, Zweibrücken - Germany.